Development of Chemical Probes for Studying K^+ in Biology

By

Zeming Wang

A dissertation submitted in partial satisfaction of the

requirements for the degree of

Doctor of Philosophy

in

Chemistry

in the

Graduate Division

of the

University of California, Berkeley

Committee in charge:

Professor Christopher J. Chang, Chair

Professor Michelle C. Chang

Professor Sanjay Kumar

Spring 2018

Development of Chemical Probes for Studying K^+ in Biology

by Zeming Wang

Abstract

Development of Chemical Probes for Studying K^+ in Biology

By Zeming Wang

Doctor of Philosophy in Chemistry

University of California, Berkeley

Professor Christopher J. Chang, Chair

Potassium (K^+) occupies 4% of human body mass and is the most abundant intracellular cation. Potassium plays a vital role in regulating intracellular fluid volume, fluid transportation, and neuron signaling. Abnormal K^+ fluctuations may lead to diseases such as anorexia, bulimia, heart disease, diabetes, and epilepsy. Recent study also has shown elevated level of K^+ channel mutation in cancer cells. However, the physiology of K^+ is insufficiently understood, due to the absence of ways to measure the change of K^+ in cellular fluids with high spatial and temporal fidelity. This dissertation chronicles the design and applications of novel imaging probes and strategies for probing K^+ both intracellularly and extracellularly. This work describes the first ratiometric probe and a new fluorescent turn-on probe for imaging intracellular K^+; both probes utilize novel lariat-ether modified crown ether structure as K^+ binding ionophore. Additionally, this work describes development of a new imaging tool for detecting H_2O_2 utilizing bioluminescence resonance energy transfer.

Table of Contents

Acknowledgments

Thanks God for all the time.
To my parents, for their love and support and for being my life role model.
And my grandma who prayed for me always and wish the best for me.
Who I am now is made of your love and support.
Special thanks to Chris who had accepted me in his group and as a mentor, he tought me how to do science and gave me the direction and support to walk the path of being a chemist. I would like to thanks Chris not only for his mentorship but also for all members in the lab. Thanks to Vivian who taught me how to set up experiment and also all the advice for the graduate school life. And also thanks to Mark and Ryan for their organic synthetic knowledge and for his friendship to be bonded to this lab. And also thank to Lakshmi, Joey, Clive and Safa for their biology-side advice and patiently taught all the bench work. Thanks to Sumin who started the graduate school at the same time and worked on alkali metals fluorescent probes in this lab even though you left me alone in potassium but it was great luck to have company like you. Thanks to other labmates, especially Kevin who shared 610 office together and be a great friend in the graduate school as well as Tyler, a great gym buddy and friend. And thanks to all of senior lab members Thom, Cheri, Allegra, Eva, and Karla who gave previous advice and support and also had fun together in entire graduate life. And all the other members like Vanessa who worked together for BRET project and all Tan 575 people who set new lab in Tan building and opened all deliveries together.
Every one of you is really valuable and helped me to become who I am now.
I cannot say how thankful I am but hope I can influence other peoples around me like you guys and be a good scientist and do good science. It won't be possible if any of you aren't there.
I also want to thank my dear friends, Jianwei who shared the house and listened to my words carefully and be my mental supporter.

Chapter 1

Design, synthesis, and application of a fluorescent turn-on K^+ probe for measuring intracellular K^+ level in living cells

Portions of this work were performed in collaboration with the following persons:

Dr. Vanessa Checchetto and Luigi Leanza from Professor Ildiko Szabo group helped perform in cellulo characterization of KGreen including HEK 293T cells imaging data and flow cytometry data (Figure 1.4-1.8)

1.1 Introduction

Potassium ion (K^+) is the most abundant metal ion in human body, and K^+ homeostasis plays an essential role in many physiological events. Intracellular K^+ levels are around 150 mM while extracellular K^+ levels are around 5 mM.[1–6] The large K^+ level difference is maintained by K^+ pump which delivers K^+ against its gradient and K^+ channel which delivers K^+ along its gradient.[7] Cellular osmolality created by K^+ gradient helps regulating intracellular pH, cell volume, enzyme function, and growth.[8–10] On the other hand, transcellular K^+ flux contributes to the regulation of processes such as neuromuscular excitability, cardiac rhythmicity, and renal absorption. K^+ misregulation, commonly caused by malfunction of K^+ channel or pump, could lead to multiple diseases such as epilepsy, arrhythmia, and kidney stones.[9–12] A better understanding of K^+ homeostasis can benefit the study of these diseases and drug discovery. Current methods for K^+ detection involve either bulk analysis such as atomic absorption, flame photometry, and ion chromatography or selective microelectrode. However, bulk analysis requires destruction of cells and cannot be used for live cell detection, while selective microelectrode can give live cell readout but suffers from low spatial resolution and low throughput issue.

Our lab has developed a fluorescent approach for detection of K^+ dynamics.[13–15] A fluorescent small molecule sensor for K^+ could provide non-invasive, fast, and sensitive read out while maintaining high temporal and spatial resolution. Despite the importance of K^+, only a limited number of fluorescent K^+ sensors have been reported due to the difficulty in selectivity of K^+ over Na^+. The majority of previously developed K^+ sensors mostly utilize cryptand or pseudo-cryptand structure as ionophore for specific K^+ binding.[16–18] However, they suffer from having a low dissociation constant (K_d) less than 10 mM and are only suitable for sensing K^+ fluxes extracellularly.[19] Also, synthetic challenges make the modification of the fluorophore structure difficult. Other crown-ether-based K^+ sensors such as PBFI have desirable K_d range but show poor selectivity for K^+ over Na^+.[20] We envisioned an improved fluorescent sensor that could provide accurate information on intracellular K^+ level and a sensitive response to cellular K^+ fluxes.

In this chapter, we report the design, synthesis, and biological evaluation of a fluorescent probe for K^+ by modulating photo-induced energy transfer (PET) between a K^+ binding ionophore and chromophore.[21] More specifically, this new probe (KGreen) utilizes a lariat-ether modified crown-ether as selective K^+ binding ionophore and control PET between aza-crown and chromophore.[22,23] This strategy can be further extended to different chromophore and thus allow multiple color turn-on probes for potassium, one of which, K rhodol, will be shown in the later chapter. KGreen showed good selectivity and sensitivity to K^+ over other biologically relevant metals especially Na^+ and is capable of a dynamic read-out of intracellular K^+ level. This result proves KGreen to be a good candidate probe for studying cellular K^+ flux in biology.

1.1. Methods

1.1.1. General synthetic methods

Reactions using moisture- or air-sensitive reagents were carried out in flame-dried glassware under an inert atmosphere of N_2. Solvent was passed over activated alumina and stored over activated 3Å molecular sieves before use when dry solvent was required. All other commercially purchased chemicals were used as received (without further purification). Lariet ether-modified crown-ether was prepared according to published procedures.[24] SiliCycle 60 F254 silica gel (pre-coated sheets, 0.25 mm thick) were used for analytical thin layer chromatography and visualized by fluorescence quenching under UV light. Silica gel P60 (SiliCycle) was used for column chromatography. ^{1}H and ^{13}C NMR NMR spectra were collected at 298 K in CDCl3 or CD3CN (Cambridge Isotope Laboratories, Cambridge, MA) at 25 °C on Bruker AVQ-400, AVB-400, AV-500, or AV-600 at the College of Chemistry NMR Facility at the University of California, Berkeley. All chemical shifts are reported in the standard notation of δ parts per mil-lion relative to residual solvent peak at 7.26 ($CDCl_3$) or 1.93 (CD_3CN) for ^{1}H and 77.16 ($CDCl_3$) or 177.7 (CD_3CN) for ^{13}C as an internal reference. Splitting patterns are indicated as follows: br, broad; s, singlet; d, doublet; t, triplet; m, multiplet; dd, doublet of doublets. Low-resolution electrospray mass spectral analyses were carried out using a LC-MS (Agilent Technology 6130, Quadrupole LC/MS and Advion expression-L Compact Mass Spectrometer). High-resolution mass spectral analyses (ESI-MS) were carried out at the College of Chemistry Mass Spectrometry Facility at the University of California, Berkeley.

1.1.2. Probe synthesis and new compound characterization

4-(1,4,7,10,13-pentaoxa-16-azacyclooctadecan-16-yl)-3-(2-methoxyethoxy)benzaldehyde, 2. POCl3 (3.72 ml, 40 mmol) was added dropwise to a vigorously stirring anhydrous DMF which was kept in ice bath under N_2. Resulting pale yellow solution was stirred at room temperature for additional 15 min. To this, DMF (2 ml) solution of 16-(2-(2-methoxyethoxy)phenyl)-aza-18-crown-6 **1** (1.65 g, 4 mmol) was then slowly introduced and the resulting dark red solution was heated at 70 ^{o}C for 3 h. Reaction was cooled to room temperature, and poured into ice-cold sat'd $NaHCO_3$ solution. The mixture was extracted 3 x 100 ml DCM/Toluene (2:1) and dried over anhydrous $MgSO_4$. Solvent was evaporated in vacuo and compound was purified by silica gel FCC using DCM:MeOH (19:1) as the eluent. Product **2** was obtained as dark red oil (820 mg, 44% yield) ^{1}H NMR (400 MHz, $CDCl_3$) δ (ppm): 3.48 (s, 3 H), 2.38 (s, 2 H), 2.00 - 1.77 (m, 11 H). ^{13}C NMR (101 MHz, $CDCl_3$) δ (ppm): 215.88, 175.71, 51.63, 45.47, 39.82, 37.98, 37.51, 26.98. LCMS calcd. for $C_{12}H_{16}O_3$ $[M + H]^+$ 414.19, found 414.2.

9-(4-(1,4,7,10,13-pentaoxa-16-azacyclooctadecan-16-yl)-3-(2-methoxyethoxy)phenyl)-6-hydroxy-3H-xanthen-3-one, 3. Aldehyde **2** (150 mg, 0.34 mmol, 1 equiv) and resorcinol (82 mg, 0.74 mmol, 2.2 equiv) were dissolved in 4.25 ml TFA in 35 ml pressure flask. The solution was then stirred at 115 °C for 13 h and rotovaped own to yield crude red oil. The red oil was taken up in silica column for purification by flash column chromatography (50%

MeCN/Toluene) to yield **3** (35 mg, 18% yield) as a bright yellow solid. ^{1}H NMR (400 MHz, $CDCl_3$) δ (ppm): 3.48 (s, 3 H), 2.38 (s, 2 H), 2.00 - 1.77 (m, 11 H). ^{13}C NMR (101 MHz, $CDCl_3$) δ (ppm): 215.88, 175.71, 51.63, 45.47, 39.82, 37.98, 37.51, 26.98. LRMS calcd. for $C_{12}H_{16}O_3$ [M + H]$^+$ 209.11, found 209.2.

1.1.3. Spectroscopic materials and methods

All aqueous solutions were prepared using Milli-Q water, and all spectroscopic experiments were carried out in 50 mM HEPES, pH 7.4, unless otherwise noted. All spectroscopic experiments were prepared using freshly prepared aliquots. Absorption spectra were acquired on a Varian Cary 50 spectrophotometer, and fluorescence spectra were acquired using a Photon Technology International Quanta Master 4 L-format scan spectro-fluorometer equipped with an LPS-220B 75-W xenon lamp and power supply, A-1010B lamp housing with integrated igniter, switchable 814 photocounting/analog photomultiplier detection unit, and MD5020 motor driver. 1-cm × 1-cm quartz cuvettes (1.4-mL volume, Starna, capped) were used for obtaining absorption and fluorescence spectra. For all fluorescence response to K^+ studies, aqueous solutions of KCl (Sigma) were used. For metal selectivity studies, aqueous metal solutions of $MgCl_2 \cdot 4H_2O$ (EMD Millipore), $CaCl_2 \cdot 2H_2O$ (EMD Millipore), $NiCl_2 \cdot 6H_2O$ (Sigma), $ZnCl_2$ (Sigma), $CuCl_2 \cdot 2H_2O$ (Baker & Adamson), $CoCl_2 \cdot 6H_2O$ (Sigma), $MgCl_2 \cdot 6H_2O$ (Sigma), NaCl (Sigma), $FeCl_2$ (Sigma), and $FeCl_3$ (Sigma) were used. Moreover, the identity of the potassium complex formed was assessed by the method of continuous variations (Job's plot) to identify a 1:1 K^+:KGreen binding stoichiometry. (Figure xxx) This information allowed for the characterization of the binding affinity for K^+ via Benesi-Hildebrand plot. (Figure)

1.1.4. Fluorescence Turn-on Responses to Potassium

2 different 50 mM HEPES (pH 7.4) was made. Solution A contains 200 mM Na^+ while solution B contains 200 mM K^+. Solution A and B was mixed in different ratio to yield 1 ml final buffer solution with 0, 1, 5, 10, 20, 50, 80, 100, 120, 150, 180, 200 mM respectively. A 2 µM solution of KGreen prepared by diluting1 mM DMSO stock solution of KGreen with each buffer 1:500 ratio into a 1-cm × 1-cm capped quartz cuvette. The probe solution was incubated at 37 °C for 5 minutes. Emission spectra (λex = 488 nm, λem = 500-700 nm) were then collected.

1.1.5. Metal Selectivity Experiments.

A 2 µM solution of Kgreen was prepared by diluting a 1 mM DMSO stock solution of probe into 1 mL HEPES. 500 µL of this solution were added to ten 1-cm × 1-cm capped quartz cuvettes and then 500 µL of the metal of interest was added to the cuvette to bring the concentration of transition metals to 10 µM and with the exception of Na^+ at 150 mM. The emission spectrum was then recorded for each metal of interest solution.

1.1.6. Cell culture

Human embryonic kidney (HEK-293) cells were maintained in culture in Dulbecco's modified Eagle medium (DMEM) supplemented with 10% FBS, 100 U/mL penicillin G, 0.1 mg/mL streptomycin and 1% non-essential amino acids (100X solution; Thermo Fisher Scientific). T lymphocytes (Jurkat cells) were grown in RPMI-1640 (Thermo Fisher Scientific), supplemented as DMEM.

1.1.7. Metal Selectivity Experiments.

HEK-293 cells (150,000 cells/well) were seeded on coverslips in a 6-well plate in 2 mL of their culture medium. After 24 h, cells were washed with 1 mL Hank's Balanced Salt Solution (HBSS) (Thermo Fisher Scientific). Then, cells were incubated in the dark at room temperature (RT) with 400 nM freshly diluted KGreen (from 400 µM stock solution in 100% DMSO) for different time points as indicated. Valinomycin (10 µM) was finally added to induce potassium release. KGreen fluorescence was followed by fluorescence microscopy using a Leica DMI 6000 fluorescence microscope equipped with confocal setup (Leica Microsystem, Wetzlar, Germany) and a GFP filter set.

Jurkat cells (1x106 cells) were washed and re-suspended in 1 mL HBSS. Cells were incubated with 1:1000 diluted KGreen for 15 minutes, followed by valinomycin (10 µM) addition. KGreen fluorescence was followed by FACS analysis using a FACSanto II (Beckton Dickinson) and data were processed by quadrant statistics using BD VISTA software.

1.1.8. Mitochondrial potential and nuclear staining

HEK-293 cells (150,000 cells/well) were seeded on coverslips in a 6-well plate in 2 mL of their culture medium. After 24 h, cells were washed with 1 mL HBSS (Thermo Fisher Scientific) and incubated 20 min at 37°C with 20 nM of the potentiometric dye Tetramethylrhodamine methyl ester (TMRM) + 300 µG/ml Hoechst 33342 (2'-[4-ethoxyphenyl]-5-[4-methyl-1-piperazinyl]-2,5'-bi-1H-benzimidazole trihydrochloride trihydrate), suitable for fixed- and live-cell fluorescent staining of DNA and nuclei. Then, in the dark at RT, 1:1000 diluted KGreen was either added or not to the cells and the three fluorescence signals (TMRM=Red; KGreen=green; Hoechst=blue) were monitored for different time points as indicated, by fluorescence microscopy using a Leica DMI 6000 fluorescence microscope equipped with confocal setup (Leica Microsystem, Wetzlar, Germany).

1.1.9. KGreen release and potassium channel inhibition

HEK-293 cells (150,000 cells/well) were seeded on coverslips in a 6-well plate in 2 mL of their culture medium. After 24 h, cells were washed with 1 mL HBSS. Then, cells were incubated in the dark at RT with 1:1000 diluted KGreen for 5 minutes. Following, cells were either pre-treated with general potassium channel inhibitors (1 mM $GdCl^{3+}$ 5 mM $BaCl^{2+}$ 5 mM Tetraethylammonium (TEA) Chloride) for further 5 minutes or left untreated. Afterwards, the medium was replaced with a solution containing 30 mM Tris-HCl pH 7.4 either containing or not

the three channel inhibitors and KGreen fluorescence was monitored for the next 10 minutes by fluorescence microscopy using a Leica DMI 4000 fluorescence microscope (Leica Microsystem, Wetzlar, Germany).

1.3. Results

1.3.1. Design and synthesis of KGreen

Our design of KGreen utilizing a lariat-ether modified crown-ether as a K^+ selective ionophore. We chose the lariat-ether modified crown-ether as K^+ binding moiety since it has been shown to have a moderate binding affinity towards K^+ but still maintain high selectivity over sodium. We then chose di-hydroxy xanthone as our fluorophore inspired by fluorescein and many of our lab's previous work to ensure a bright and stable signal. We envision that before binding K^+ nitrogen lone pair will quench fluorescence of the fluorophore. After binding K^+, PET quenching effect from nitrogen lone pair on KGreen to the chromophore is inhibited and the probe thus gives out a turn-on response at 521 nm emission. Information of K^+ can be provided using emission profiles for green fluorescein channel.
The synthesis of KGreen is briefly described below. The lariat-ether modified phenyl aza-crown was synthesized according to literature procedure. It was then converted to aldehyde through vilsmeier haack reaction and then into KGreen by further condensation with resorcinol.

1.3.2. Reactivity and K+ Selectivity of KGreen in Aqueous Buffer.

After synthesizing KGreen, we evaluate its fluorescence response to K^+ in aqueous buffer (50 mM HEPES, pH 7.4). KGreen showed absorption maxima at 488 nm with molar attenuation coefficient of ε488 = 17600 M-1 cm-1 (Figure) and emission maxima at 521 nm (Figure)

We next evaluate turn-on response of KGreen with K^+ titration. With the increase of K^+ / Na^+ concentration in the buffer, we observe a significant increase in emission intensity of the probe. At the range of 0 mM to 150 mM K^+ increase with Na^+ as the counter ion, the probe showed 10 fold turn-on. To further calculate the dissociation constant (K_d), binding analysis of the formed K^+ complex was conducted using the method of continuous variations (Job's plot) to make sure a 1:1 K^+ : probe complex is formed for the fluorescence turn-on response. After confirmation of 1:1 binding Benesi-Hildebrand plot was obtained from the titration experiment, and was calculated to be 37 mM, which is much higher than cryptand based probe as expected. (Figure)

1.3.3. Application of KGreen to Imaging K^+ in Living Cells

In the next series of experiments, human embryonic kidney (HEK 293T) cells were loaded using the membrane permeant KGreen at 400 nM concentration. Quantification of the dye uptake was achieved by using confocal microscopy and exciting the cells at 488 nm, while

detecting emission in the 505-525 nm range. Uptake of the dye was efficient and reached a plateau within 10 minutes (Figure 1A). This property of KGreen contrasts with the poor loading efficiency usually reported for the other K^+ -sensitive dye PBFI AM. Uptake was homogenous and occurred in all cells (Figure 1B and Figure 2). Within the cells, KGreen exhibited a distribution that is typical of that of cytosolic dyes and was largely excluded from the nucleus (Figure 1B). The probe exhibited a remarkable intracellular stability, with negligible photobleaching or cell leakage (see e.g. Figure 1 B, 2, 3). KGreen did not cause either loss of mitochondrial membrane potential or nuclear fragmentation, as assessed using TMRM and Hoechst 33342 dyes, respectively (Figure 2). Cell viability was not altered upon incubation of the cells with up to 4 µM KGreen for 24 hours as assessed by MTT assay [25] (not shown, n=12).

Next, we applied the potassium-specific ionophore, valinomycin in order to demonstrate that the dye responds to variations in the intracellular potassium concentration. Valinomycin is a cell-permeant compound that can bind to K+ ions with relatively high selectivity over other cations, replacing the hydration shell of K^+. Consequently, K^+ ions shielded by valinomycin molecules can pass across the plasma membrane without a requirement for opening a K^+-permeable channel. Valinomycin was used at 10 µM concentration which is sufficient to allow K^+ ions to freely cross the plasma membrane and therefore to promote potassium efflux and to cause plasma membrane hyperpolarization.[26] Valinomycin indeed brings the membrane potential of the plasmamembrane closer to the K^+ diffusion potential, while it collapses the membrane potential of the mitochondria in the high [K^+] cytoplasm.[27] The resting membrane potential in HEK293 cells was measured to range between -35 and -50 mV in a typical intracellular (130 mM K^+) and extracellular (6 mM K^+) recording solution.[28] Following application of valinomycin, the resulting fluorescence signal was recorded (Fig. 3). In contrast to untreated HEK-293 cells, in those treated with valinomycin, a sustained decrease of the fluorescent signal was observable, in accordance with the expected decrease of intracellular [K+]. Similar results were obtained using Jurkat T lymphocytes, where uptake of the dye and valinomycin-induced KGreen fluorescent decrease were evaluated by FACS analysis (Figure S1). In addition to valinomycin, we also used a more physiological stimulus to induce potassium efflux from HEK-293 cells. Under hypo-osmotic conditions, acute volume regulation occurs in order to prevent cell bursting.[29] Osmotic swelling is followed by cell-intrinsic regulatory processes that are called regulatory volume decrease (RVD) which tend to restore the initial cell volume. RVD usually involves the net export of K^+, Cl^- and organic osmolytes like taurine. Loss of K^+ may occur through K^+ channels. HEK-293 cells harbours different K^+ channels, including voltage-gated potassium channels (K_v) which can be partially inhibited using Tetraethylammonium chloride (TEACl), a classical general blocker of K^+ channels.[30] In addition, Barium and Gadolinium are also able to block potassium currents.[31] Therefore, we investigated whether KGreen fluorescence can reflect an osmotic-stress induced channel-mediated exit of potassium and whether this process was sensitive to general potassium channel blockers. Figure S2 exemplifies that indeed cell volume was increased while KGreen fluorescence was decreased upon osmotic shock and both processes were at least partially responding to the mixture of potassium channel inhibitors comprising TEA, Ba^{2+} and Gd^{3+}.

1.4. Conclusion

To conclude, we have shown the design, synthesis, in *vivo* an in *vitro* characterization of KGreen, a unique K^+ fluorescent probe with turn-on response through PET mechanism. KGreen utilize a new lariat-ether modified crown-ether structure to ensure moderate binding affinity towards K^+ KGreen demonstrated selective response to K^+ and is able to report on changes in levels of intracellular K^+ flux induced by K^+ artificial pore valinomycin or K^+ channel blocker. KGreen has shown its potential to help study intracellular K^+ dynamics in biological system.

1.5. Reference

(1) Ghosh, T.; Cho, K. Y.; Ullah, K.; Nikam, V.; Park, C. Y.; Meng, Z. Da; Oh, W. C. High Photonic Effect of Organic Dye Degradation by CdSe-Graphene-TiO2particles. *J. Ind. Eng. Chem.* **2013**, *19* (3), 797–805.

(2) Tian, H.; Zhu, W. 2014 - In Vivo and in Situ Tracking Cancer Chemotherapy by Highly Photostable NIR Fluorescent Theranostic Prodrug.pdf. **2013**.

(3) Edalat, F. NIH Public Access. **2012**, *40* (6), 1301–1315.

(4) Alder, J. F.; Ashworth, D. C.; Narayanaswamy, R. An Ion. **1987**, *112* (August), 1191–1192.

(5) Gelling, A.; Jeffery, J. C.; Poveycand, C.; Went, M. J.; Chemistry, I.; Its, B. B. S. Chemical Corn M U N Ications. **1991**, *346* (6), 349–351.

(6) He, F. J.; MacGregor, G. A. Beneficial Effects of Potassium on Human Health. *Physiol. Plant.* **2008**, *133* (4), 725–735.

(7) Amédée, T.; Robert, A.; Coles, J. A. Potassium Homeostasis and Glial Energy Metabolism. *Glia* **1997**, *21* (1), 46–55.

(8) Ge, L.; Hoa, N. T.; Wilson, Z.; Arismendi-Morillo, G.; Kong, X. T.; Tajhya, R. B.; Beeton, C.; Jadus, M. R. Big Potassium (BK) Ion Channels in Biology, Disease and Possible Targets for Cancer Immunotherapy. *Int. Immunopharmacol.* **2014**, *22* (2), 427–443.

(9) Tian, C.; Zhu, R.; Zhu, L.; Qiu, T.; Cao, Z.; Kang, T. Potassium Channels: Structures, Diseases, and Modulators. *Chem. Biol. Drug Des.* **2014**, *83* (1), 1–26.

(10) Yu, S. P. Regulation and Critical Role of Potassium Homeostasis in Apoptosis. *Prog. Neurobiol.* **2003**, *70* (4), 363–386.

(11) Huang, X.; Jan, L. Y. Targeting Potassium Channels in Cancer. *J. Cell Biol.* **2014**, *206* (2), 151–162.

(12) Felipe, A.; Vicente, R.; Villalonga, N.; Roura-Ferrer, M.; Martínez-Mármol, R.; Solé, L.; Ferreres, J. C.; Condom, E. Potassium Channels: New Targets in Cancer Therapy. *Cancer Detect. Prev.* **2006**, *30* (4), 375–385.

(13) Dickinson, B. C.; Chang, C. J. Chemistry and Biology of Reactive Oxygen Species in Signaling or Stress Responses. *Nat. Chem. Biol.* **2011**, *7* (8), 504–511.

(14) Dickinson, B. C.; Chang, C. J. A Targetable Fluorescent Probe for Imaging Hydrogen

Peroxide in the Mitochondria of Living Cells. *J. Am. Chem. Soc.* **2008**, *130* (30), 9638–9639.
(15) Srikun, D.; Albers, A. E.; Chang, C. J. A Dendrimer-Based Platform for Simultaneous Dual Fluorescence Imaging of Hydrogen Peroxide and pH Gradients Produced in Living Cells. *Chem. Sci.* **2011**, *2* (6), 1156.
(16) Sui, B.; Yue, X.; Tichy, M. G.; Liu, T.; Belfield, K. D. Improved Synthesis of the Triazacryptand (TAC) and Its Application in the Construction of a Fluorescent TAC-BODIPY Conjugate for K+ Sensing in Live Cells. *European J. Org. Chem.* **2015**, *2015* (6), 1189–1192.
(17) Valeur, B. Design Principles of Fluorescent Molecular Sensors for Cation Recognition. *Coord. Chem. Rev.* **2000**, *205* (1), 3–40.
(18) Carpenter, R. D.; Verkman, A. S. Function-Oriented Synthesis of a Didesmethyl Triazacryptand Analogue for Fluorescent Potassium Ion Sensing. *European J. Org. Chem.* **2011**, No. 7, 1242–1248.
(19) Han, Y.; Jiang, Y.; Chen, C. F. Cryptand-Based Hosts for Organic Guests. *Tetrahedron* **2015**, *71* (4), 503–512.
(20) Meuwis, K.; Boens, N.; De Schryver, F. C.; Gallay, J.; Vincent, M. Photophysics of the Fluorescent K+ Indicator PBFI. *Biophys. J.* **1995**, *68* (6), 2469–2473.
(21) Savariar, E. N.; Felsen, C. N.; Nashi, N.; Jiang, T.; Ellies, L. G.; Steinbach, P.; Tsien, R. Y.; Nguyen, Q. T. Real-Time in Vivo Molecular Detection of Primary Tumors and Metastases with Ratiometric Activatable Cell-Penetrating Peptides. *Cancer Res.* **2013**, *73* (2), 855–864.
(22) Woodroofe, C. C.; Lippard, S. J. A Novel Two-Fluorophore Approach to Ratiometric Sensing of Zn2+. *J. Am. Chem. Soc.* **2003**, *125* (38), 11458–11459.
(23) Schultz, R. A.; White, B. D.; Dishone, D. M.; Arnold, K. A.; Gokel, G. W. 12-, 15-, and 18-Membered-Ring Nitrogen-Pivot Lariat Ethers: Syntheses, Properties, and Sodium and Ammonium Cation Binding Properties1-. *J. Am. Chem. Soc.* **1985**, *107* (23), 6659–6668.
(24) Ast, S.; Schwarze, T.; Müller, H.; Sukhanov, A.; Michaelis, S.; Wegener, J.; Wolfbeis, O. S.; Körzdörfer, T.; Dürkop, A.; Holdt, H. J. A Highly K+-Selective Phenylaza-[18]crown-6-Lariat-Ether-Based Fluoroionophore and Its Application in the Sensing of K+ Ions with an Optical Sensor Film and in Cells. *Chem. - A Eur. J.* **2013**, *19* (44), 14911–14917.
(25) Leanza, L.; Romio, M.; Becker, K. A.; Azzolini, M.; Trentin, L.; Managò, A.; Venturini, E.; Zaccagnino, A.; Mattarei, A.; Carraretto, L.; et al. Direct Pharmacological Targeting of a Mitochondrial Ion Channel Selectively Kills Tumor Cells In Vivo. *Cancer Cell* **2017**, *31* (4), 516–531.e10.
(26) Ndukwe Erlingsson, U. C.; Iacobazzi, F.; Liu, A.; Ardon, O.; Pasquali, M.; Longo, N. The Effect of Valinomycin in Fibroblasts from Patients with Fatty Acid Oxidation Disorders. *Biochem. Biophys. Res. Commun.* **2013**, *437* (4), 637–641.
(27) Nicholls, D. G. Simultaneous Monitoring of Ionophore- and Inhibitor-Mediated Plasma and Mitochondrial Membrane Potential Changes in Cultured Neurons. *J. Biol. Chem.* **2006**, *281* (21), 14864–14874.
(28) Chemin, J.; Monteil, A.; Briquaire, C.; Richard, S.; Perez-Reyes, E.; Nargeot, J.; Lory, P. Overexpression of T-Type Calcium Channels in HEK-293 Cells Increases Intracellular Calcium without Affecting Cellular Proliferation. *FEBS Lett.* **2000**, *478* (1–2), 166–172.
(29) Jentsch, T. J. VRACs and Other Ion Channels and Transporters in the Regulation of Cell Volume and Beyond. *Nat. Rev. Mol. Cell Biol.* **2016**, *17* (5), 293–307.

(30) Jiang, B.; Sun, X.; Cao, K.; Wang, R. Endogenous KV Channels in Human Embryonic Kidney (HEK-293) Cells. *Mol. Cell. Biochem.* **2002**, *238* (1/2), 69–79.
(31) Yellen, G. Permeation in Potassium Channels: Implications for Channel Structure. *Annu. Rev. Biophys. Biophys. Chem.* **1987**, *16* (1), 227–246.

Figures

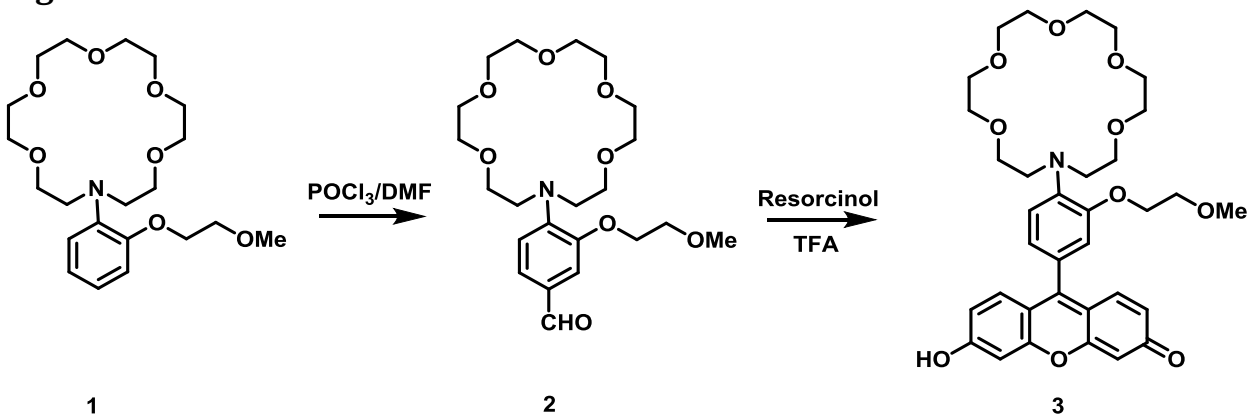

Scheme 1.1. Synthesis of K^+ fluorescent probe KGreen

Reagents and conditions: (i) $POCl_3$, DMF, 0 °C to r.t. 15 min, r.t. to 80 °C 4 h; (ii) Resorcinol, TFA , 115 °C., 12 h

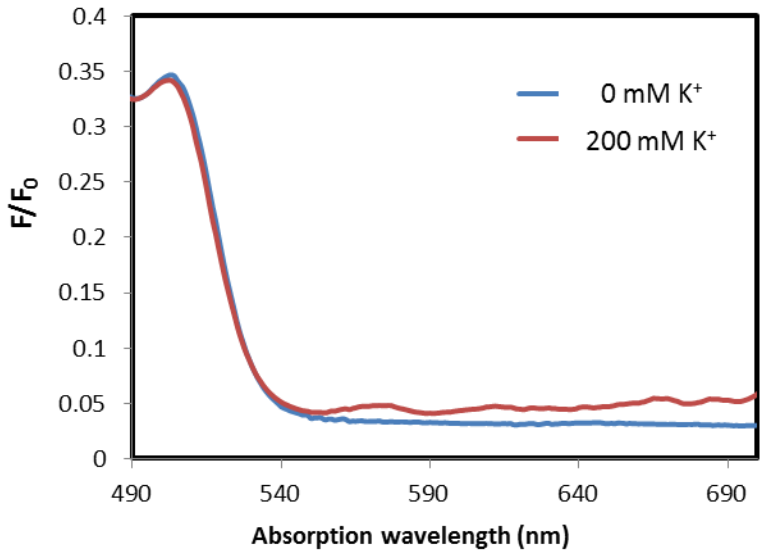

Figure 1.1. UV-Visible spectra of KGreen. Spectra were obtained in 50 mM HEPES (pH 7.4) with 2 µM KGreen.).

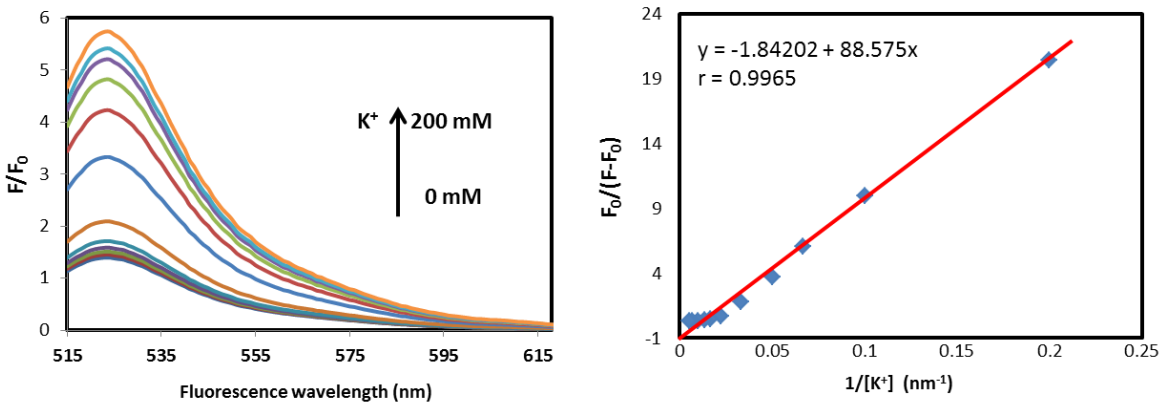

Figure 1.2. (a) Fluorescence intensity of 2 μM KGreen with response of buffer with various K^+ level from 0 mM to 200 mM in 50 mM HEPES (pH 7.4) (b) Benesi-Hildebrand plot was made using the fluorescence intensity information with reference to K^+ concentration. K_d was calculated to be 37 mM.

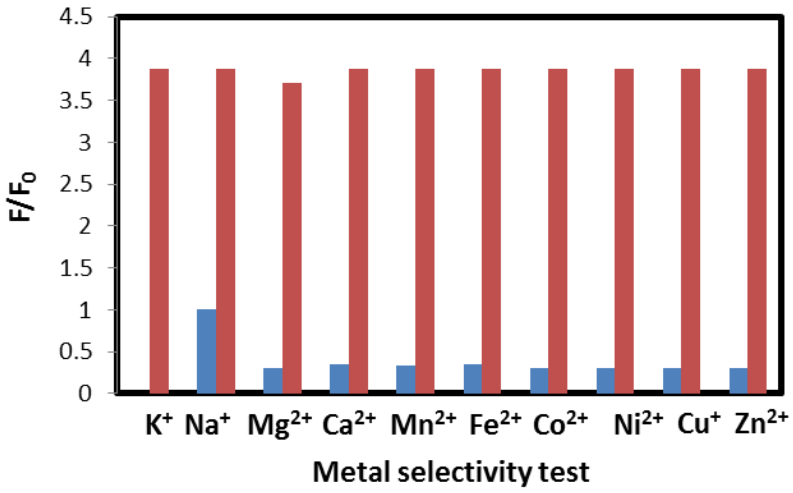

Figure 1.3. Fluorescence response of 2 μM KGreen to biologically relevant d-block (10 μM) and s-block (1 mM) metals with the exception of Na^+ (150 mM). Blue bar shows the fluorescence information of mere metal buffer solution and Red bar shows the fluorescence information of buffer balanced by K^+ to 150 mM.

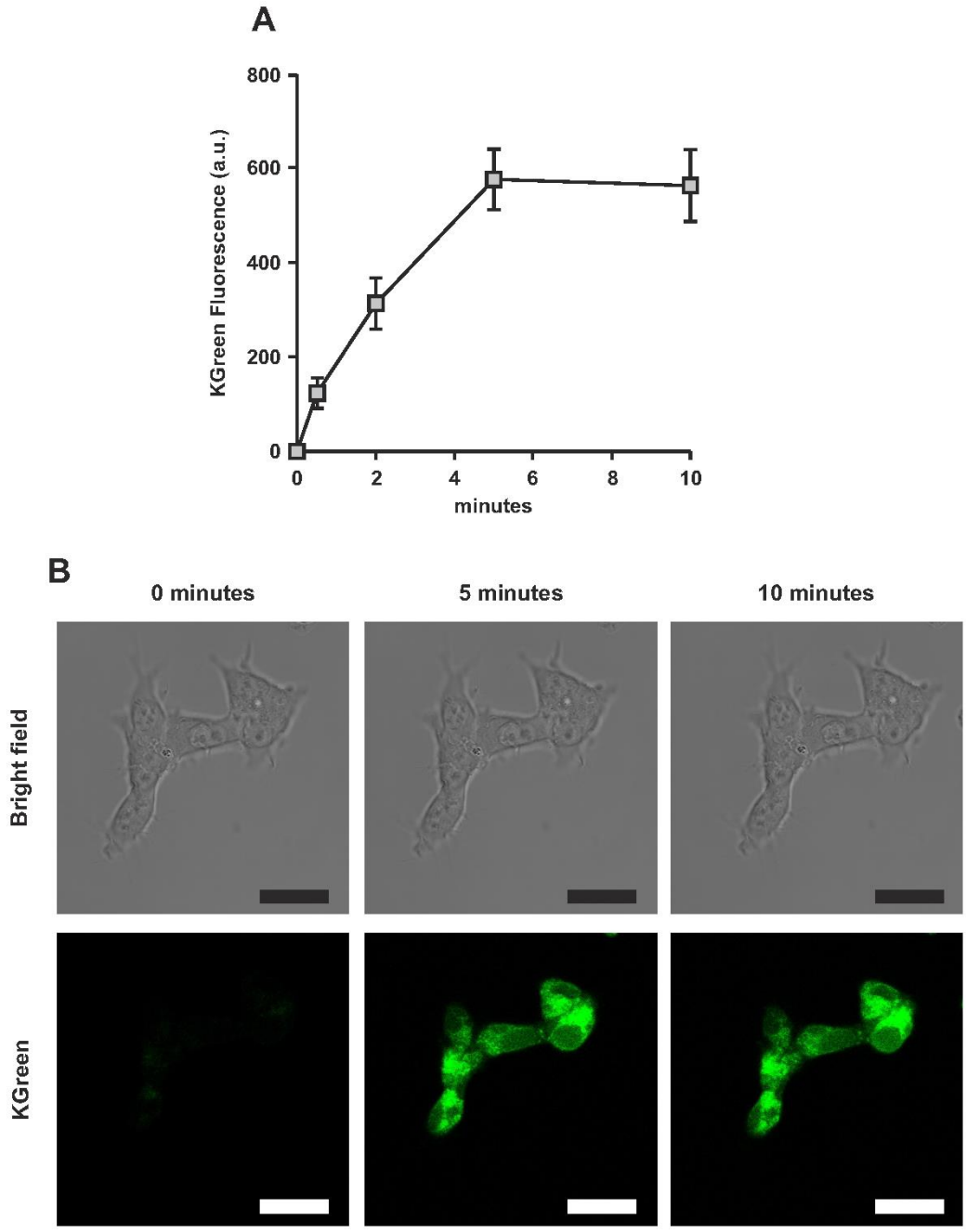

Figure 1.4. KGreen is efficiently taken up into HEK-293 cells. A) HEK-293 cells were incubated with 400 nM KGreen for the indicated time. KGreen fluorescence was detected by a Leica DMI6000 confocal microscopy and the intensity was determined analyzing the obtained images by Fiji software (n=13 +/- S.D.). **B)** Representative images obtained as described in A. Bright field and KGreen fluorescence are shown. Bars: 25 µm.

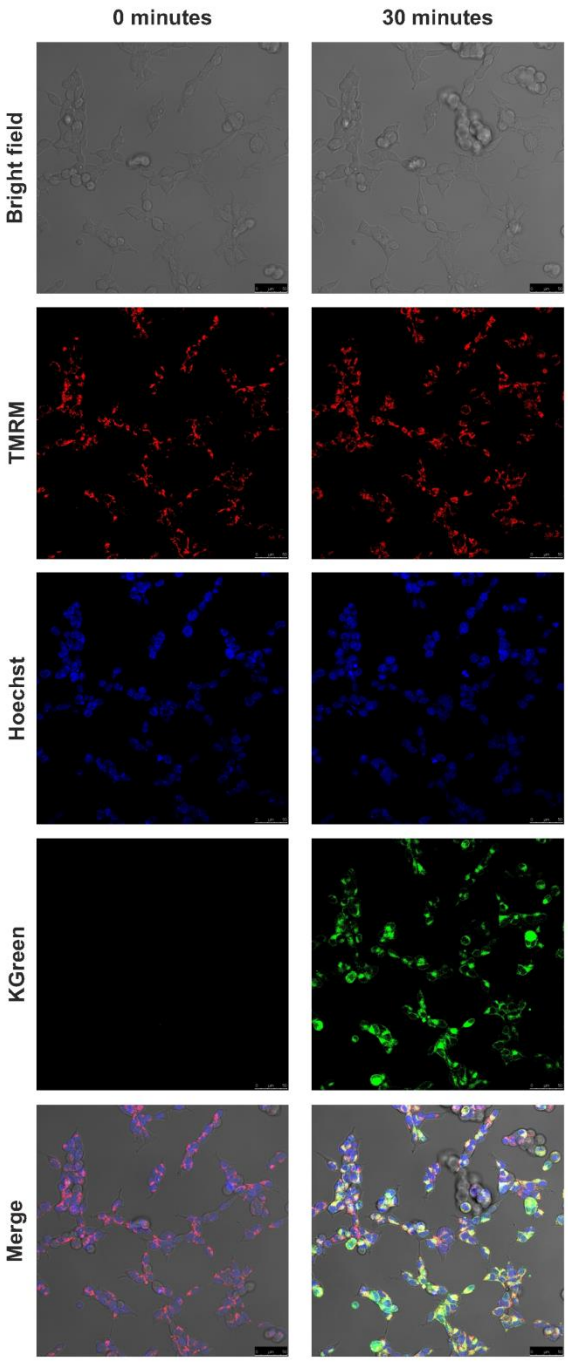

Figure 1.5. Mitochondrial membrane potential and nuclear morphology are not affected by incubation with KGreen. HEK-293 cells were incubated with 400 nM KGreen for 30 minutes. Mitochondrial membrane potential and nuclear morphology were evaluated by using 20 nM TMRM staining and 300 µg/ml Hoechst33342 staining, respectively. KGreen, TMRM, and Hoechst fluorescence were detected by confocal microscope (n=3). From the top of the figure: Bright field, TMRM, Hoechst, KGreen fluorescence and merged images are shown. Bars: 50 µm.

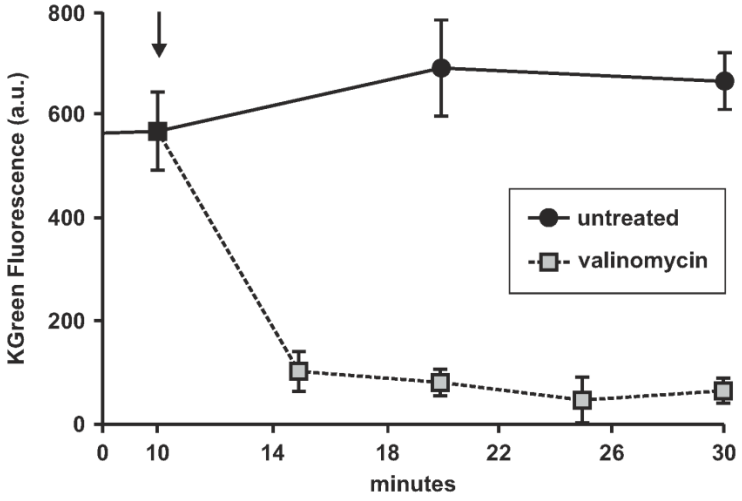

Figure 1.6. The potassium-selective ionophore valinomycin induces a decrease of the KGreen fluorescence signal. Cells were incubated with 400 nM KGreen for 10 minutes at 37°C and then were either left untreated or incubated with Valinomycin (10 μM, as indicated by the arrow) for further 30 minutes. KGreen fluorescence was detected as in figure 1. (n=13 +/- S.D.).

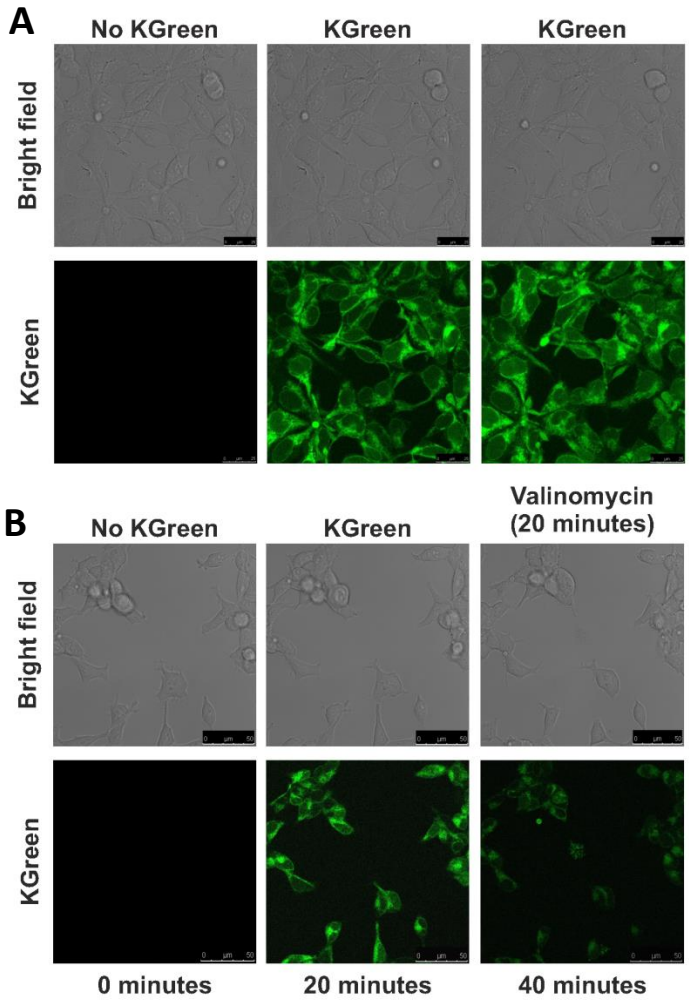

Figure 1.7. The potassium-selective ionophore valinomycin induces a decrease of the KGreen fluorescence signal. A) Representative images obtained of HEK-293 cells (untreated and incubated with 400 nM KGreen as in A, for 40 minutes). Bright field and KGreen fluorescence images are shown. Bars: 25 µm. **B)** Representative images obtained of HEK-293 cells incubated with 400 nM KGreen for 20 minutes and then treated with Valinomycin as in A. Bright field and KGreen fluorescence images are shown. Bars: 50 µm.

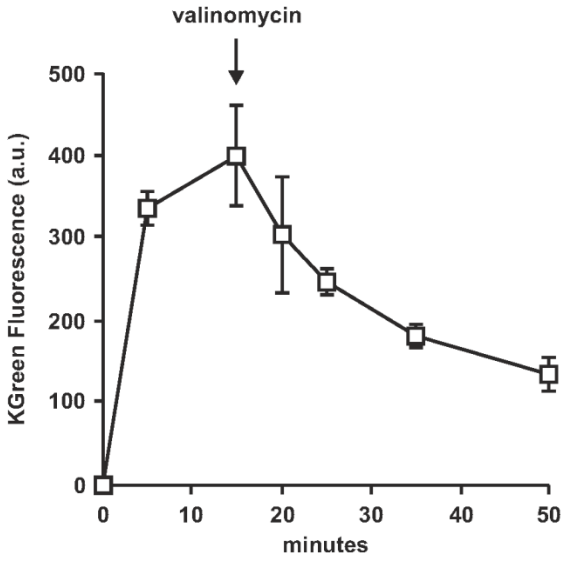

Figure 1.8. KGreen uptake study in Jurkat cells. Jurkat T lymphocytes were incubated with 400 nM KGreen for 15 min and then cells were incubated with Valinomycin (10 μM, as indicated by the arrow) for further 35 minutes. KGreen fluorescence was detected by FACS analysis and the median intensity of the fluorescence was determined (n=3 +/- S.D.).

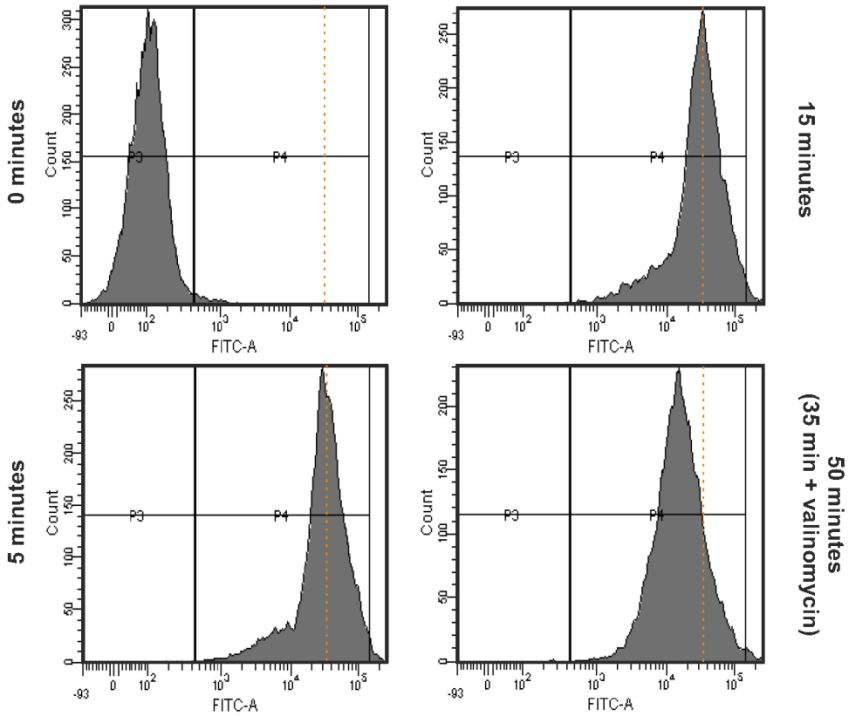

Figure 1.9. Flow cytometry study of KGreen cell uptake into Jurkat cells. Representative graphs obtained by FACS with Jurkat cells treated as described in A. Data were acquired at 0, 5, 15 minutes after addition of KGreen and after 35 minutes following application of 10 μM valinomycin (50 minutes total incubation time).

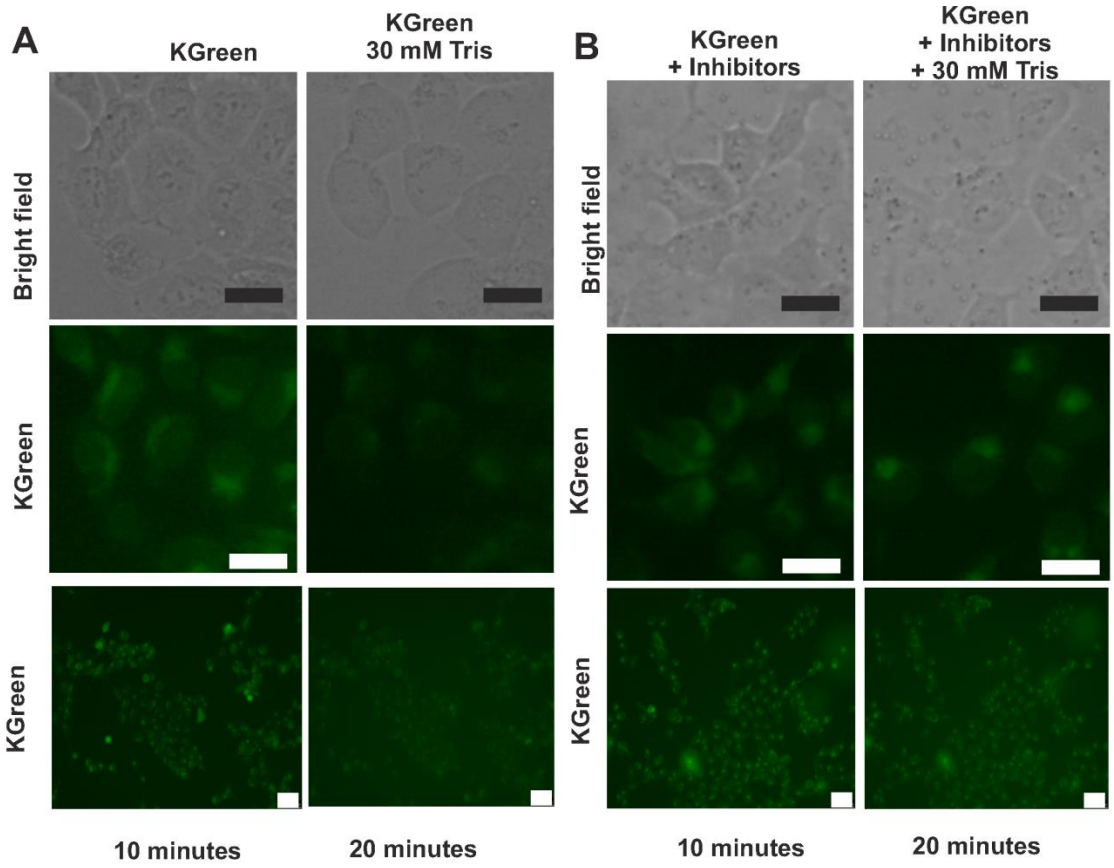

Figure 1.10. Decrease of KGreen fluorescence upon hypo-osmotic shock is prevented by pre-treatment with K^+ channel inhibitors. A) HEK-293 cells were incubated with 400 nM KGreen for 10 min and then were incubated with 30 mM Tris-HCl pH 7.4 for further 10 minutes. Bright field and KGreen fluorescence are shown. Bars: 25 μm. (n=3). Lower panels: bars 50 μm. **B)** HEK-293 cells were incubated with 400 nM KGreen for 5 min and then cells were pretreated for 5 more minutes with potassium channel inhibitors TEACl 5 mM + $GdCl_3$ 1 mM + $BaCl_2$ 5 mM. After pre-treatment, cells were incubated in 30 mM Tris-HCl pH 7.4 supplemented with the previously indicated potassium blockers for further 10 minutes. Bright field and KGreen fluorescence images are shown. Bars: 25 μm. (n=3). Lower panels: bars 50 μm.

Chapter 2

Design, synthesis, and application of a ratiometric K^+ probe for measuring intracellular K^+ level in living cells

Portions of this work were performed in collaboration with the following persons:

Dr. Cheri Ackerman and Tyler Detomasi helped generate ICP-MS data for measuring resting K^+ level in various cell lines (Figure 2.6,2.7)

2.1 Introduction

Potassium ions (K^+) are among the most abundant metal ions in the human body.[1,2] Potassium ion regulation of cellular osmolality and potential contributes to many physiological processes, including neuron firing[3–5], muscle contraction[6,7], and hormone regulation[8–10]. Cellular potassium homeostasis is maintained by membrane K^+ channels and pumps, giving physiological K^+ concentrations ranging from 5 mM (extracellular) to 150 mM (intracellular). Elevation or depletion of intracellular K^+ caused by the malfunction of K^+ channels or pumps can lead to various diseases including diabetes, arrhythmia, heart disorders, and epilepsy.[11,12] K^+ channels have been intensively studied for the past few years and the overexpression of K^+ channels is implicated in various cancer models.[12–17] However, these studies are hindered by the limitations of existing tools for studying K^+ dynamics in live cells.

Fluorescent sensors are non-invasive, high signal-to-noise tools that can accurately map a variety of biological analytes. While small-molecule fluorescent sensors for potassium have been developed, these sensors suffer various shortcomings which hamper their utilization for the visualization of intracellular potassium in biological samples. [18–27] The first potassium probe, termed PBFI (potassium benzofuran isophthalic acid), was developed by Salim and co-workers. PBFI suffers from slow cellular uptake kinetics due to its high molecular weight.[28] Verkman and other research groups have successfully developed several extracellular potassium sensors based on a triaza-cryptand potassium ionophore.[23,29–32] These potassium sensors have extremely high binding affinities and selectivity of potassium over sodium. However, they are not suitable for intracellular potassium studies due to the high binding affinity value. (Scheme 2.1) Also, the poor-yielding, multistep synthesis of triaza-cryptand makes further modification and functionalization of these sensors difficult.

Our potassium ion sensor design described in chapter one features lariat-ether modified crown ethers[20,33,34] as potassium ionophores with decreased binding affinity compared to Verkman's cryptand ionophores. The binding affinity of our sensor (KGreen) is calculated to be around 37 mM which roughly matches intracellular potassium level. Although KGreen shows desired photo-properties and has been utilized in live cell K^+ imaging as a fluorescent sensor with turn-on response, KGreen suffers two key disadvantages. Since the observed fluorescence intensity of KGreen is based on the quantity of K^+-bound fluorophore, it is not only influenced by intracellular K^+ concentration but also by intracellular KGreen concentration, making our readout based on relative rather than absolute K^+ concentration changes. Moreover, KGreen can detect dynamic K^+ flux within the same cells, but may not be useful in detecting or comparing K^+ levels in different cell lines since intracellular delivery of KGreen may vary among cell types. Inspired by previous work on ratiometric zinc sensors[35], we have sought to address these flaws by introducing a ratiometric readout which enables internal self-calibration through a conjugated standard fluorophore. Ratiometric calibration minimizes interference arising from analyte-independent phenomena such as sample thickness,

heterogeneity, and variations in light intensity, and also enables quantitative readout of K^+ levels among cell lines.[36]

In this chapter, we report the design, synthesis, and biological evaluation of a first-generation ratiometric fluorescent probe for K^+ composed of a dual fluorophore system. Specifically, potassium ratiometric probe 1 (KR-1) utilizes an ester linker that can be cleaved by cellular esterase to detach the standard fluorophore Coumarin 343.[35] This chemical modification strategy of converting a turn-on probe to a ratiometric probe is broadly applicable to a variety of fluorescent probes for different analytes as long as the emission spectrum of the turn-on probe does not overlap with that of the standard fluorophore. KR-1 demonstrates high selectivity and sensitivity to K^+ over competing biologically relevant metals and is able to monitor intracellular K^+ fluxes. Moreover, the ratiometric readout of this probe also facilitates comparative screening of K^+ levels across a variety of cell types, in particular identifying cancer cell types that possess higher resting concentrations of K^+.[13–15]

2.2 Methods

2.2.1. General synthetic and spectroscopic methods

Reactions using moisture- or air-sensitive reagents were carried out in flame-dried glassware under an inert atmosphere of N_2. Solvent was passed over activated alumina and stored over activated 3Å molecular sieves before use when dry solvent was required. All other commercially purchased chemicals were used as received (without further purification). SiliCycle 60 F254 silica gel (pre-coated sheets, 0.25 mm thick) were used for analytical thin layer chromatography and visualized by fluorescence quenching under UV light. Silica gel P60 (SiliCycle) was used for column chromatography. ^{1}H and ^{13}C NMR NMR spectra were collected at 298 K in CDCl3 or CD3OD (Cambridge Isotope Laboratories, Cambridge, MA) at 25 °C on Bruker AVQ-400, AVB-400, AV-500, or AV-600 at the College of Chemistry NMR Facility at the University of California, Berkeley or on Bruker 900 at the QB3 Central California 900 MHz NMR Facility. All chemical shifts are reported in the standard notation of δ parts per million relative to residual solvent peak at 7.26 ($CDCl_3$) or 3.31 (CD_3OD) for ^{1}H and 77.16 ($CDCl_3$) or 49.00 (CD_3OD) for ^{13}C as an internal reference. Splitting patterns are indicated as fol-lows: br, broad; s, singlet; d, doublet; t, triplet; m, multiplet; dd, doublet of doublets. Low-resolution electrospray mass spectral analyses were carried out using a LC-MS (Agilent Technology 6130, Quadrupole LC/MS and Advion expression-L Compact Mass Spectrometer). High-resolution mass spectral analyses (ESI-MS) were carried out at the College of Chemistry Mass Spectrometry Facility at the University of California, Berkeley.

9-(4-(1,4,7,10,13-pentaoxa-16-azacyclooctadecan-16-yl)-3-(2-methoxyethoxy)phenyl)-3-oxo-3H-xanthen-6-yl trifluoromethanesulfonate (1). Compound **1** (20.0 g, 51.7 mmol), 2-(2-(2-chloroethoxy)ethoxy)ethan-1-ol (12.0 mL, 77.5 mmol), potassium carbonate (35.8 g, 250 mmol), and potassium iodide (17.1 g, 103 mmol) were suspended in dry DMF (80 mL) and heated to 70 °C while stirring under nitrogen. After 24 h, the reaction was poured into brine (700 mL), and the mixture was extracted with ethyl acetate (3 × 200 mL). The combined organic layers were

dried over sodium sulfate, filtered, and concentrated via rotary evaporation. The crude residue was purified by column chromatography (silica gel, 30-100% EtOAc in hexanes) to afford **3** as a transparent, yellow oil (26.0 g, 50.0 mmol, 97%). ^{1}H NMR (400 MHz, $CDCl_3$): δ 8.28 (d, 2H, *J* = 8.8 Hz), 7.84 (d, 2H, *J* = 9.2 Hz), 7.21 (d, 1H, *J* = 8.4 Hz), 7.09 (dd, 1H, *J* = 8.4, 2.0 Hz), 6.91 (d, 1H, *J* = 2.0 Hz), 3.71-3.66 (m, 3H), 3.56-3.51 (m, 8H), 3.35 (s, 3H). ^{13}C NMR (101 MHz, $CDCl_3$): δ 156.46, 149.93, 145.99, 134.71, 128.82, 125.07, 124.30, 123.97, 123.76, 115.57, 72.54, 70.42, 69.08, 61.84, 55.35, 49.43. LRMS calcd. for $C_{35}H_{40}F_3NO_{12}S$ $[M + H]^+$ 755.76; found: 755.70.

tert-butyl 4-(9-(4-(1,4,7,10,13-pentaoxa-16-azacyclooctadecan-16-yl)-3-(2-methoxyethoxy)phenyl)-3-oxo-3H-xanthen-6-yl)piperazine-1-carboxylate (2). Compound **2** (26.0 g, 50 mmol) and triethylamine (41 mL, 300 mmol) were dissolved in methylene chloride (200 mL) and cooled to 0 °C while stirring. Tosyl chloride (19.0 g, 100 mmol) was added, and the reaction was allowed to warm to ambient temperature while stirring. After 24 h, the reaction was concentrated via rotary evaporation, and the resulting residue was purified by column chromatography (silica gel, 25% EtOAc in hexanes to 10% MeOH in EtOAc) to afford **4** as a tan solid (28.0 g, 42 mmol, 84%). ^{1}H NMR (400 MHz, $CDCl_3$): δ 8.35 (d, 2H, *J* = 8.2 Hz), 7.91 (d, 2H, *J* = 6.8 Hz), 7.83 (d, 2H, *J* = 8.4 Hz), 7.46 (d, 2H, *J* = 8.0 Hz), 7.24 (d, 1H, *J* = 8.0 Hz), 7.17-7.13 (m, 2H), 4.15 4.17-4.14 (m, 2H), 3.62 (t, 2H, *J* = 4.4 Hz), 3.43-3.40 (m, 8H), 3.41 (s, 3H), 2.47 (s, 3H). ^{13}C NMR (101 MHz, $CDCl_3$): δ 164.25, 157.24, 152.89, 152.51, 141.87, 139.99, 137.24, 135.91, 134.98, 132,44, 131.21, 130.74, 130.39, 124.57, 122.88, 67.21, 62.46, 56.49, 28.01, 20.85.

9-(4-(1,4,7,10,13-pentaoxa-16-azacyclooctadecan-16-yl)-3-(2-methoxyethoxy)phenyl)-6-(piperazin-1-yl)-3H-xanthen-3-one (3). *Tert*-butyl 4-amino-3-methoxybenzoate (2.2 g, 9.9 mmol) was dissolved in a 2:1 mixture of methylene chloride/pyridine (75 mL) and cooled to 0 °C. Nosyl chloride (4.0 g, 18.0 mmol) was dissolved in a 2:1 mixture of methylene chloride/pyridine (75 mL) was added dropwise over 30 min while stirring. The reaction was allowed to warm to ambient temperature for 1 h and then poured into dilute sulfuric acid (1 N, 700 mL, 0 °C) in a separatory funnel. The mixture was extracted with methylene chloride (3 × 200 mL), and the combined organic layers were washed with water (100 mL) and brine (200 mL). The washed organic phase was dried over sodium sulfate, filtered, and then concentrated via rotary evaporation. The crude residue was purified by column chromatography (silica gel, 20% EtOAc in hexanes) to afford **1** as a pale yellow powder (3.0 g, 7.4 mmol, 74%). ^{1}H NMR (600 MHz, $CDCl_3$): δ 8.18 (d, 2H, *J* = 8.4 Hz), 7.95 (d, 2H, *J* = 9.0 Hz), 7.70 (s, 1H), 7.49 (s, 2H), 7.34 (s, 1H), 3.67 (s, 3H), 1.48 (s, 9H). ^{13}C NMR (101 MHz, $CDCl_3$): δ 164.75, 150.09, 148.86, 144.58, 128.76, 128.42, 124.06, 122.62, 119.56, 81.22, 55.78, 27.92.

methyl 2-(4-(9-(4-(1,4,7,10,13-pentaoxa-16-azacyclooctadecan-16-yl)-3-(2-methoxyethoxy)phenyl)-3-oxo-3H-xanthen-6-yl)piperazin-1-yl)acetate (4). Compound **3** (6.8 g, 10.1 mmol), Compound **4** (4.1 g, 10.1 mmol), potassium carbonate (5.6 g, 41 mmol), and potassium iodide (3.4 g, 20 mmol) were suspended in dry DMF (40 mL) and heated to 70 °C while stirring under nitrogen. After 24 h, the reaction was poured into brine (600 mL), and the mixture was extracted with ethyl acetate (3 × 100 mL). The combined organic layers were dried over sodium sulfate, filtered, and concentrated via rotary evaporation. The crude residue was

passed through a silica plug (100 g, 10% MeOH in EtOAc), filtered, and concentrated to afford **5** as a foamy yellow solid (9.0 g, 98%). ^{1}H NMR (400 MHz, $CDCl_3$): δ 8.29-8.26 (m, 4H), 7.87-7.82 (m, 4H), 7.59 (dd, 1H, *J* = 8.0, 1.6 Hz), 7.41 (d, 1H, *J* = 1.6 Hz), 7.37 (d, 1H, *J* = 8.0 Hz), 7.171 (d, 1H, *J* = 8.0 Hz), 7.08 (dd, 1H, *J* = 8.4, 2.0 Hz), 6.92 (d, 1H, *J* = 2.0 Hz), 3.54-3.43 (m, 12H), 3.40 (s, 3H), 3.36 (s, 3H), 1.59 (s, 9H). ^{13}C NMR (101 MHz, $CDCl_3$): δ 166.42, 147.65, 145.88, 141.95, 137.27, 124.21, 123.71, 119.45, 112.76, 110.76, 109.81, 107.97, 107.79, 79.96, 70.36, 70.33, 69.58, 69.47, 55.63, 55.47, 43.18, 42.73, 28.36. HRMS-ESI calculated for $C_{37}H_{41}BrN_4O_{14}S_2Na$ [M + Na^+]: 931.1142; found: 931.1183.

Krhodol (5). Compound **5** (4.5 g, 5.0 mmol), thiophenol (3.5 mL, 35 mmol), and potassium carbonate (7.0 g, 50 mmol) were suspended in DMF (70 mL) and stirred at ambient temperature. After 2 h, the reaction was poured into brine (700 mL), and the mixture was extracted with ethyl acetate (3 × 100 mL). The combined organic layers were dried over sodium sulfate, filtered, and concentrated via rotary evaporation. The crude residue was purified by column chromatography (silica gel, 20-40% EtOAc in hexanes) to afford **6** as a light yellow powder (23 mg, 0.24 mmol, 78%). ^{1}H NMR (400 MHz, $CDCl_3$): δ 7.56 (dd, 1H, *J* = 8.3, 2.0 Hz), 7.36 (s, 1H), 6.95 (dd, 1H, *J* = 8.5, 2.0 Hz), 6.83 (d, 1H, *J* = 2.0 Hz), 6.53-6.47 (m, 2H), 3.84 (s, 3H), 3.79 (s, 3H), 3.74 (t, 4H, *J* = 5.0 Hz), 3.67 (s, 4H), 3.37 (t, 2H, *J* = 5.5 Hz), 3.29 (t, 2H, *J* = 5.5 Hz), 1.57 (s, 9H). ^{13}C NMR (101 MHz, $CDCl_3$): δ 166.01, 147.32, 145.55, 141.72, 137.07, 123.97, 123.42, 119.03, 112.40, 110.36, 109.49, 107.48, 79.50, 70.02, 69.98, 69.22, 69.10, 55.27, 55.12, 42.83, 42.40, 28.07. HRMS-ESI calculated for $C_{25}H_{36}BrN_2O_6$ [M + H^+]: 739.1757; found: 739.1764.

***KR-1* (6).** Compound **6** (23 mg, 0.24 mmol) and glycoyl chloride (0.23 mL, 1.90 mmol) were separately dissolved in anhydrous benzene (50 mL) under nitrogen. Using two syringe pumps (KDS-100, KD Scientific), the two solutions were added dropwise over 24 h to a stirring solution of anhydrous pyridine (1.5 mL, 19 mmol) and anhydrous benzene (1.0 L) in a flame-dried, three-neck round bottom flask under nitrogen. After completion of addition, the reaction was heated to reflux while stirring under nitrogen. After 16 h, the solvent was removed via rotary evaporation, and the crude residue was purified by column chromatography (basic alumina, 0-5% MeOH in CH_2Cl_2) to afford **7** as a foamy orange oil (13 mg, 0.16 mmol, 36%). ^{1}H NMR (400 MHz, $CDCl_3$): δ 8.29-8.26 (m, 4H), 7.87-7.82 (m, 4H), 7.59 (dd, 1H, *J* = 8.0, 1.6 Hz), 7.41 (d, 1H, *J* = 1.6 Hz), 7.37 (d, 1H, *J* = 8.0 Hz), 7.171 (d, 1H, *J* = 8.0 Hz), 7.08 (dd, 1H, *J* = 8.4, 2.0 Hz), 6.92 (d, 1H, *J* = 2.0 Hz), 3.54-3.43 (m, 12H), 3.40 (s, 3H), 3.36 (s, 3H), 1.59 (s, 9H). ^{13}C NMR (101 MHz, $CDCl_3$): δ 166.42, 147.65, 145.88, 141.95, 137.27, 124.21, 123.71, 119.45, 112.76, 110.76, 109.81, 107.97, 107.79, 79.96, 70.36, 70.33, 69.58, 69.47, 55.63, 55.47, 43.18, 42.73, 28.36. HRMS-ESI calculated for $C_{37}H_{41}BrN_4O_{14}S_2Na$ [M + Na^+]: 931.1142; found: 931.1183

2.2.2. Spectroscopic Materials and Methods

All aqueous buffers were prepared using Millipore water. Krhodol were aliquoted into polypropylene PCR tubes (50 nmol per tube), vacuum-dried in a dessicator, and stored in a –20 °C freezer for preservation. Aliquots were reconstituted in DMSO (20 μL for a stock concentration of 1 mM) prior to diluting into aqueous buffer to a final concentration of 2 μM). Molar extinction coefficients (ε) were calculated from the slope of the best-fit line correlating absorbance (at λ_{max}) with sensor concentration. For the fluorescence profiles and binding curves,

sodium sensor was diluted into aqueous HEPES (50 mM, pH 7.4) with metal (M = Na^+ or K^+ such that $[Na + K]_{tot}$ = 200 mM). Fluorescence spectra were recorded at varying K/Na ratios. The fold turn-on was calculated as the response to 200 mM KCl *versus* 200 mM NaCl, and the apparent dissociation constant (K_d) was calculated according to Equation 1, where F is the observed fluorescence, F_{max} is the fluorescence response to 200 mM potassium, and F_{min} is the fluorescence response to 200 mM potassium:

$$\frac{(F - F_{min})}{(F_{max} - F_{min})} = \frac{[K^+]}{[K^+] + K_d} \quad (1)$$

The sodium concentration corresponding to half the fold turn-on from the fit at $[Na^+]$ = 135 mM was taken as the K_d.

For metal selectivity, HEPES buffer (50 mM, pH 7.4) was charged with Krhodol (2 μM), then competing metal, and then potassium. The fluorescence response was recorded after each addition and normalized to the response to dye only. The following concentrations of competing metals were used: 150 mM (Na^+), 1-5 mM (Li^+, Ca^{2+}, Mg^{2+}), 50-100 μM (transition metals).

2.2.3. Preparation and staining of cell cultures

All cells were maintained at exponential growth as a monolayer in Dulbeco's Modified Eagle Medium (DMEM, Invitrogen). Cells were supplemented with 10% fetal bovine serum (FBS, Hyclone) and incubated at 37 °C in 5% CO_2. Cells were plated in phenol red-free medium on borosilicate chamber slides (Nunc) and allowed to grow to 60% confluence 1 d prior to imaging. Cells were stained by incubating a 10 μM solution of KR-1 in DMEM for 20 min. For the gramicidin sodium calibration, the DMEM media was exchanged out for phosphate buffered metal solution (PBM, pH 7.4, M = Na or K such that $[Na + K]_{tot}$ = 160 mM) containing 2-10 μM gramicidin (Invitrogen). The cells were allowed to equilibrate in the new media for 15 min prior to imaging.

2.2.4. Confocal image method

Microscopy experiments were performed on a Zeiss laser scanning microscope (model 710) equipped with a 40x water objective lens and 2010 Zeiss software (Carl Zeiss). Cells were imaged in a 37 °C stage incubator connected to 5% CO_2 gas inlet to buffer the media. The focal plane with the highest fluorescence was selected for each field of cells. Fields of cells were sampled from the bright field images only.

2.3. Results and discussion

2.3.1. Design and synthesis of K^+ responsive

Our design of KR-1 is composed of a K^+ responsive moiety linked to a standard fluorophore for ratiometric calibration. The K^+ responsive moiety was designed to be a turn-on

fluorescent sensor that responds sensitively to intracellular K^+. To achieve this, it is necessary that the equilibrium dissociation constant (K_d) of the sensor be roughly equivalent to the intracellular K^+ concentration (150 mM). We thus chose a lariat ether modified aza-crown ether to be the ionophore of the K^+ responsive moiety. This structure is shown to have a weaker binding affinity for K^+ compared to cryptand and G-quadruplex ionophores (Figure), which match intracellular K^+ concentration. As for the fluorophore, we chose a rhodol-based structure since it has been used in multiple probe designs and has shown advantageous properties such as high brightness and photostability.

The synthesis of this K^+ responsive moiety (K rhodol) is briefly described as follows: K rhodol was synthesized in 7 steps from crown ether derivative **1** (scheme). Lariat ether modified aza-crown ether **1** was synthesized using published procedures and then converted to xanthene **2** through a Vilsmeier-Haack reaction and resorcinol condensation. The hydroxyl on xanthene **2** was then converted to a triflate followed by Hartwig-Buchwald amination and deprotection to attach a piperazinyl group to yield **3**. Finally, a carboxylate group was attached to give K rhodol.

2.3.2. In vitro characterization of K rhodol.

With K rhodol in hand, its fluorescence response to K^+ was tested in aqueous buffer (50 mM HEPES, pH 7.4). K rhodol shows maximum absorption at 514 nm (Figure) with calculated absorption coefficients $\varepsilon_{([K^+]=0)} = 13800\ M^{-1}cm^{-1}$ and $\varepsilon_{([K^+]=200\ mM)} = 14980\ M^{-1}cm^{-1}$ and maximum emission at 552 nm (Figure). When exposed to K^+, K rhodol shows an increase in fluorescence emission. The K_d value of the probe was calculated to be 137 mM based on the K^+ titration response using a Benesi-Hildebrand plot (Figure S) which matches intracellular K^+ levels as expected.

We next evaluated the selectivity of K rhodol for K^+ compared to a panel of biologically relevant alkali, alkaline earth, and transition metals (Figure), confirming that K rhodol responds selectively to K^+. Notably, we were pleased to see that K rhodol showed greater than fivefold selectivity for K^+ over Na^+, a major competing monovalent cation present in cells, thus indicating the probe's adequate sensitivity for intracellular usage.

2.3.3. Design and synthesis of KR-1.

To achieve the function of a ratiometric probe, we envisioned attaching a second fluorophore to our K rhodol K^+ sensor. Based on the design of the zinc probe (name reference), we chose coumarin 343 as the standard fluorophore since coumarins are nonresponsive toward K^+. Coumarin 343 is linked to K rhodol via an ester bond and PEG linker to make KR-1. After KR-1 is delivered into the cells, cellular esterase will cleave the ester bond to give two separate fluorophores, K rhodol as the K^+ responsive fluorophore and coumarin 343 as a K^+ non-responsive fluorophore, in a 1:1 ratio. And both of the fluorophores are cell-trappable. By assessing the ratio of emission profiles for K rhodol and coumarin 343 we can obtain a quantitative readout of intracellular K^+ concentration.

Synthesis of KR-1 requires 2 additional synthetic steps after the synthesis of K rhodol. Coumarin linker **6** is first synthesized based on literature procedures (reference). Esterification of **6** and K rhodol yielded KR-1 (scheme).

2.3.4. Application of KR-1 to imaging K^+ dynamics in live cells.

Given the ability of K rhodol to respond selectively to intracellular K^+ levels in aqueous buffer, we next examined its ability to read out changes of K^+ in living cells through ratiometric fluorescence imaging. The data establish that KR-1 is indeed able to visualize both increases and decreases in intracellular K^+ levels. HeLa cells were treated with 10 μM KR-1 for 3 h and then imaged. Both K rhodol fluorescence (Green channel) and coumarin fluorescence (Blue channel) were obtained and combined to give ratio images (Green/Blue ratio). HeLa cells were then treated with 5 μM valinomycin—a potassium-specific transporter—for 1 h or left in the same conditions as the control group. Valinomycin created artificial holes in cell membranes that led to decreases in intracellular K^+ levels. In particular, we observed a clear decrease in Green/Blue ratio intensity in the HeLa cells that were treated with valinomycin compared to the cells in the control group (Figure). Cells treated with valinomycin were shown to have decreased levels of intracellular K^+ by inductively coupled plasma mass spectrometry (ICP-MS; Figure SI), consistent with the interpretation that KR-1 is responding to decreased K^+ concentrations. Additionally, cell viability in both the absence and the presence of KR-1 was verified by propidium iodide staining, which confirmed that cell viability was not affected under these conditions (SI).

After verifying that KR-1 was able to detect decreases in K^+ levels, we examined the ability of KR-1 to detect increases in K^+ levels. HT29 cells are known to express significantly higher numbers of HERG potassium channels compared to other cancer cell lines such as HeLa and A549. So we envisioned that by incubating HT29 cells with astemizole—a HERG potassium channel blocker—and artificially elevated extracellular K^+, we could increase intracellular K^+ concentrations. We first incubated all three cell types (using HeLa and A549 as comparison cells) in 10 μM KR-1 for 3 hours. We then replaced this media with 5 μM astemizole and 30 mM K^+ in HEPES buffer and imaged cells after incubating for 1 hour. We observed an increase in Green/Blue ratio fluorescence in the HT29 cells compared to the control cell lines. The difference in K^+ concentration alterations in HT29, HeLa, and A549 cells after astemizole treatment was additionally confirmed by ICP-MS (Figure S), consistent with our imaging results.

2.3.5. KR-1 enables mapping of K^+ levels in different live cancer cells.

After establishing that KR-1 is capable of reading out variable concentrations of intracellular K^+, we sought to expand the application of KR-1 to map intracellular K^+ levels in different cancer cell types. Cancer cell lines are known to exhibit elevated K^+ channel expression and some studies have shown elevated intracellular K^+ levels in these cell lines. This might be caused by the increased proliferation rate of cancer cells and thus the need for higher levels of intracellular K^+. Despite the growing recognition of the importance of K^+ channels in cancer cell lines, the dynamics of K^+ flux remain insufficiently understood, in part due to a relative lack of tools for directly assaying intracellular K^+ levels in living specimens.

Given the ability of KR-1 to measure relative intracellular K^+ level in cells such as HeLa, A549, and HT29, we turned our attention to acquiring relative basal K^+ levels for a series of other cells. We incubated all the cells with KR-1 and imaged them to obtain ratio information. We observed that most cancer cell lines (with the exception of RKO) have increased intracellular K^+ level compared to noncancer cell lines (MCF-10A) which is consistent with our hypotheses. To

validate the readout of KR-1 we also conducted ICP-MS measurements of intracellular K^+ level for these cell lines (Figure S). The results showed similar patterns, confirming that cancer cells show elevated intracellular K^+ level.

2.4. Conclusion

To summarize, we have presented the design, synthesis, characterization, and biological application of KR-1, a novel first-generation chemical probe for ratiometric quantitation of intracellular K^+ concentration. KR-1 is composed of K rhodol as a turn-on K^+ responsive fluorophore and coumarin 343 as a K^+ nonresponsive fluorophore, both of which are released after cleavage of an intramolecular ester bond in KR-1 by cellular esterase. KR-1 can sensitively and specifically respond to K^+ at intracellular levels as well as report changes in intracellular K^+ levels. Moreover, due to its ratiometric response KR-1 can be used to assay basal K^+ levels in different cell lines. Excitingly, KR-1 has enabled access to previously inaccessible data concerning intracellular K^+ concentrations in live specimens.

2.5. Reference

(1) Palmer, B. F. Regulation Of Potassium Homeostasis. *Clin. J. Am. Soc. Nephrol.* **2014**, *10* (6), 1050–1060.

(2) D'Adamo, M. C.; Catacuzzeno, L.; Di Giovanni, G.; Franciolini, F.; Pessia, M. K+ Channelepsy: Progress in the Neurobiology of Potassium Channels and Epilepsy. *Front. Cell. Neurosci.* **2013**, *7* (September), 1–21.

(3) Baylor, D. A.; Nicholls, J. G. Changes in Extracellular Potassium Concentration Produced by Neuronal Activity in the Central Nervous System of the Leech. *J. Physiol.* **1969**, *203* (3), 555–569.

(4) Grace, A. A.; Bunney, B. S. The Control of Firing Pattern in Nigral Dopamine Neurons: Burst Firing. *J. Neurosci.* **1984**, *4* (11), 2877–2890.

(5) Fortin, D. L.; Banghart, M. R.; Dunn, T. W.; Borges, K.; Wagenaar, D. A.; Gaudry, Q.; Karakossian, M. H.; Otis, T. S.; Kristan, W. B.; Trauner, D.; et al. Photochemical Control of Endogenous Ion Channels and Cellular Excitability. *Nat. Methods* **2008**, *5* (4), 331–338.

(6) Juel, C. Potassium and Sodium Shifts during in Vitro Isometric Muscle Contraction, and the Time Course of the Ion-Gradient Recovery. *Pflgers Arch. Eur. J. Physiol.* **1986**, *406* (5), 458–463.

(7) Hudgins, P. M.; Weiss, G. B. DIFFERENTIAL EFFECTS OF CALCIUM REMOVAL UPON VASCULAR SMOOTH MUSCLE CONTRACTION INDUCED BY

NOREPINEPHRINE, HISTAMINE AND POTASSIUM. *J. Pharmacol. Exp. Ther.* **1968**, *159* (1).
(8) Storey, N. M.; O'Bryan, J. P.; Armstrong, D. L. Rac and Rho Mediate Opposing Hormonal Regulation of the Ether-A-Go-Go-Related Potassium Channel. *Curr. Biol.* **2002**, *12* (1), 27–33.
(9) Féraille, E.; Doucet, A. Sodium-Potassium-Adenosinetriphosphatase-Dependent Sodium Transport in the Kidney: Hormonal Control. *Physiol. Rev.* **2001**, *81* (1), 345–418.
(10) Bia, M. J.; DeFronzo, R. A. Extrarenal Potassium Homeostasis. *Am. J. Physiol.* **1981**, *240* (4), F257-68.
(11) Tian, C.; Zhu, R.; Zhu, L.; Qiu, T.; Cao, Z.; Kang, T. Potassium Channels: Structures, Diseases, and Modulators. *Chem. Biol. Drug Des.* **2014**, *83* (1), 1–26.
(12) Ge, L.; Hoa, N. T.; Wilson, Z.; Arismendi-Morillo, G.; Kong, X. T.; Tajhya, R. B.; Beeton, C.; Jadus, M. R. Big Potassium (BK) Ion Channels in Biology, Disease and Possible Targets for Cancer Immunotherapy. *Int. Immunopharmacol.* **2014**, *22* (2), 427–443.
(13) Urrego, D.; Tomczak, A. P.; Zahed, F.; Stühmer, W.; Pardo, L. A.; Stuehmer, W. Potassium Channels in Cell Cycle and Cell Proliferation. *Phil. Trans. R. Soc. B 2014* **2014**, No. February, 1–9.
(14) Felipe, A.; Vicente, R.; Villalonga, N.; Roura-Ferrer, M.; Martínez-Mármol, R.; Solé, L.; Ferreres, J. C.; Condom, E. Potassium Channels: New Targets in Cancer Therapy. *Cancer Detect. Prev.* **2006**, *30* (4), 375–385.
(15) Salyer, S. A.; Olberding, J. R.; Distler, A. A.; Lederer, E. D.; Clark, B. J.; Delamere, N. A.; Khundmiri, S. J. Vacuolar ATPase Driven Potassium Transport in Highly Metastatic Breast Cancer Cells. *Biochim. Biophys. Acta - Mol. Basis Dis.* **2013**, *1832* (10), 1734–1743.
(16) Huang, X.; Jan, L. Y. Targeting Potassium Channels in Cancer. *J. Cell Biol.* **2014**, *206* (2), 151–162.
(17) Wulff, H.; Castle, N. A.; Pardo, L. A. Voltage-Gated Potassium Channels as Therapeutic Targets. *Nat. Rev. Drug Discov.* **2009**, *8* (12), 982–1001.
(18) Fan, X.; Li, H.; Zhao, J.; Lin, F.; Zhang, L.; Zhang, Y.; Yao, S. A Novel Label-Free Fluorescent Sensor for the Detection of Potassium Ion Based on DNAzyme. *Talanta* **2012**, *89*, 57–62.
(19) Thibori, A.; Pierre, V. C. A Highly Selective Luminescent Sensor for the Time-Gated Detection of Potassium. *J. Am. Chem. Soc.* **2009**, *131* (2), 434–435.
(20) Ast, S.; Schwarze, T.; Müller, H.; Sukhanov, A.; Michaelis, S.; Wegener, J.; Wolfbeis, O. S.; Körzdörfer, T.; Dürkop, A.; Holdt, H. J. A Highly K+-Selective Phenylaza-[18]crown-6-Lariat-Ether-Based Fluoroionophore and Its Application in the Sensing of K+ Ions with an Optical Sensor Film and in Cells. *Chem. - A Eur. J.* **2013**, *19* (44), 14911–14917.
(21) He, H.; Mortellaro, M. A.; Leiner, M. J. P.; Fraatz, R. J.; Tusa, J. K. A Fluorescent Sensor with High Selectivity and Sensitivity for Potassium in Water. *J. Am. Chem. Soc.* **2003**, *125* (6), 1468–1469.
(22) Kong, X.; Su, F.; Zhang, L.; Yaron, J.; Lee, F.; Shi, Z.; Tian, Y.; Meldrum, D. R. A Highly Selective Mitochondria-Targeting Fluorescent K+Sensor. *Angew. Chemie - Int. Ed.* **2015**, *54* (41), 12053–12057.
(23) Sui, B.; Yue, X.; Tichy, M. G.; Liu, T.; Belfield, K. D. Improved Synthesis of the Triazacryptand (TAC) and Its Application in the Construction of a Fluorescent TAC-BODIPY Conjugate for K+ Sensing in Live Cells. *European J. Org. Chem.* **2015**, *2015*

(6), 1189–1192.
(24) Akenaka, S. T.; Uskowiak, B. J. Fluorescence Detection of Potassium Ion Using the G-Quadruplex Structure. **2011**, *27* (December).
(25) Nagatoishi, S.; Nojima, T.; Juskowiak, B.; Takenaka, S. A Pyrene-Labeled G-Quadruplex Oligonucleotide as a Fluorescent Probe for Potassium Ion Detection in Biological Applications. *Angew. Chemie* **2005**, *117* (32), 5195–5198.
(26) He, F.; Tang, Y.; Wang, S.; Li, Y.; Zhu, D. Fluorescent Amplifying Recognition for DNA G-Quadruplex Folding with a Cationic Conjugated Polymer: A Platform for Homogeneous Potassium Detection. *J. Am. Chem. Soc.* **2005**, *127* (35), 12343–12346.
(27) Swiatkowska, A.; Juskowiak, B. Effect of Cholesterol Anchoring Group on the Properties of G-Quadruplex-Based FRET Probes for Potassium Ion. *Chemosensors* **2014**, *2* (4), 267–286.
(28) Meuwis, K.; Boens, N.; De Schryver, F. C.; Gallay, J.; Vincent, M. Photophysics of the Fluorescent K+ Indicator PBFI. *Biophys. J.* **1995**, *68* (6), 2469–2473.
(29) Carpenter, R. D.; Verkman, A. S. Function-Oriented Synthesis of a Didesmethyl Triazacryptand Analogue for Fluorescent Potassium Ion Sensing. *European J. Org. Chem.* **2011**, No. 7, 1242–1248.
(30) Padmawar, P.; Yao, X.; Bloch, O.; Manley, G. T.; Verkman, A. S. K+waves in Brain Cortex Visualized Using a Long-Wavelength K+-Sensing Fluorescent Indicator. *Nat. Methods* **2005**, *2* (11), 825–827.
(31) Namkung, W.; Padmawar, P.; Mills, A. D.; Verkman, A. S. Cell-Based Fluorescence Screen for K+ Channels and Transporters Using an Extracellular Triazacryptand-Based K+ Sensor. *J. Am. Chem. Soc.* **2008**, *130* (25), 7794–7795.
(32) Han, Y.; Jiang, Y.; Chen, C. F. Cryptand-Based Hosts for Organic Guests. *Tetrahedron* **2015**, *71* (4), 503–512.
(33) Schultz, R. A.; White, B. D.; Dishone, D. M.; Arnold, K. A.; Gokel, G. W. 12-, 15-, and 18-Membered-Ring Nitrogen-Pivot Lariat Ethers: Syntheses, Properties, and Sodium and Ammonium Cation Binding Properties1-. *J. Am. Chem. Soc.* **1985**, *107* (23), 6659–6668.
(34) Gokel, G. W.; Barbour, L. J.; Ferdani, R.; Hu, J. Lariat Ether Receptor Systems Show Experimental Evidence for Alkali Metal Cation-Pi Interactions. *Acc. Chem. Res.* **2002**, *35* (10), 878–886.
(35) Woodroofe, C. C.; Lippard, S. J. A Novel Two-Fluorophore Approach to Ratiometric Sensing of Zn2+. *J. Am. Chem. Soc.* **2003**, *125* (38), 11458–11459.
(36) Gee, K. R.; Archer, E. A.; Lapham, L. A.; Leonard, M. E.; Zhou, Z. L.; Bingham, J.; Diwu, Z. New Ratiometric Fluorescent Calcium Indicators with Moderately Attenuated Binding Affinities. *Bioorganic Med. Chem. Lett.* **2000**, *10* (14), 1515–1518.

Figures

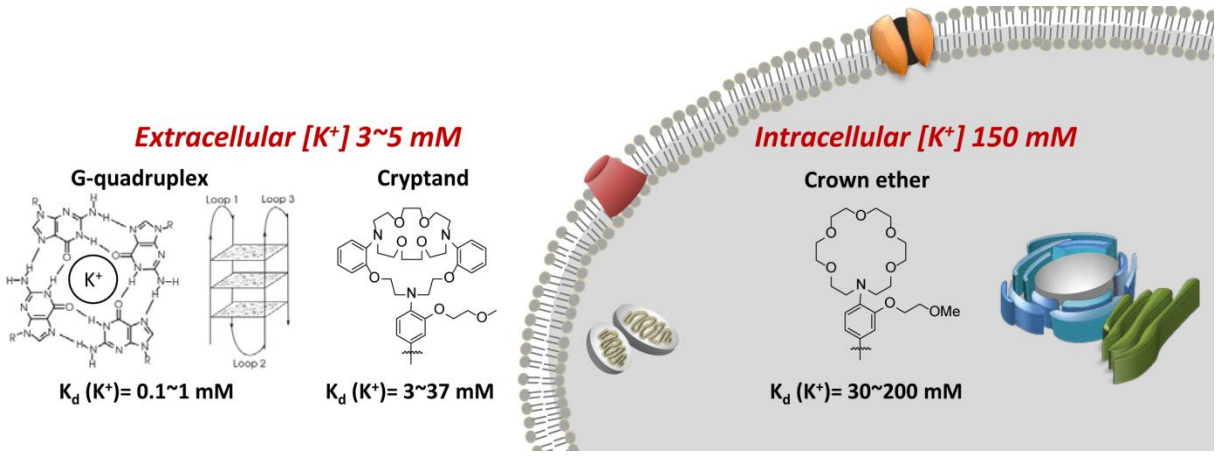

Scheme 2.1. Various K^+ ionophores and their K_d value

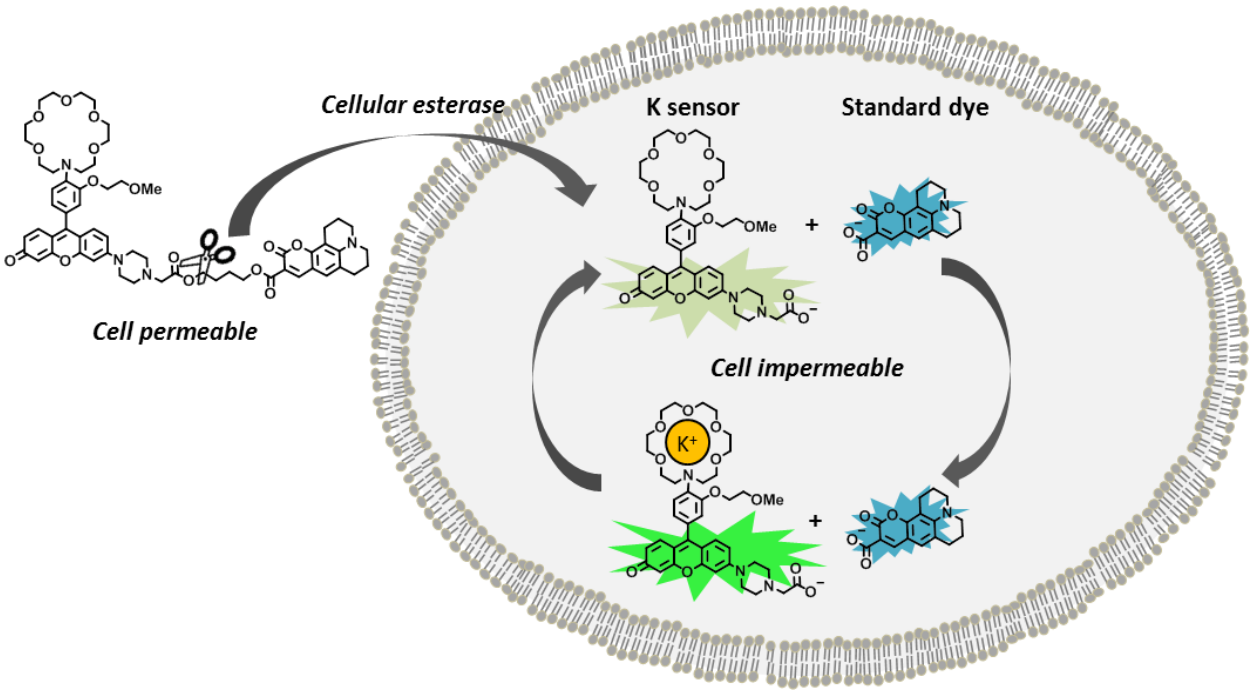

Scheme 2.2. Design of ratiometric potassium Probe (KR-1).

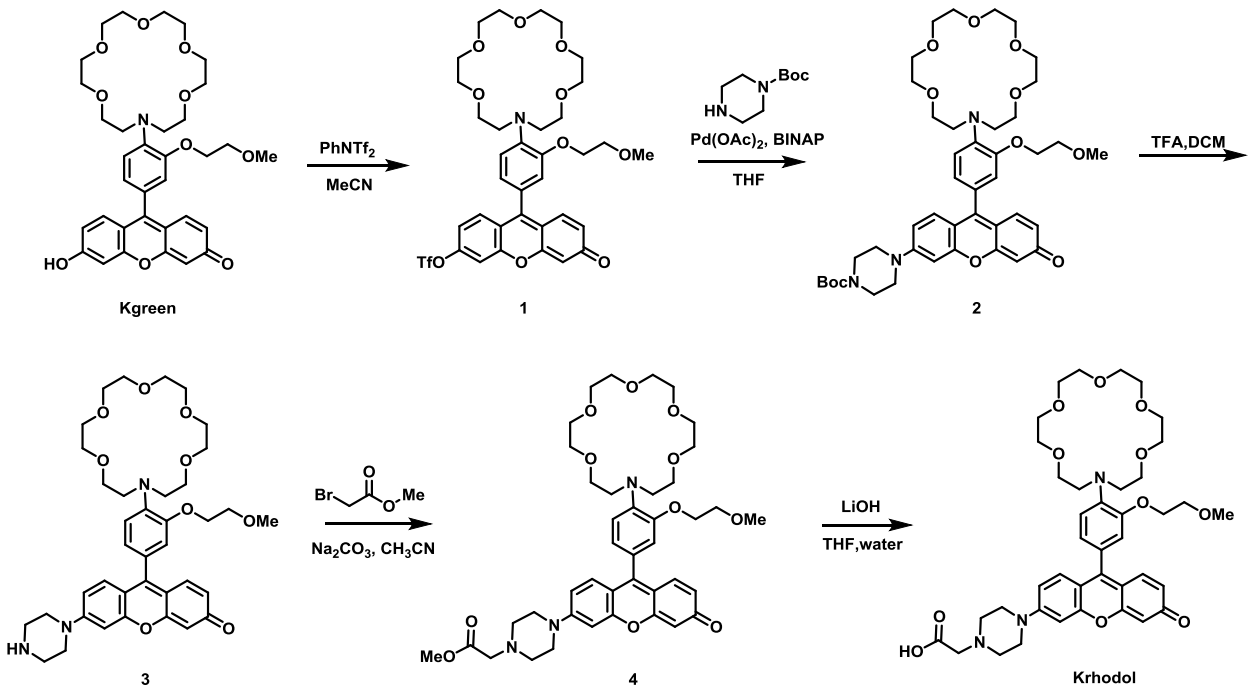

Scheme 2.3. Synthesis of intermediate, turn-on probe K rhodol

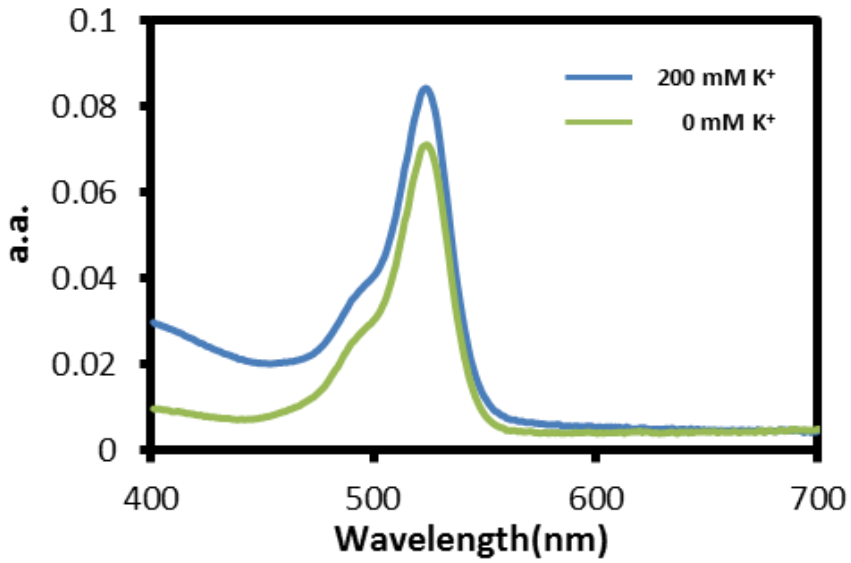

Figure 2.1. UV-Visible spectra of Krhodol. Spectra were obtained in 50 mM HEPES (pH 7.4) with 2 µM Krhodol (solid) and after treatment with 200 mM K^+

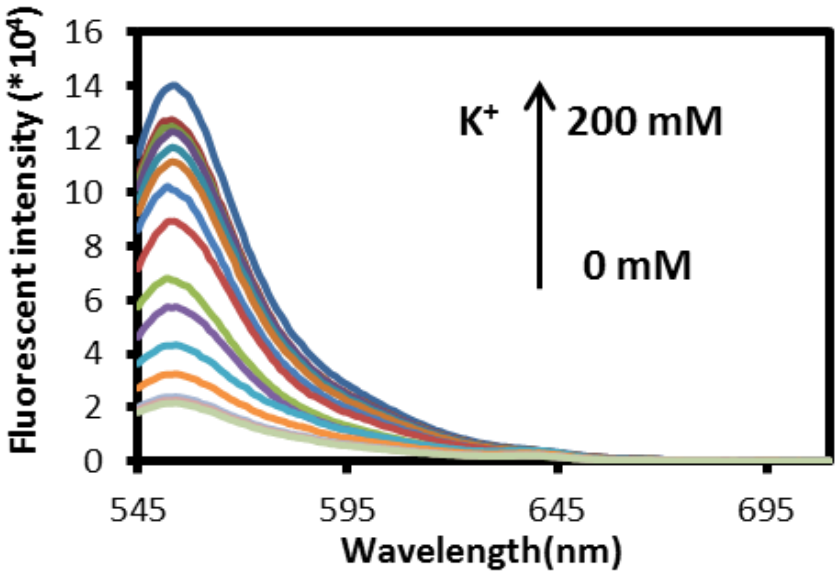

Figure 2.2. (a) Fluorescence intensity of 2 μM Krhodol with titration of K^+ (0, 15, 30, 45, 60, 75, 90, 105, 120, 135, 150, 175, 200 mM K^+ balanced by Na^+) Spectra were acquired in 50 mM HEPES (pH 7.4) when monitoring intensity at λ_{ex} = 525 nm, collecting emission between 545 – 700 nm.

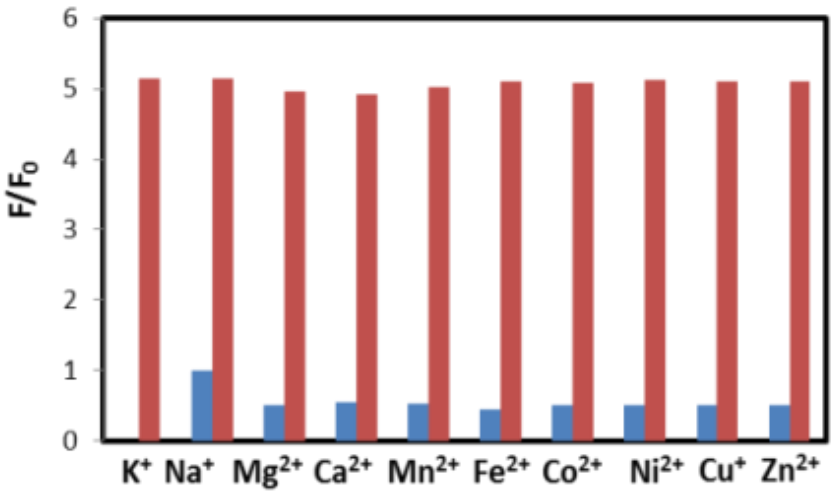

Figure 2.3. Fluorescence response of 2 μM Krhodol to biologically relevant d-block (10 μM) and s-block (1 mM) metals except for Na^+ (150 mM). Spectra were acquired in 50 mM HEPES (pH 7.4) when monitoring intensity at λ_{ex} = 525 nm, collecting emission between 545 – 700 nm.

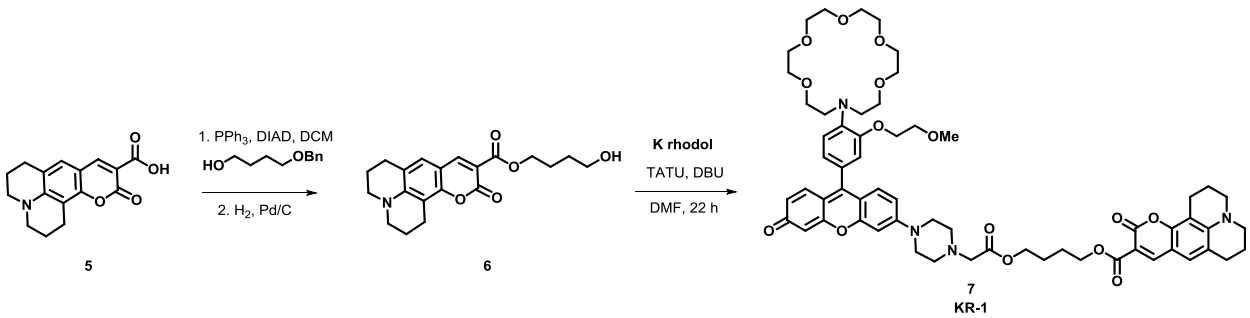

Scheme 2.4. Synthesis of Ratiometric Potassium Probe KR-1 from Krhodol

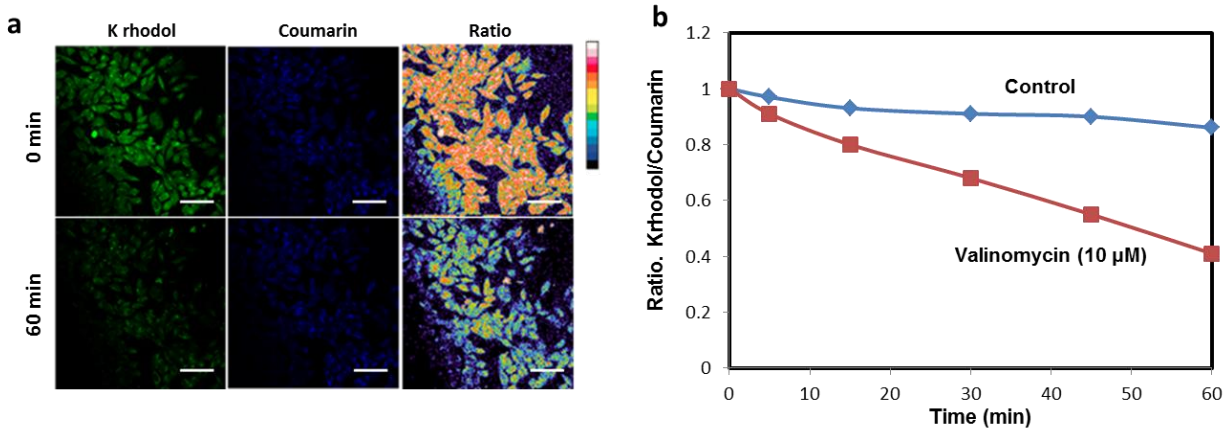

Figure 2.4. Representative ratiometric confocal microscopy images of live HEK 293T cells loaded with KR-1. Cells were treated with 10 µM KR-1 in DMEM for 90 minutes then washed 2x with DMEM before acquiring images. Cells were then treated with 10 µM valinomycin for 60 min, or not treated as control group for 60 min. Images were taken every 10 min and mean Krhodol/Coumarin ratios of HEK 293T were calculated. Scale bar = 25 µm.

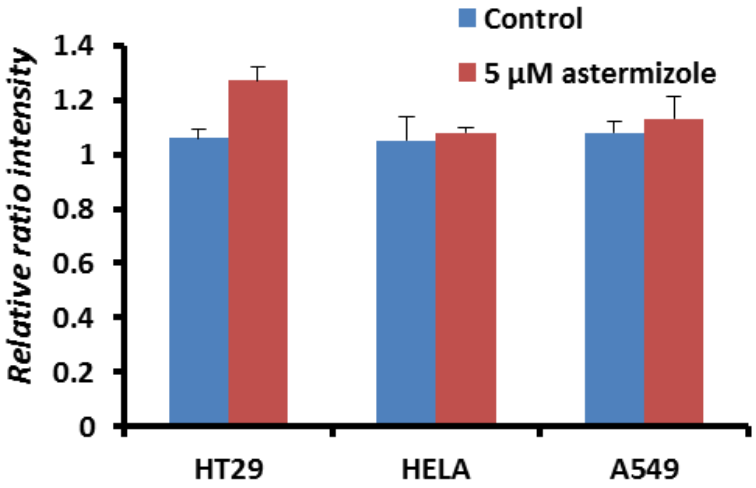

Figure 2.5. Imaging effect of K^+ channel blocker astermizole on various cell lines. HT29, HELA, A549 cells were treated with 10 µM KR-1 in DMEM for 90 minutes then washed 2x with DMEM before acquiring images. Then cells were either treated with 5 µM astermizole or astermizole exclusive high K buffer for 30 min. Relative ratio intensity was calculated by dividing final mean ratio value by initial mean ratio value. Error bars denote SEM, n=3.

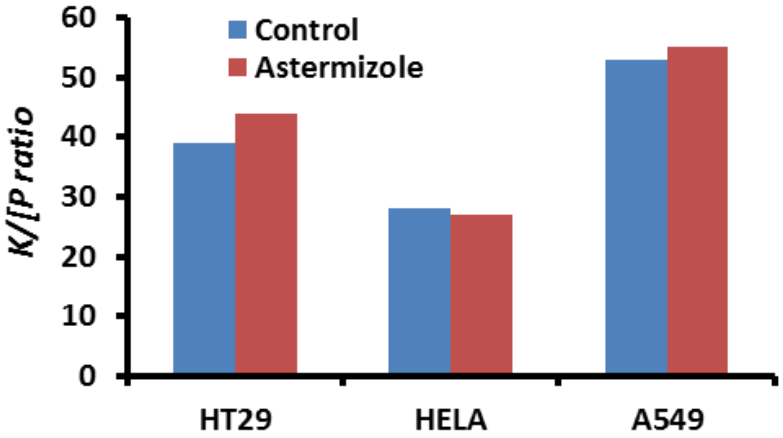

Figure 2.6. Total potassium content of astermizole-treated various cell lines. HT29, HELA, A549 cells were treated with 10 μM KR-1 in DMEM for 90 minutes then washed 2x with DMEM. Then cells were either treated with 5 μM astermizole or astermizole exclusive high K buffer for 30 min. Cellular ^{39}K and phosphorous content was measured by ICP-MS. Error bars denote SEM, n=3.Error bars denote SEM, n=3.

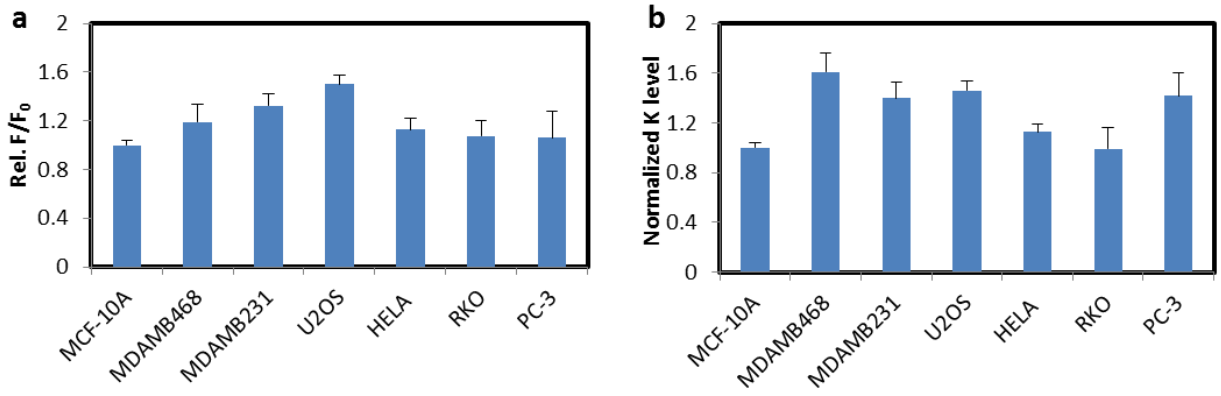

Figure 2.7. Resting potassium levels of various cancer cell lines. MCF-10A, MDAMB468, MDAMB231, U2OS, HELA, RKO, PC-3 were incubated with 10 μM KR-1 in DMEM for 90 minutes then washed 2x with DMEM before acquiring the image. Cellular ^{39}K and phosphorous content was measured by ICP-MS. Error bars denote SEM, n=3.Error bars denote SEM, n=3.

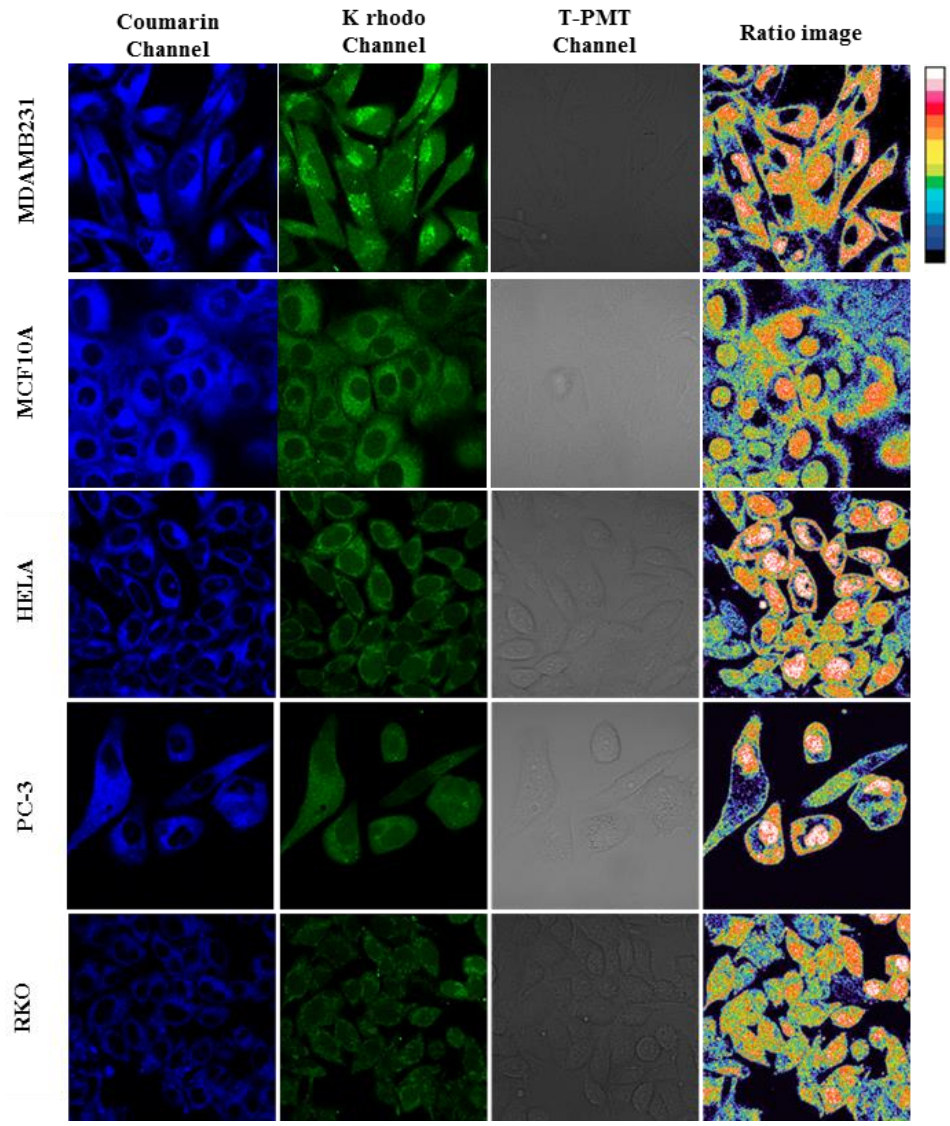

Figure 2.8. Resting potassium levels of various cancer cell lines. MCF-10A, MDAMB468, MDAMB231, U2OS, HELA, RKO, PC-3 were incubated with 10 μM KR-1 in DMEM for 90 minutes then washed 2x with DMEM before acquiring the image. Ratio images were generated with imageJ.

Chapter 3

Development of a bioluminescence resonance energy transfer (BRET) based platform for detecting H_2O_2 in living cells

3.1 Introduction

Bioluminescence resonance energy transfer (BRET), first observed in marine organisms such as *Renilla reniformis*[1,2] depicts a nonradiative energy transfer between two optical components, BRET donor and acceptor. The donor is usually an enzyme such as luciferase and its derivatives which can that can catalyze light-producing chemical reactions in living organisms.[3–6] The acceptor can be either fluorescent proteins or fluorophores that can be excited with the donor energy and emit at a longer wavelength. BRET shares similar features with fluorescence resonance energy transfer (FRET) as both require some degree of spectral overlap between the emission spectrum of the donor and the excitation wavelength of the acceptor. In addition, both FRET and BRET efficiency are inversely proportional to the sixth power of the donor-acceptor distance.[7–9] But compared to FRET, BRET does not require an external light source, therefore, BRET does not suffer from auto-fluorescence and does not cause photo-damage in biological systems. Due to this special characteristic, BRET provides high signal-to-noise ratio, is non-destructive, and can be used in living cells. Thus, BRET has been utilized in the fields of protein-protein interaction studies as well as protein signaling and trafficking studies. Several examples mainly take advantage of the influence of donor-acceptor distance on BRET efficiency and in most cases BRET acceptors are fluorescent proteins.[5,10–12] (Scheme 3.1)

As described in previous chapters, fluorescent sensors can provide selective and sensitive read-out with good temporal and spatial resolution, Due to these advantages, our lab has developed several novel fluorescent probes and utilized them to study the signaling and trafficking of cellular analytes including ROS and transition metals.[13–15] However, recognition-based fluorescent probe which is one of two general strategies of fluorescent turn-on[16] have a caveat, false signal of signal-to-noise in the cell application. Even with the development of targetable organelles labeling tools such as SNAP-tag or HALO-tag, labeling of fluorescent sensors still suffered from the issues of non-specific labelling or the necessity of extra washing. It is worth noting that most of these problems come from the external light input.

In this chapter, we report the design and characterization of the novel H_2O_2 probe using BRET strategy modified from our fluorescent H_2O_2 sensors.[17–19] We envision utilizing the engineered luciferase, Nanoluciferase (NLuc)[20–25] as the BRET donor in conjunction with the small molecule fluorescent H_2O_2 sensor as the acceptor.[26] In order to bring the donor and the acceptor in close proximity, we turned to the HaloTag labeling technology[27–30] which is based on an engineered haloalkane dehalogenase enzyme which can covalently interact with a choloroalkane conjugated H_2O_2 probe. We generated a fusion protein of NLuc and the HaloTag protein, which can be expressed in living cells. Upon reacting with the halo protein, the modified H_2O_2 probe can specifically label the Nanoluc halo proteins. In the presence of H_2O_2, the fluorophore is unmasked and can serve as a BRET acceptor to produce a H_2O_2 responsive BRET signal. This BRET pair will give us high signal-to-noise for detection of cellular H_2O_2 levels without the use of excitation light source. This modular BRET design strategy can be employed to detect other biologically important analytes by coupling the donor to a wide range of fluorescent sensors which have good overlap between excitation spectrum of fluorophore and the

emission spectrum of BRET donor. This BRET method for H_2O_2 detection can provide a valuable starting point for the further development of BRET sensors for bio-analyte studies.

3.2. Methods

3.2.1. General Synthetic Methods

Reactions using moisture- or air-sensitive reagents were carried out in flame-dried glassware under an inert atmosphere of N_2. Solvent was passed over activated alumina and stored over activated 3Å molecular sieves before use when dry solvent was required. All other commercially purchased chemicals were used as received (without further purification). Fmoc-piperazine rhodol boronate was prepared according to published procedures.[19] SiliCycle 60 F254 silica gel (pre-coated sheets, 0.25 mm thick) were used for analytical thin layer chromatography and visualized by fluorescence quenching under UV light. Silica gel P60 (SiliCycle) was used for column chromatography. ^{1}H and ^{13}C NMR NMR spectra were collected at 298 K in CDCl3 or CD3CN (Cambridge Isotope Laboratories, Cambridge, MA) at 25 °C on Bruker AVQ-400, AVB-400, AV-500, or AV-600 at the College of Chemistry NMR Facility at the University of California, Berkeley. All chemical shifts are reported in the standard notation of δ parts per million relative to residual solvent peak at 7.26 ($CDCl_3$) or 1.93 (CD_3CN) for ^{1}H and 77.16 ($CDCl_3$) or 177.7 (CD_3CN) for ^{13}C as an internal reference. Splitting patterns are indicated as follows: br, broad; s, singlet; d, doublet; t, triplet; m, multiplet; dd, doublet of doublets. Low-resolution electrospray mass spectral analyses were carried out using a LC-MS (Agilent Technology 6130, Quadrupole LC/MS and Advion expression-L Compact Mass Spectrometer). High-resolution mass spectral analyses (ESI-MS) were carried out at the College of Chemistry Mass Spectrometry Facility at the University of California, Berkeley.

3.2.2. Probe Synthesis and New Compound Characterization

4-(1,4,7,10,13-pentaoxa-16-azacyclooctadecan-16-yl)-3-(2-methoxyethoxy)benzaldehyde, 2. POCl3 (3.72 ml, 40 mmol) was added dropwise to a vigorously stirring anhydrous DMF which was kept in ice bath under N_2. Resulting pale yellow solution was stirred at room temperature for additional 15 min. To this, DMF (2 ml) solution of 16-(2-(2-methoxyethoxy)phenyl)-aza-18-crown-6 **1** (1.65 g, 4 mmol) was then slowly introduced and the resulting dark red solution was heated at 70 ^{o}C for 3 h. Reaction was cooled to room temperature, and poured into ice-cold sat. $NaHCO_3$ solution. The mixture was extracted 3 x 100 ml DCM/Toluene (2:1) and dried over anhydrous $MgSO_4$. Solvent was evaporated in vacuo and compound was purified by silica gel FCC using DCM:MeOH (19:1) as the eluent. Product **2** was obtained as dark red oil (820 mg, 44% yield) ^{1}H NMR (400 MHz, $CDCl_3$) δ (ppm): 3.48 (s, 3 H), 2.38 (s, 2 H), 2.00 - 1.77 (m, 11 H). ^{13}C NMR (101 MHz, $CDCl_3$) δ (ppm): 215.88, 175.71, 51.63, 45.47, 39.82, 37.98, 37.51, 26.98. LCMS calcd. for $C_{12}H_{16}O_3$ $[M + H]^+$ 414.19, found 414.2.

9-(4-(1,4,7,10,13-pentaoxa-16-azacyclooctadecan-16-yl)-3-(2-methoxyethoxy)phenyl)-6-hydroxy-3H-xanthen-3-one, 3. Aldehyde **2** (150 mg, 0.34 mmol, 1 equiv) and resorcinol (82 mg, 0.74 mmol, 2.2 equiv) were dissolved in 4.25 ml TFA in 35 ml pressure flask. The solution was then stirred at 115 °C for 13 h and rotovaped own to yield crude red oil. The red oil was

taken up in silica column for purification by flash column chromatography (50% MeCN/Toluene) to yield **3** (35 mg, 18% yield) as a bright yellow solid. ^{1}H NMR (400 MHz, $CDCl_3$) δ (ppm): 3.48 (s, 3 H), 2.38 (s, 2 H), 2.00 - 1.77 (m, 11 H). ^{13}C NMR (101 MHz, $CDCl_3$) δ (ppm): 215.88, 175.71, 51.63, 45.47, 39.82, 37.98, 37.51, 26.98. LRMS calcd. for $C_{12}H_{16}O_3$ [M + H]$^+$ 209.11, found 209.2.

PY1-Halo 2-(2-((6-chlorohexyl)oxy)ethoxy)ethan-1-amine B was synthesized following literature procedures.10 Compound (14) (0.0159 g, 0.01968 mmol, 1 eq), B (0.0132 g, 0.059 mmol, 3 eq), and HATU (0.0262 g, 0.0689 mmol, 3.5 eq) were added to an oven-dried round-bottom flask with 1 mL DMF. Then DIPEA (0.02057 mL, 0.11808 mmol, 6 eq) was added, and the reaction was stirred at room temperature overnight. The reaction was concentrated in vacuo, then was loaded on silica gel for purification by flash chromatography (10% MeOH in DCM) to yield P Y1-HALO (0.0068 g, 34%). 1H NMR (400 MHz, CDCl3) δ (ppm): 7.94 (s, 1 H), 7.79 – 7.78 (d, 1 H), 6.85 – 6.82 (m, 4 H), 6.63 – 6.59 (d, 1 H), 6.55 (s, 1 H), 3.84 (s, 2 H), 3.59 – 3.45 (m, 12 H), 3.11 (s, 2 H), 2.84 – 2.56 (s, 24 H), 1.28 (m, 6 H).

3.2.3. Spectroscopic Materials and Methods.

Millipore water was used to prepare all aqueous solutions. All spectroscopic measurements were performed in 20 mM HEPES buffer, pH 7. Absorption spectra were recorded on a Varian Cary 50 spectrophotometer (Walnut Creek, CA) and fluorescence spectra were recorded on a Photon Technology International Quanta Master 4 L-format scanning spectrofluorometer (Lawrenceville, NJ) equipped with an LPS-220B 75-W xenon lamp and power supply, A-1010B lamp housing with integrated igniter, switchable 814 photon-counting/analog photomultiplier detection unit, and MD5020 motor driver. Samples for absorption and emission measurements were contained in 1-cm × 1-cm quartz cuvettes (1.5-mL volume, Starna, Atascadero, CA).

3.2.4. Preparation and Staining of Cell Cultures.

HEK293T cells were cultured in DMEM (Invitrogen) supplemented with 10% fetal bovine serum (FBS, Hyclone) and glutamine (2 mM). Two days before imaging, cells were passaged and plated on 18-mm glass coverslips. For all experiments, solutions of dyes (from 5 mM stocks in DMSO) were made in DBPS with calcium chloride and magnesium chloride (Sigma). H_2O_2 was added by bath application to the medium from a 100 mM aqueous stock. For paraquat treatment, HeLa cells were cultured as described above. One day prior to imaging, 1 mM paraquat was added to cells from a 0.5 M stock solution in water. An equal amount of water was added to control cells at the same time. Cells were then incubated at 37 °C, 5% CO2. After 24 hours, the media was exchanged for DPBS with 5 μM dye and incubated for 1 hour.

3.2.5. Fluorescence Imaging Experiments.

Confocal fluorescence imaging studies were performed with a Zeiss LSM510 NLO Axiovert 200 laser scanning microscope and a 63x Achroplan IR water-immersion objective lens. Excitation of PY1-loaded cells at 510 nm was carried out with an Ar laser and emission was collected using a META detector between 527-580 nm. MitoTracker Deep Red was excited with a 633-nm line and emission was collected between 666-698 nm. LysoTracker Red was excited with a 543-nm line and emission was collected between 580-644 nnm. Excitation of Hoechst 33342 was carried out using a MaiTai two-photon laser at 780-nm pulses (mode-locked Ti:sapphire laser, Tsunami Spectra Physics) and emission was collected between 452-537 nm. Image analysis was performed in Adobe Photoshop.

3.2.6. Cell plating and transfection

Plate 9 mL of HEK293T cells in a 10 cm dish at a cell density of 1.1 $x10^5$ /mL and incubated at 37°C, 5% CO_2 for 24 h. Cells were then transfected with NLuc-HaloTag Vector (Promega) using lipofectamine 3000 and incubated at 37°C, 5% CO2 for 24 h. The cells were harvested by trypsinization followed by centrifugation for 5 minutes at 200 x g. The cell pellet was then resuspended in 2 mL PBS, divided into two tubes and centrifuged for 5 minutes at 200 x g to obtain cell pellet. The cell pellets were stored in -80°C until further use.

3.2.7. Binding analysis

The cell pellet was resuspended in 400 µL lysis buffer (Promega) and incubated for 15 minutes at room temperature with constant mixing. The solution was then diluted 1:2 with PBS for a final volume of 1.2 mL diluted cell lysate. At this point, 60 µL of the lysate was removed and labeled as Time 0. A 4 µM HaloTag TMR ligand solution in PBS was prepared and 20 µL of 4 µM HaloTag TMR solution was added to the Time 0 aliquot for a final concentration of 1 µM and incubated for 15 minutes at room temperature. This represents 100% available HaloTag not treated with the chloroalkane derivatized compound and will be used as reference in the calculations. To the remainder of the lysate, the chloroalkane derivatized compound was added at a final concentration of 1 µM and incubated at room temperature with constant mixing. Sequentially after 5, 10, 15, 30, 45, and 60 minutes incubation time, 60 µL lysate was removed and 20 µL of 4µM HaloTag TMR ligand was added immediately and incubated at room temperature for 15 minutes. The TMR-HaloTag ligand will bind to HaloTag which was not already bound to the chloroalkane derivatized compound. After labeling, 26µl of 4 X SDS Loading buffer was added to all the samples and 10-15 µL of each sample was loaded in an SDS-PAGE. The fluorescent gel was imaged with the Chemi Doc imager and the band intensities were used to calculate the percentage of labeled protein at the various time points.

3.3. Results

3.3.1. Design, Synthesis, and Characterization of BRET-based H_2O_2 sensor

Our design of this BRET-based H_2O_2 probe includes three components, the BRET donor, the BRET acceptor, and the linker. We chose Nanoluc luciferase (Nluc), a new bioluminescent enzyme as our BRET donor. NLuc is a 19.1 kDa luciferase enzyme that relies on the substrate furimazine to produce high intensity, glow-type luminescence. NLuc was shown to exhibit multiple photo-properties superior to traditional luciferases. Also, the H_2O_2 sensor (PY1) which revealed the high selectivity toward H_2O_2 and high quantum yield was chosen as the BRET acceptor and modified it with halo-tag reactive handle for labeling Nluc (Halo-PY1). We envisioned in *cellulo* labeling of modified PY1 probe on co-expressed Nluc-Halotag fusion protein. Before reacting with peroxide, PY1 is not activated and only bioluminescence at Nluc emission wavelength will be observed (around 460 nm). However, after the reaction of PY1 probe with cellular hydrogen peroxide, boronic ester on PY1 will be hydrolyzed and unmasked to yield an excitable fluorescein species. Then upon stimulation of bioluminescence with furimazine, BRET process will occur between Nluc and activated PY1, resulting in an increase in activated PY1 emission at 545 nm. Information of cellular H_2O_2 level can thus be monitored using the ratio of emission profiles for PY1 channel and Nluc channel (BRET ratio).

The synthesis of Halo-PY1 is described briefly as follows. Fmoc-PY1 was synthesized in four steps from commercially available starting material according to literature procedure (Scheme 3.2). Deprotection of Fmoc group gives yield to piperazine modified rhodol 2. The free secondary amine on molecule 2 further reacted with succinic anhydride to afford rhodol 3 with carboxylate acid functional group. Halo-tag reactive handle was then attached to rhodol 3 using HATU facilitated amination reaction to yield Halo-PY1.

3.3.2. Reactivity and binding affinity of the probe

We next examined the response of Halo-PY1 for H_2O_2 in aqueous buffer (50 mM HEPES, pH 7.4). The oxidized probe showed absorption maxima at 515 nm and emission maxima at 545 nm and upon the addition of 100 μM H_2O_2, the probe showed over 25 fluorescent turn-on, which matches the features of previous PY1 probe. (Figure 3.1) The data also showed that Halo-PY1 retained the sensitive response to H_2O_2 around physiological level (< 200 μM). Also, reaction of the probe in buffer with various H_2O_2 level showed the rate of reaction increases with increasing concentrations of H_2O_2 (1 μM to 1 mM). (Figure 3.2)

After confirming reactivity of Halo-PY1 towards peroxide, we tested out reactivity of the Halo-PY1 towards Nluc-Halotag protein. The experiment was conducted with cell lysate of Nluc-Halotag transfected in HEK293T cells. The result showed a fast and efficient labeling between Halo-PY1 and Nluc-Halotag proteins. The rate of labeling was comparable to that of TMR-halo as a standard labeling reagent. Labeling reaction was determined to be completed within 15 min by imaging the fluorescent gel. (Figure 3.3)

3.3.3. Cellular staining and response of the labeled probe to H_2O_2

Halo-PY1 was then tested for its ability to both specifically label Nluc-HaloTag protein and respond to H_2O_2 in living biological systems. HEK293T was transfected with Nluc-Halotag protein vector. The transfected cells were then incubated with 5 μM Halo-PY1 for 1h at 37 ^{o}C and washed 3 times before imaging. No signal was observed before peroxide addition by confocal microscopy. However after the addition of 100 μM H_2O_2 to transfected cells loaded with Halo-PY1, we observed strong fluorescent signal from the transfected cells after 30 min incubation and it even showed staining pattern. This suggests that the probe can sensitively read out the increases of cellular H_2O_2. Moreover, the staining pattern demonstrated that not all the cells in the imaging field had fluorescent signal, indicating that only cells that were successfully transfected with Nluc-Halotag construct can be labeled by Nluc-PY1. In addition, control experiments were conducted with non-transfected HEK293T under same condition. No signal was observed both before and after the addition of 100 μM H_2O_2. The result suggested that the unlabeled probe was not retained in the untransfected cells during the washing process and this further confirmed specific labeling of Halo-PY1 to Nluc-Halotag protein. (Figure 3.4)

3.4. Reference

(1) Ward, W. W.; Cormier, M. J. Energy Transfer Via Protein-Protein Interaction in Renilla Bioluminescence. *Photochem. Photobiol.* **1978**, *27* (4), 389–396.

(2) Lorenz, W. W.; McCann, R. O.; Longiaru, M.; Cormier, M. J. Isolation and Expression of a cDNA Encoding Renilla Reniformis Luciferase. *Proc. Natl. Acad. Sci.* **1991**, *88* (10), 4438–4442.
(3) Badr, C. E.; Tannous, B. A. Bioluminescence Imaging: Progress and Applications. *Trends Biotechnol.* **2011**, *29* (12), 624–633.
(4) Paley, M. A.; Prescher, J. A. Bioluminescence: A Versatile Technique for Imaging Cellular and Molecular Features. *MedChemComm* **2014**, *5* (3), 255–267.
(5) Xia, Z.; Rao, J. Biosensing and Imaging Based on Bioluminescence Resonance Energy Transfer. *Curr. Opin. Biotechnol.* **2009**, *20* (1), 37–44.
(6) Prinz, A.; Diskar, M.; Herberg, F. W. Application of Bioluminescence Resonance Energy Transfer (BRET) for Biomolecular Interaction Studies. *ChemBioChem* **2006**, *7* (7), 1007–1012.
(7) Sapsford, K. E.; Berti, L.; Medintz, I. L. Materials for Fluorescence Resonance Energy Transfer Analysis: Beyond Traditional Donor–Acceptor Combinations. *Angew. Chem. Int. Ed.* **2006**, *45* (28), 4562–4589.
(8) Rao, J.; Dragulescu-Andrasi, A.; Yao, H. Fluorescence Imaging in Vivo: Recent Advances. *Curr. Opin. Biotechnol.* **2007**, *18* (1), 17–25.
(9) Clapp, A. R.; Medintz, I. L.; Mauro, J. M.; Fisher, B. R.; Bawendi, M. G.; Mattoussi, H. Fluorescence Resonance Energy Transfer Between Quantum Dot Donors and Dye-Labeled Protein Acceptors. *J. Am. Chem. Soc.* **2004**, *126* (1), 301–310.
(10) Compan, V.; Baroja-Mazo, A.; Bragg, L.; Verkhratsky, A.; Perroy, J.; Pelegrin, P. A Genetically Encoded IL-1β Bioluminescence Resonance Energy Transfer Sensor To Monitor Inflammasome Activity. *J. Immunol.* **2012**, *189* (5), 2131–2137.
(11) Wu, C.; Mino, K.; Akimoto, H.; Kawabata, M.; Nakamura, K.; Ozaki, M.; Ohmiya, Y. In Vivo Far-Red Luminescence Imaging of a Biomarker Based on BRET from Cypridina Bioluminescence to an Organic Dye. *Proc. Natl. Acad. Sci.* **2009**, *106* (37), 15599–15603.
(12) Pichler, A.; Prior, J. L.; Luker, G. D.; Piwnica-Worms, D. Generation of a Highly Inducible Gal4→Fluc Universal Reporter Mouse for in Vivo Bioluminescence Imaging. *Proc. Natl. Acad. Sci.* **2008**, *105* (41), 15932–15937.
(13) Chan, J.; Dodani, S. C.; Chang, C. J. Reaction-Based Small-Molecule Fluorescent Probes for Chemoselective Bioimaging. *Nat. Chem.* **2012**, *4* (12), 973–984.
(14) Gonçalves, M. S. T. Fluorescent Labeling of Biomolecules with Organic Probes. *Chem. Rev.* **2009**, *109* (1), 190–212.
(15) Silva, A. P. de; Moody, T. S.; Wright, G. D. Fluorescent PET (Photoinduced Electron Transfer) Sensors as Potent Analytical Tools. *Analyst* **2009**, *134* (12), 2385–2393.
(16) Aron, A. T.; Ramos-Torres, K. M.; Cotruvo, J. A.; Chang, C. J. Recognition- and Reactivity-Based Fluorescent Probes for Studying Transition Metal Signaling in Living Systems. *Acc. Chem. Res.* **2015**, *48* (8), 2434–2442.
(17) Lin, V. S.; Dickinson, B. C.; Chang, C. J. Chapter Two - Boronate-Based Fluorescent Probes: Imaging Hydrogen Peroxide in Living Systems. In *Methods in Enzymology*; Cadenas, E., Packer, L., Eds.; Hydrogen Peroxide and Cell Signaling, Part A; Academic Press, 2013; Vol. 526, pp 19–43.
(18) Chang, M. C. Y.; Pralle, A.; Isacoff, E. Y.; Chang, C. J. A Selective, Cell-Permeable Optical Probe for Hydrogen Peroxide in Living Cells. *J. Am. Chem. Soc.* **2004**, *126* (47), 15392–15393.

(19) Dickinson, B. C.; Chang, C. J. A Targetable Fluorescent Probe for Imaging Hydrogen Peroxide in the Mitochondria of Living Cells. *J. Am. Chem. Soc.* **2008**, *130* (30), 9638–9639.
(20) Luker, K. E.; Smith, M. C. P.; Luker, G. D.; Gammon, S. T.; Piwnica-Worms, H.; Piwnica-Worms, D. Kinetics of Regulated Protein–protein Interactions Revealed with Firefly Luciferase Complementation Imaging in Cells and Living Animals. *Proc. Natl. Acad. Sci.* **2004**, *101* (33), 12288–12293.
(21) Coppola, J. M.; Ross, B. D.; Rehemtulla, A. Noninvasive Imaging of Apoptosis and Its Application in Cancer Therapeutics. *Clin. Cancer Res.* **2008**, *14* (8), 2492–2501.
(22) Ilagan, M. X. G.; Lim, S.; Fulbright, M.; Piwnica-Worms, D.; Kopan, R. Real-Time Imaging of Notch Activation with a Luciferase Complementation-Based Reporter. *Sci Signal* **2011**, *4* (181), rs7-rs7.
(23) Sun, C.; Gardner, C. L.; Watson, A. M.; Ryman, K. D.; Klimstra, W. B. Stable, High-Level Expression of Reporter Proteins from Improved Alphavirus Expression Vectors To Track Replication and Dissemination during Encephalitic and Arthritogenic Disease. *J. Virol.* **2014**, *88* (4), 2035–2046.
(24) Karlsson, E. A.; Meliopoulos, V. A.; Savage, C.; Livingston, B.; Mehle, A.; Schultz-Cherry, S. Visualizing Real-Time Influenza Virus Infection, Transmission and Protection in Ferrets. *Nat. Commun.* **2015**, *6*, 6378.
(25) Hall, M. P.; Unch, J.; Binkowski, B. F.; Valley, M. P.; Butler, B. L.; Wood, M. G.; Otto, P.; Zimmerman, K.; Vidugiris, G.; Machleidt, T.; et al. Engineered Luciferase Reporter from a Deep Sea Shrimp Utilizing a Novel Imidazopyrazinone Substrate. *ACS Chem. Biol.* **2012**, *7* (11), 1848–1857.
(26) BRET, NanoLuc Luciferase and Protein:Protein Interactions https://www.promega.com/resources/pubhub/features/bret-nanoluc-luciferase-and-protein-protein-interactions/ (accessed May 7, 2018).
(27) Sletten, E. M.; Bertozzi, C. R. Bioorthogonal Chemistry: Fishing for Selectivity in a Sea of Functionality. *Angew. Chem. Int. Ed.* **2009**, *48* (38), 6974–6998.
(28) Prescher, J. A.; Bertozzi, C. R. Chemistry in Living Systems. *Nat. Chem. Biol.* **2005**, *1* (1), 13–21.
(29) Stagge, F.; Mitronova, G. Y.; Belov, V. N.; Wurm, C. A.; Jakobs, S. Snap-, CLIP- and Halo-Tag Labelling of Budding Yeast Cells. *PLOS ONE* **2013**, *8* (10), e78745.
(30) Mazza, D.; Abernathy, A.; Golob, N.; Morisaki, T.; McNally, J. G. A Benchmark for Chromatin Binding Measurements in Live Cells. *Nucleic Acids Res.* **2012**, *40* (15), e119–e119.

Figures

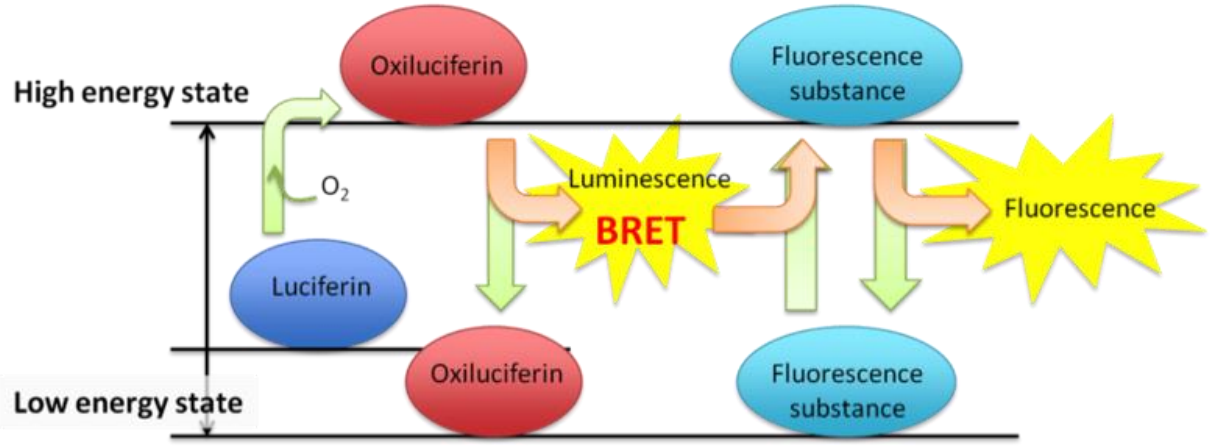

Scheme 3.1. Mechanism of bioluminescence resonance energy transfer (BRET)

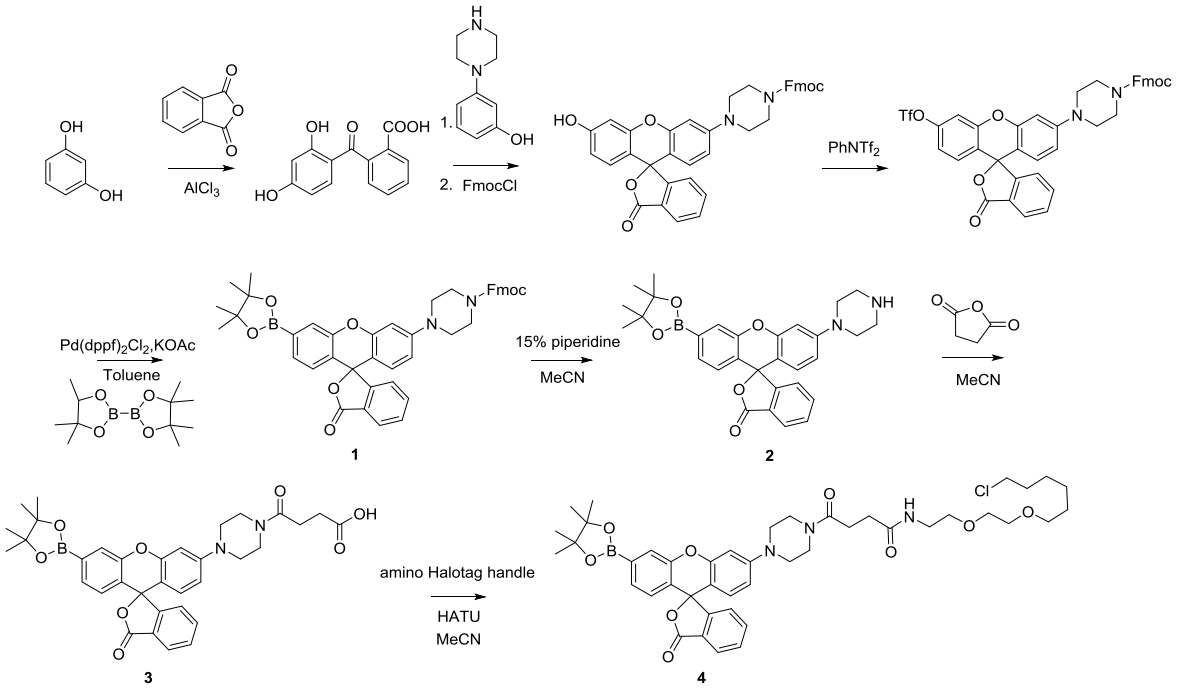

Scheme 3.2. Synthesis of Halo-tag reactive H_2O_2 sensor PY1-Halo

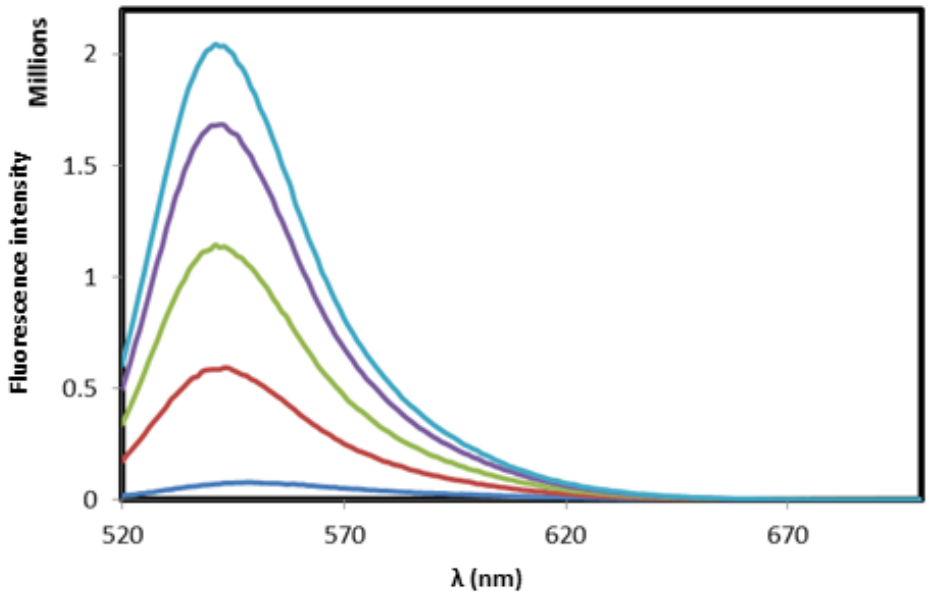

Figure 3.1. Fluorescence turn-on response of 5 μM PY1-Halo to H_2O_2. Data were acquired at 37 ^{0}C in 20 mM HEPES, pH 7.4 with excitation at λ = 503 nm Emission were collected between 520 and 700 nm. Time points represent 0, 5, 15, 30, 45, and 60 min after addition of 100 μM H_2O_2. Reactions are not complete at these times.

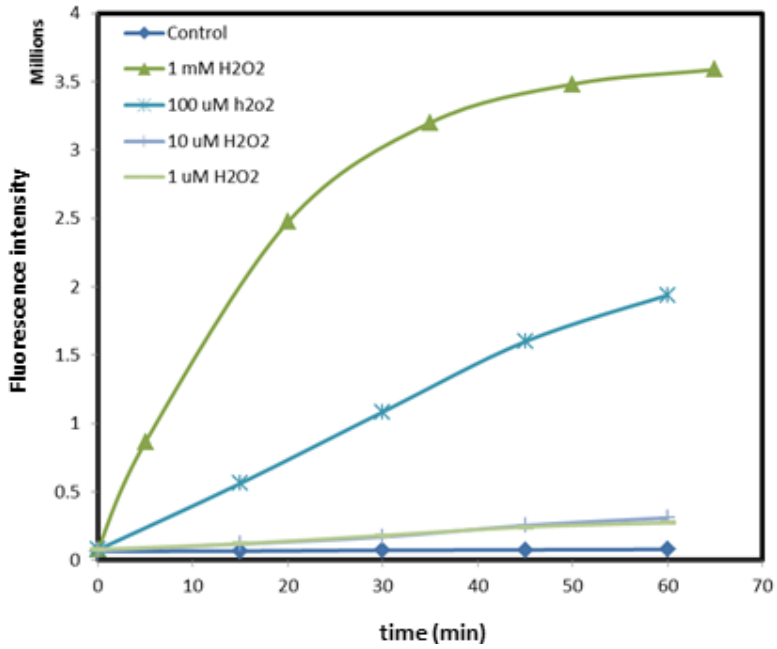

Figure 3.2. Kinetic study of fluorescence turn-on response of PY1-Halo to H_2O_2. Data were acquired at 37 ^{0}C in 20 mM HEPES, pH 7.4 with excitation at λ = 503 nm Emission were collected between 520 and 700 nm. Time points represent 0, 5, 15, 30, 45, and 60 min after addition of 1, 10, 100, and 1000 µM H_2O_2. Reactions are not complete at these times.

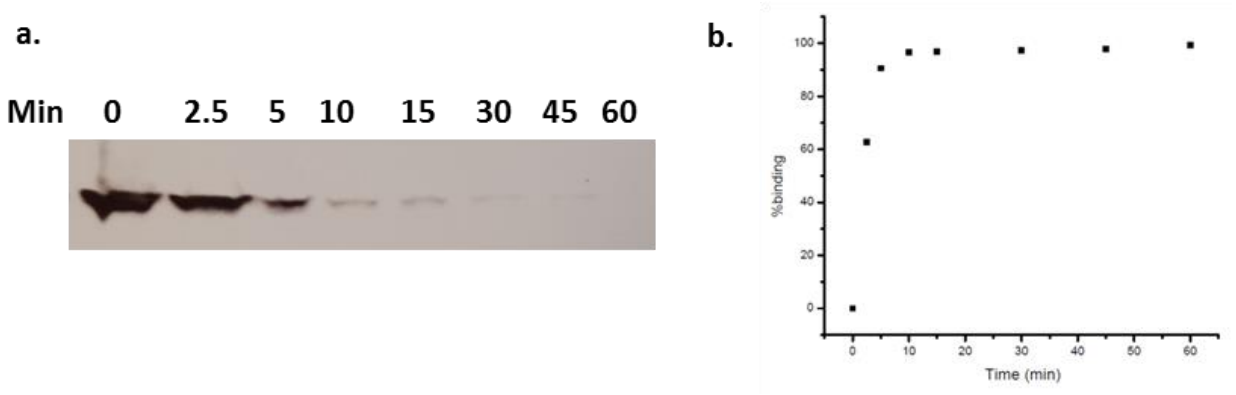

Figure 3.3. Fig 1: Binding kinetics of PY1-Halo to HaloTag in cell lysate. a. SDS–PAGE analysis of binding to HaloTag. b. % binding with time. Results indicates sufficient binding to HaloTag within the 15 minutes capture time frame. TMR-Halo was used as comparison group

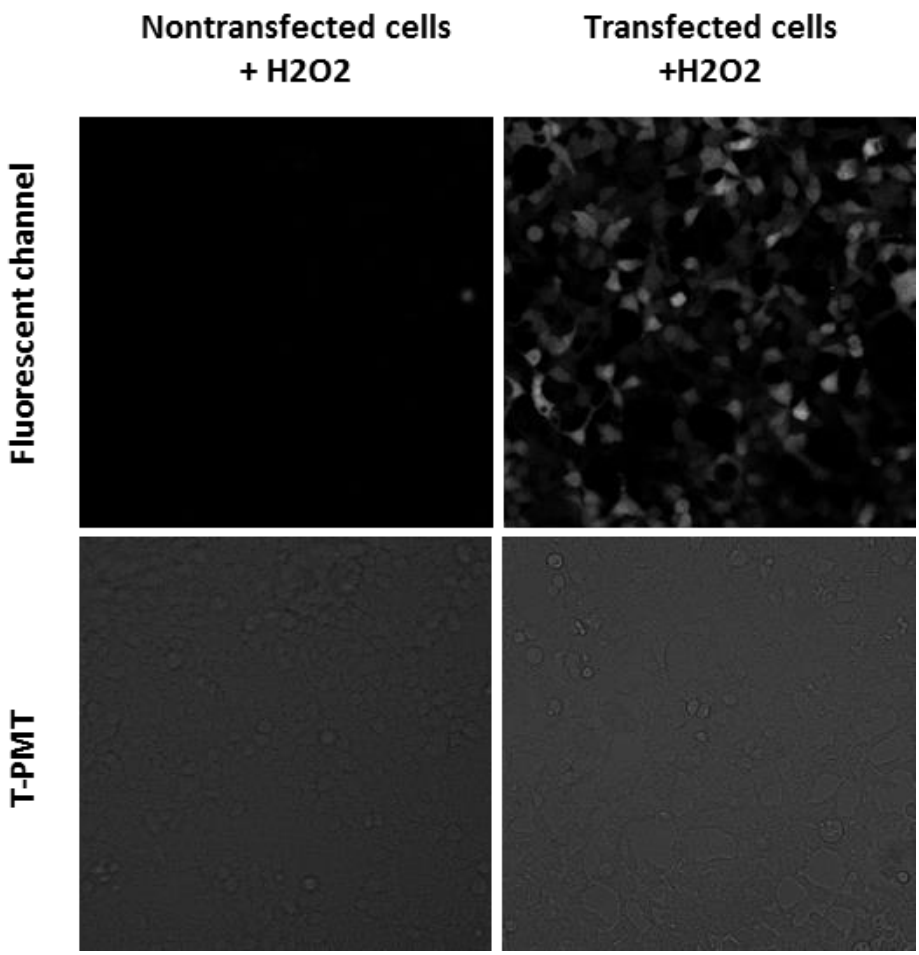

Figure 3.4: Both HeLa cells (on two coverslips each in separate petri dishes) transfected with Nanoluc-Halo construct and non-transfected were incubated with 5 μM PY1-Halo in DPBS for 30 minutes. 100 μM H2O2 was then added to one of the petri dishes. (3.2 μsec pixel time, 100% laser power for 514 line, 4.1% laser power for the 633 line, 26% laser power for the 543 line, scanned using 12-bit multi-track scan mode using a constant receiver gain). Shown above are signals from PY1-Halo 20 μm scale bar shown for all images.

Appendix 1

Design, synthesis of a fluorescent turn-on K^+ probe for measuring extracellular K^+ level in living cells

A.1.1. Introduction

As the most abundant intracellular cation, potassium (K^+) occupies 4% of human body mass and plays a vital role in regulating intracellular fluid volume, fluid transportation, and neuron signaling. In general, physiological extracellular K^+ concentrations are around 5 mM, while the concentration of intracellular K^+ is typically around 150 mM. During normal K^+ fluctuations in activities such as such as neurotransmission, muscle contraction, and heart function, extracellular K^+ can rise up to 10 mM, while intracellular K^+ levels remain relatively on a constant higher concentration. Abnormal K^+ fluctuations may lead to diseases such as anorexia, bulimia, heart disease, diabetes, and cancer. [1, 2, 3, 4] However, the current knowledge of physiology of K^+ is very limited, due to the absence of efficient ways to measure the change of K^+ in both cellular and extracellular fluids with high spatial and temporal fidelity. [5] A fluorescent approach might be a promising candidate for studying the dynamics of K^+ levels as it is non-invasive to biology system and sensitive for target molecules.

Potassium-binding benzofuran isophthalate (PBFI), one of the earliest fluorescent potassium ion probes, uses diaza-18-crown-6 as the ion receptor and a benzofuran derivative as the fluorophore. However, PBFI suffers from poor selectivity for potassium ion over sodium ion. [7] A new triazacryptand platform was introduced as the potassium ionophore by He et al. to improve selectivity over sodium (Na^+). [6] Later, Verkman's group developed related probes for extracellular sensing by applying the same triazacryptand platform but altering the dissociation constant (Kd). [7~10] However, previous probes suffered from issues like low turn-on ratio and poor solubility, and hence the likelihood of applications of the probes to study extracellular potassium of live cells has been significantly excluded.

Since extracellular potassium concentration is much lower than intracellular potassium concentration, a more drastic change of potassium concentration will happen in extracellular fluids during the fluctuation of potassium ion which could result in a better sensitivity for fluorescent detection. For instance, extracellular potassium concentration can increase up to 2-fold during neuronal activity, while intracellular potassium stays stable. Physiological evidence indicate that the small amount of liberated K^+ does not immediately diffuse away from the neuron; instead, it appears to accumulate in a restricted space just outside the membrane, where it gives rise to a temporary increase in K^+ concentration in that area. [11] Thus we aim at developing an extracellular potassium ion probe. It is worthy to note that there are several principles we must consider in designing improved fluorescent potassium sensors. First of all, fluorophores with excitation in the visible range are preferred in biological systems, preferably at excitation (> 400 nm) and emission (> 500 nm) wavelengths that minimize the effects of the background fluorescence of biological systems. Second, sensors with reasonable dissociation constant (K_d) values around 5 mM to detect potassium efflux outside the cell are desired. Moreover, due to the much higher level of the extracellular sodium ion (~ 140 mM) with respect to potassium ion level, the sensor with high selectivity over Na^+ ion, as well as good water solubility, and high turn-on ratio is expected.

A.1.3. Methods

A.1.3.1. General synthetic methods

Reactions using moisture- or air-sensitive reagents were carried out in flame-dried glassware under an inert atmosphere of N_2. Solvent was passed over activated alumina and stored over activated 3Å molecular sieves before use when dry solvent was required. All other commercially purchased chemicals were used as received (without further purification). SiliCycle 60 F254 silica gel (pre-coated sheets, 0.25 mm thick) were used for analytical thin layer chromatography and visualized by fluorescence quenching under UV light. Silica gel P60 (SiliCycle) was used for column chromatography. ^{1}H and ^{13}C NMR NMR spectra were collected at 298 K in CDCl3 or CD3CN (Cambridge Isotope Laboratories, Cambridge, MA) at 25 °C on Bruker AVQ-400, AVB-400, AV-500, or AV-600 at the College of Chemistry NMR Facility at the University of California, Berkeley. All chemical shifts are reported in the standard notation of δ parts per mil-lion relative to residual solvent peak at 7.26 ($CDCl_3$) or 1.93 (CD_3CN) for ^{1}H and 77.16 ($CDCl_3$) or 177.7 (CD_3CN) for ^{13}C as an internal reference. Splitting patterns are indicated as follows: br, broad; s, singlet; d, doublet; t, triplet; m, multiplet; dd, doublet of doublets. Low-resolution electrospray mass spectral analyses were carried out using a LC-MS (Agilent Technology 6130, Quadrupole LC/MS and Advion expression-L Compact Mass Spectrometer). High-resolution mass spectral analyses (ESI-MS) were carried out at the College of Chemistry Mass Spectrometry Facility at the University of California, Berkeley.

A.1.3.2. Probe synthesis and new compound characterization

Synthesis of 1-(2-bromoethoxy)-2-nitrobenzene, 1.

Compound 1 (27.8 g, 200 mmol), 1,2-dibromoethane (86 ml, 1 mol), potassium carbonate (27.6 g, 200 mmol) were suspended in dry DMF (100 mL) and heated to 110 °C while stirring under nitrogen. After 1 h, the reaction was mixed with 250 ml of water and extracted with chloroform (250 ml). The organic layer was then washed by NaOH solution (1 N) until the water layer was pale yellow. Then the organic layer was dried over sodium sulfate, filtered and concentrated via rotary evaporation. The resulting oil (30 ml) was triturated with methanol and stored at -20 °C overnight. The solution was filtered and dried in air for 3 h to obtain a light yellow powder. The powder was then purified by column chromatography (silica gel, 30% ethyl acetate in hexanes) to afford the product as pale yellow crystal (13.0 g, 62.0 mmol 31%). 1H NMR (400 MHz, CDCl3): δ 7.85 (dd, 1H), 7.57 (td, 1H), 7.21 (d, 1H), 7.09-7.13 (m, 2H), 4.50 (t, 2H), 3.70 t, 2H) 13C NMR (101 MHz, CDCl3): δ 150.91, 140.31, 131.55, 127.52, 121.19, 115.29, 67.28, 29.21.

Synthesis of 5-(5,5-dimethyl-1,3-dioxan-2-yl)-2-nitrophenol, 2

3-hydroxy-4-benzaldehyde (10.0 g, 60 mmol), 2,2-dimethylpropane-1,3-diol (25.6 g, 300 mmol) were dissolved in benzene (300 ml) and H2SO4 (3 ml) was then added. The solution was heated at 120 °C for overnight. After cooling down, the solution was treated with potassium carbonate (10 g) and washed with sodium bicarbonate. The organic layer was then dried over sodium sulfate, filtered and concentrated via rotary evaporation to afford bright yellow powder (13.4 g, 58 mmol, 97%). 1H NMR (400 MHz, CDCl3): δ 8.13 (d, 1H), 7.30 (d, 1H), 7.16 (dd, 1H), 5,41 (s, 1H), 3.82 (d, 2H), 3.69 (d, 2H), 1.30 (s, 3H), 0.85 (s, 3H) 13C NMR (101 MHz, CDCl3): δ 153.03, 144.88. 132.92, 125.17, 119.54, 114.02, 109.59, 78.31, 76.22, 30.09, 24.11, 20.08

Synthesis of 2-(3-(2-methoxyethoxy)-4-nitrophenyl)-5, 5-dimethyl-1, 3-dioxane. (3)

5-(5,5-dimethyl-1,3-dioxan-2-yl)-2-nitrophenol (2 g, 8 mmol), 1-chloro-2-methoxyeth- ane (2.4 ml, 24 mmol), potassium carbonate (2.1 g, 16 mmol), and potassium iodide (2.5g, 16mmol) were suspended in DMF (80 ml) and heated to 80 °C under nitrogen. After 12 h, the reaction was poured into water (200 ml) and extracted with chloroform (200 ml). Then the organic layer was evaporated down to afford a yellow oil (2.3 g). The product was further purified by chromatography (silica gel, 20-50% ethyl acetate in hexanes) to afford the final product (2.2 g, 7 mmol, 83.2%) 1H NMR (400 MHz, CDCl3): δ 8.05 (d, 1H), 7.27 (s, 1H), 7.08 (dd, 1H), 5,39 (s, 1H), 4.29 (t, 2H), 3.75-3.82 (m, 4H), 3.66 (d, 2H), 3.46 (s, 3H) , 1.26 (s, 3H)), 0.82 (s, 3H). 13C NMR (101 MHz, CDCl3): δ 150.31, 143.98. 139.92, 124.36, 118.66, 112.31, 109.59, 78.31, 76.27, 72.11, 69.99, 59.34, 30.11, 24.11, 20.08

4-(5, 5-dimethyl-1,3-dioxan-2-yl)-2-(2-methoxyethoxy)aniline. (4)

2-(3-(2-methoxyethoxy)-4-nitrophenyl)-5,5-dimethyl-1,3-dioxane (1.8 g, 5.8 mmol), sodium borohydride (660 mg, 18 mmol), Raney nickel (2 ml in a slurry) was suspended in 300 ml of methanol. It was stirred at room temperature for 45 min. The product was filtered over Celite and rotary evaporated all the solvent. Then the slurry was treated with 100 ml of water and 100 ml of ethyl acetate. The organic layer was dried and evaporated down to afford light orange oil (1.64 g, 4 mmol, 87%) 1H NMR (400 MHz, CDCl3): δ 6.99 (s, 1H), 6.90 (d, 1H), 6.70 (dd, 1H), 4.12 (t, 2H), 4.64-4.74 (m, 6H), 3.75-3.82 (m, 4H), 3.42 (s, 3H), 1.26 (s, 3H)), 0.77 (s, 3H). 13C NMR (101 MHz, CDCl3): δ 144.08, 136.52. 127.88, 119.77, 116.82, 112.41, 109.52, 78.31, 76.27, 72.07, 69.05, 59.32, 30.11, 24.11, 20.08

4-(5,5-dimethyl-1,3-dioxan-2-yl)-2-(2-methoxyethoxy)-N,N-bis(2-(2 nitrophenoxy)ethyl)anil -ine. (5)

4-(5,5-dimethyl-1,3-dioxan-2-yl)-2-(2-methoxyethoxy)aniline (2 g,7 mmol), 1-(2-bromoethoxy)-2-nitrobenzene (5 g, 21 mmol), potassium carbonate (2.9 g, 21 mmol), potassium iodide (2.1 g, 14 mmol) was suspended in 30 ml of acetonitrile and heated to 80 °C under nitrogen. After 20 h, 1-(2-bromoethoxy)-2-nitrobenzene (1.7 g, 7 mmol) was added and after another 20 h 1-(2-bromoethoxy)-2-nitrobenzene (1.7 g, 7 mmol) was added. After 20 h, the solution was cooled down and the solvent was evaporated. Then 100 ml of water and 100 ml of chloroform were poured into the product. The organic layer was extracted, dried and evaporated down to afford a light brown oil (2.1 g). The crude residue was purified by two sequential columns (1: 20-70% ethyl acetate in hexanes; 2: 0-3% methanol in DCM (containing 1% triethylamine)) to afford (1.3 g , 2.12 mmol, 33%). 1H NMR (400 MHz, CDCl3): δ 7.74 (d, 2H), 7.43 (t, 2H), 6.99-7.05 (m,

5H), 6.93 (t, 2H), 5.31 (s, 1H), 4.10-4.18 (m, 6H), 3.68-3.74 (m, 8H), 3.59-3.63 (m 2H), 3,32 (s, 3H), 1.26 (s, 3H)), 0.77 (s, 3H). 13C NMR (101 MHz, CDCl3): δ 161.41, 150.95, 142.11, 140.32, 131.58, 127.57, 127.43, 121.32, 119.96, 114.88, 114.32, 113.54, 78.31, 76.27, 72.07, 69.05, 65.39, 59.43, 59.32, 30.11, 24.11, 20.08. HRMS-ESI calculated for C31H38O10N3 612.2552; found 612.2550

N,N-bis(2-(2-aminophenoxy)ethyl)-4-(5,5-dimethyl-1,3-dioxan-2-yl)-2-(2-methoxyethoxy)aniline. (6)

4-(5,5-dimethyl-1,3-dioxan-2-yl)-2-(2-methoxyethoxy)-N,N-bis(2-(2-nitrophenoxy)ethyl) aniline (780 mg, 1.1 mmol), sodium borohydride (210 mg, 7 mmol), and Raney nickel (2 ml in a water slurry) were suspended in 200 ml of methanol and stirred for 40 min. The reaction was filtered over Celite and dried by sodium sulfate and then evaporate. Then water (100 ml) and ethyl acetate (100 ml) were added to extract the product. The organic layer was collected, dried and evaporated down to afford red oil. The oil was further purified by column chromatography (0-5% methanol in DCM (containing 1% TEA)) to afford light brown oil (520 mg, 0.9 mmol, 81%). 1H NMR (400 MHz, MeOD): δ 7.06-7.08 (m, 4H), 6.69-6.81 (m, 7H), 5.33 (s, 1H), 3.67-4.20 (m, 16H), 3,43 (s, 3H), 1.35 (s, 3H)), 0.84 (s, 3H). 13C NMR (101 MHz, CDCl3): δ 161.42, 147.23, 142.18, 137.41, 127.41, 122.29, 121.11, 119.88, 115.06, 114.84, 113.50, 112.55, 109.74, 79.99, 76.02, 72.22, 69.00, 66.43, 59.48, 59.32, 30.10, 24.46, 20.13.

22-(4-(5,5-dimethyl-1,3-dioxan-2-yl)-2-(2-methoxyethoxy)phenyl)-9,10,21,22,23,24-hexahydro-5H,12H,20H-dibenzo[h,q][1,4,10,16]tetraoxa[7,13,19]triazacyclohenicosine-6,13(7H,14H)-dione. (7)

N,N-bis(2-(2-aminophenoxy)ethyl)-4-(5,5-dimethyl-1,3-dioxan-2-yl)-2-(2-methoxyethoxy)ani - line (1.00 g, 1.8 mmol) and 2,2'-(ethane-1,2-diylbis(oxy))diacetyl chloride (408 mg, 1.90 mmol) were separately dissolved in anhydrous benzene (50 mL) under nitrogen. Using two syringe pumps (KDS-100, KD Scientific), the two solutions were added dropwise over 24 h to a stirring solution of anhydrous pyridine (1.5 mL, 19 mmol) and anhydrous benzene (1.0 L) in a flame-dried, three-neck round bottom flask under nitrogen. After completion of addition, the reaction was heated to reflux while stirring under nitrogen. After 16 h, the solvent was removed via rotary evaporation, and the crude residue was purified by column chromatography (basic alumina, 0-80% ethyl acetate in hexanes) to afford the product as a sticky light orange oil (791 mg, 1.18 mmol, 72%). 1H NMR (400 MHz, MeOD): δ 8.16 (dd, 2H), 6.74-7.05 (m, 9H), 5.32 (s, 1H), 3.59-4.15 (m, 24H), 3,36 (s, 3H), 1.23 (s, 3H)), 0.76 (s, 3H). 13C NMR (101 MHz, CDCl3): δ 168.24, 161.46, 155.64, 142.18, 127.89, 127.45, 126.93, 120.58, 119.92, 119.92, 114.83, 112.96, 112.55, 111.67, 78.24, 76.55, 73.84, 72.22, 69.04, 68.00, 67.92, 59.42, 59.32, 30.18, 24.67, 20.63.

22-(4-(5,5-dimethyl-1,3-dioxan-2-yl)-2-(2-methoxyethoxy)phenyl)-6,7,9,10,13,14,21,22,23,24-decahydro-5H,12H,20H-dibenzo[h,q][1,4,10,16]tetraoxa[7,13,19]triazacyclohenicosine. (8)

Compound 7 (700 mg, 0.10 mmol) was dissolved in anhydrous tetrahydrofuran (21 mL) in a flamed-dried, round bottom flask equipped with a reflux condenser. The resulting solution was cooled to 0 °C, and diborane (4.9 mL, 1.0 M in anhydrous tetrahydrofuran, 1.0 mmol) was added dropwise. The reaction was heated to reflux under nitrogen for 1 h, and the solvent was removed

via rotary evaporation. The crude residue was purified by column chromatography (silica, 50-100% EtOAc in hexanes) to afford 8 as a transparent, pale yellow oil (412 mg, 0.06 mmol, 58%). 1H NMR (400 MHz, CDCl3): δ 7.14-7.08 (m, 3H), 6.90 (t, 2H), 6.50-6.71 (m, 6H), 5.38 (s, 1H), 4.24 (t, 2H), 4.09 (t, 2H), 3.91 (t, 2H), 3.86-3.79 (m, 8H), 3.75 (s, 2H), 3.72-3.65 (d, 2H), 3.48 (s, 3H), 3.38 (t, 4H), 1.35 (s, 3H), 0.85 (s, 3H). 13C NMR (101 MHz, CDCl3): δ 165.40, 149.28, 142.18, 137.43, 124.46, 121.24, 120.60, 117.79, 114.82, 112.52, 110.41, 110.27, 108.65, 79.28, 75.82, 72.21, 71.76, 70.34, 69.08, 67.93, 59.44, 59.30, 52.67, 30.11, 24.84, 20.97. HRMS-ESI: calculated for C37H51O8N3 665.8161; found 665.8169.

TAC-actal. (9)

Compound 8 (390 mg, 0.58 mmol) and 2,2'-(ethane-1,2-diylbis(oxy))diacetyl chloride (127 mg, 0.60 mmol) were separately dissolved in anhydrous benzene (50 mL) under nitrogen. Using two syringe pumps (KDS-100, KD Scientific), the two solutions were added dropwise over 24 h to a stirring solution of anhydrous pyridine (0.5 mL, 5.8 mmol) and anhydrous benzene (1.0 L) in a flame-dried, three-neck round bottom flask under nitrogen. After completion of addition, the reaction was heated to reflux while stirring under nitrogen. After 16 h, the solvent was removed via rotary evaporation, and the crude residue was purified by column chromatography (silica, 0-15% methanol in dichloromethane) to afford the product as a light yellow oil (197 mg, 0.23 mmol, 48%). 1H NMR (400 MHz, CDCl3): δ 7.35 (dd, 2H), 7.30-7.22 (m, 2H), 6.90-7.14 (m, 7H), 4.84 (s, 1H), 3.49-4.25 (m, 36H), 3.40 (s, 3H), 1.26 (s, 3H), 0.79 (s, 3H).

A.1.3.3. Spectroscopic materials and methods

All aqueous solutions were prepared using Milli-Q water, and all spectroscopic experiments were carried out in 50 mM HEPES, pH 7.4, unless otherwise noted. Absorption spectra were acquired on a Varian Cary 50 spectrophotometer, and fluorescence spectra were acquired using a Photon Technology International Quanta Master 4 L-format scan spectro-fluorometer equipped with an LPS-220B 75-W xenon lamp and power supply, A-1010B lamp housing with integrated igniter, switchable 814 photocounting/analog photomultiplier detection unit, and MD5020 motor driver. 1-cm × 1-cm quartz cuvettes (1.4-mL volume, Starna, capped) were used for obtaining absorption and fluorescence spectra. For all fluorescence response to K^+ studies, aqueous solutions of KCl (Sigma) were used. For metal selectivity studies, aqueous metal solutions of $MgCl_2 \cdot 4H_2O$ (EMD Millipore), $CaCl_2 \cdot 2H_2O$ (EMD Millipore), $NiCl_2 \cdot 6H_2O$ (Sigma), $ZnCl_2$ (Sigma), $CuCl_2 \cdot 2H_2O$ (Baker & Adamson), $CoCl_2 \cdot 6H_2O$ (Sigma), $MgCl_2 \cdot 6H_2O$ (Sigma), NaCl (Sigma), $[Cu(CH_3CN)_4]PF_6$ (Sigma), and $FeCl_3$ (Sigma) were used. GSH (Sigma) was used for selectivity studies

A.1.3.4. Fluorescence Turn-on Responses to Potassium

2 different 50 mM HEPES (pH 7.4) was made. Solution A contains 200 mM Na^+ while solution B contains 200 mM K^+. Solution A and B was mixed in different ratio to yield 1 ml final buffer solution with 0, 1, 5, 10, 20, 50, 80, 100, 120, 150, 180, 200 mM respectively. A 2 µM solution of TAC-green prepared by diluting1 mM DMSO stock solution of TAC-green with each buffer 1:500 ratio into a 1-cm × 1-cm capped quartz cuvette. The probe solution was incubated at 37 °C for 5 minutes. Emission spectra (λex = 488 nm, λem = 500-700 nm) were then collected.

A.1.3. Result and discussion

A.1.3.3. Design strategy for a new fluorescent K^+ sensor

Crown ether derivatives have been known as good alkali metal binding molecules. Previously, fluorescent K+ sensors were based on crown ether derivatives, namely PBFI (Scheme 1, a). However, crown ether derivatives suffered from poor selectivity for K^+ over Na^+. New potassium sensors with good selectivity for potassium ion were derived from a potassium selective receptor based on a triazacryptand structure, developed by He et al. [6] The ring size and the three dimensional cavity structure of this potassium receptor provided good selectivity for K^+ over Na^+. This potassium receptor can be covalently linked to various fluorophores to construct molecular probes. Herein, the project focuses on synthesizing a key potassium receptor derivative with an aldehyde group. (Scheme 1, c) The aldehyde group was added to the design of the potassium receptor for further development of fluorophores since it is a useful handle to condense with pyrrole and 3-aminophenol to generate boron-dipyrromethene (BODIPY) and rhodamine cores respectively. (Scheme 1, d) BODIPY sensors have the advantage of a versatile biological labeling and are widely used in biology since they are more resistant to photobleaching and chemical degradation.[11] The basic BODIPY fluorophore, composed of 3-ethyl-2,4-dimethyl-1H-pyrrole, were reported to have quantum yields as high as 0.70.[12] Recent work reported by Courtis et al. showed changing of fluorine to methoxy or ethoxy group in BODIPY could contribute to improved solubility and shift emission wavelengths.[13] This development drastically increases the solubility of the BODIPY group and renders it more suitable for biological imaging In addition, rhodamine-based fluorescent sensors can also be derived from the aldehyde group.

A.1.3.3. Synthesis effort towards triazacryptand based fluorescent K^+ sensor

Two main routes towards the synthesis of the triazacryptand derivative were developed by Verkman's group and He's group. [6, 8] Verkman's route was attempted first due to its reported higher overall yield. However, we encountered problem at the first step with the N-aryl coupling reaction. Various conditions were attempted by altering the catalyst, the ligand, the temperature and the reaction time. The best reaction condition was based on Zhang's paper [14] (Scheme 3) with a yield of 23%, which compared with the yield from Verkman's group (76%) was still low. We then decided to pursue a route based on He's synthesis. (Scheme 2) However, He's potassium receptor lacked the key aldehyde group needed for further functionalization. The addition of the aldehyde group required changes to the synthetic route performed by He et al. In addition, the two essential macrocyclization reactions showed low yields (48%, 36%). Thus we modified the synthetic route for our target molecule.

First, we used 3-hydrox-4-nitro-benzaldehyde as the precursor to introduce an aldehyde group at para position of the aryl amine for the final product, and protected the aldehyde as an acetal to prevent the undesired reduction. Acetal group was used as the protecting group for the extra aldehyde group. We chose to use 2, 2-dimethyl-1, 3-propanediol to make a 6-membered ring acetal group. Earlier attempts to use glycol to make a 5-membered ring acetal group were less successful. Using 2, 2-dimethyl-1, 3-propanediol as the acetal percursor, we obtained a 97% yield.

In the original paper, the reduction of the aryl nitro group to an aniline group was performed using zinc dust and ammonium chloride. Considering the sensitivity of acetal protecting group toward acidic conditions, a different reduction agent was needed. First, a simple hydrogenation reaction was attempted with palladium on carbon as the catalyst. However, the dimethyl acetal group was unstable under the reaction conditions and various byproducts were formed, resulting in a low yield (< 35%). Sodium borohydride and Raney nickel were used as an alternative reducting agent. [14] (Scheme 2, d) Fortunately, a good yield (87%) was obtained by controlling the reaction time (1 h) and equivalents of sodium borohydride (3 equivalents), thus preventing the degeneration and reduction of the acetal group as well as achieving an improved yield.

Two key macrocyclization steps are used in our synthetic route. The yields reported in He's original synthesis were relatively low (45% for the first macrocyclization and 40% for the second macrocyclization) mainly because, in original synthesis, addition funnels were used, lacking a good control of the addition rate. However, we used syringe pumps adding two starting materials separately to better control the addition rate. In our method, both starting materials were added to the reaction flask with a slow rate (< 0.1 mmol/h) and were diluted to a great extent (< 2 mmol/L). The change was made to avoid the intermolecular reaction and favor the intramolecular reaction. After the process change, we observed an increase in the yield of both macrocyclization steps (72 % for the first macrocyclization and 48% for the second macrocyclization).

Following the macrocyclization reactions, we sought to reduce the amide functionalities to amines. We again found the need to optimize our reaction conditions to make the reducing conditions compatible with the acetal-protected aldehyde. Early experiments showed either partial reduction of the acetal group to hydroxyl neopentyl ether group or complete reduction of the acetal to a methyl group using borane and tetrahydrofuran (THF) as the reduction agent. This result was hypothesized to occur as a result of the influence of the electron rich aniline moiety connected to the acetal group and borane acting as a Lewis acid. Additional experiments showed that shortening the reaction time (from overnight to 1 h), increasing the temperature (from room temperature to 80 oC) raising the equivalents of borane reagent (from 3 equivalents to 6 equivalents), and slowing down the addition of borane to ensure an even dispersion could help increase the yield. After incorporating all these major changes, a maximum yield of 58% has been achieved at present.

A.1.4. Conclusion

Thus far, we have presented the synthesis of the key potassium receptor derivative, Compound 10. Our route was based on the original route published by He et al. with changes and optimization of some key steps in the original route, enabling an aldehyde group to be introduced in the structure for further fluorophore attachment. Based on our understandings of previous research efforts, a primary goal for potassium sensor development is preparation of extracellular dyes with high fluorescence turn-on for use in mammalian cell culture models. Specifically, we want to attach our sensor to the outside cell membrane to obtain better temporal and spatial information regarding potassium efflux during a certain cell activities.

To accomplish this goal, first, we will finish the synthesis of the potassium receptor Compound 11. Fluorescent sensors will be synthesized by using the aldehyde group to conjugate BODIPY, rhodamine, and xanthene cores. (Scheme 1, d) These probes will be characterized further to evaluate the specificity and response to potassium ions under physiological conditions. Fluorescent probes which show good turn-on ratio, Kd around 5 mM, and good selectivity for potassium under high sodium concentration around 140 mM will then be evaluated in cellular model system. During potassium fluctuations, the extracellular potassium levels in the vicinity of the cells will undergo larger changes compared with those in distant area. Thus, we would like to attach our potassium sensor to the outside of the membrane. SNAP-tag technology is a good method for site-specific labeling of small molecules on a protein of interest. Our group has previously exploited the versatility of this method for the fluorescent detection of extracellular hydrogen peroxide with a modified boronate probe. [15] In the future we would like to apply the SNAP-tag or Clip-tag technology and attach our potassium sensor to the exterior surface membrane, thus achieving better temporal and spatial detection of the potassium efflux.

A.1.5. Reference

(1) Hudgins, P. M.; Weiss, G. B. J. Pharmacol. Exp. Ther. 1968; 159, 91–97.
(2) Gadsby, D. C.; Niedergerke, R.; Page, S. Nature. 1971; 232, 651–653.
(3) Kofuji, P.; Newman, E. A. Neuroscience. 2004; 129, 1043–1054.
(4) Stanton, B. A.; Biemesderfer, D.; Wade, J. B.; Giebisch, G. Kidney Int. 1981; 19, 36–48.
(5) Frant, M. S.; Ross, J. W. 1970; 167, 987–988.
(6) He, H.; Mortellaro, M. A.; Leiner, M. J. P.; Fraatz, R. J.; Tusa, J. K. J. Am. Chem. Soc. 2003; 125, 1468–1469.
(7) Jezek, P.; Mahdi, F.; Garlid, K. D. J Biol Chem. 1990, 265, 10522–10526.
(8) Namkung, W.; Padmawar, P.; Mills, A. D.; Verkman, A. S. J. Am. Chem. Soc. 2008, 130, 7794–7795.
(9) Namkung, W.; Song, Y.; Mills, A. D.; Padmawar, P.; Finkbeiner, W. E.; Verkman, A. S. J. Biol. Chem. 2009, 284, 15916–15926.
(10) Padmawar, P.; Yao, X.; Bloch, O.; Manley, G. T.; Verkman, A. S. Nat. Methods 2005, 2, 825–827.
(11) BAYLOR, D. A.; NICHOLLS, J. G. J. Physiol. 1969, 203, pp. 555-569
(12) Won, Y.-J.; Ono, F.; S. R. Ikeda, PLos ONE, 2012, 7, 42602
(13) Boens, N.; Leen, V.; Dehaen, W. Chem. Soc. Rev. 2012, 41, 1130
(14) Zhang, X.X.; Buchwald, S.L. J. Org. Chem. 2000, 65, 8027
(15) Courtis, A. M.; Santos, S. A.; Guan, Y.; Hendricks, J. A.; Ghosh, B.; Szantai-Kis, D.M.; Reis, S. A.; Shah, J. V.; Mazitschek, R. Bioconjug Chem. 2014, 25,1043.

(16) Pogoreli´c et al. Journal of Molecular Catalysis A: Chemical 274 (2007).
(17) Srikun, D.; Aaron, E.; Albers, C. I; Nam, A. T.; Chang, C. J. J. Am. Chem. Soc. 2010, 132, 4455–4465.
(18) Garmestani, K.; Link, J. M.; Kronr, K. A. Journal of Labelled Compounds and Radiopharmaceuticals-Vol. XXVIII, No. 10 Ward, W. W.; Cormier, M. J. Energy.

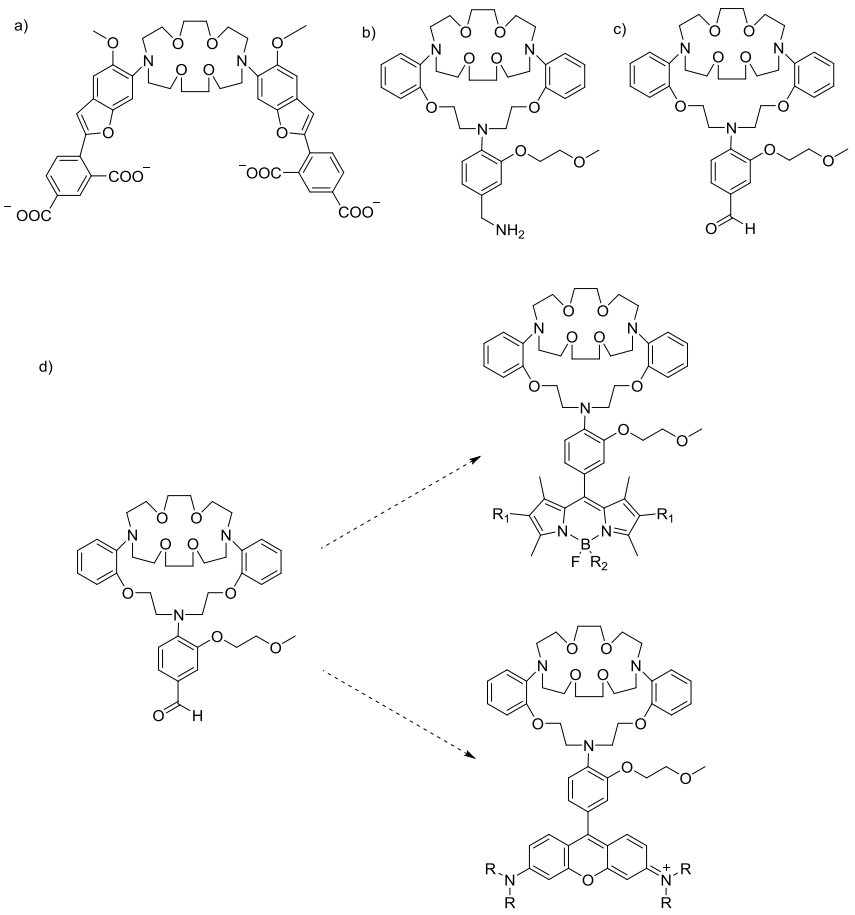

Scheme 1. a) Crown ether based potassium ion sensor PBFI. b) Original potassium receptor moiety synthesized by He *et al.* c) Our design of potassium ion sensor with an aldehyde group for fluorophore attachment. d) Two kinds of fluorophores that can be developed based on the aldehyde group.

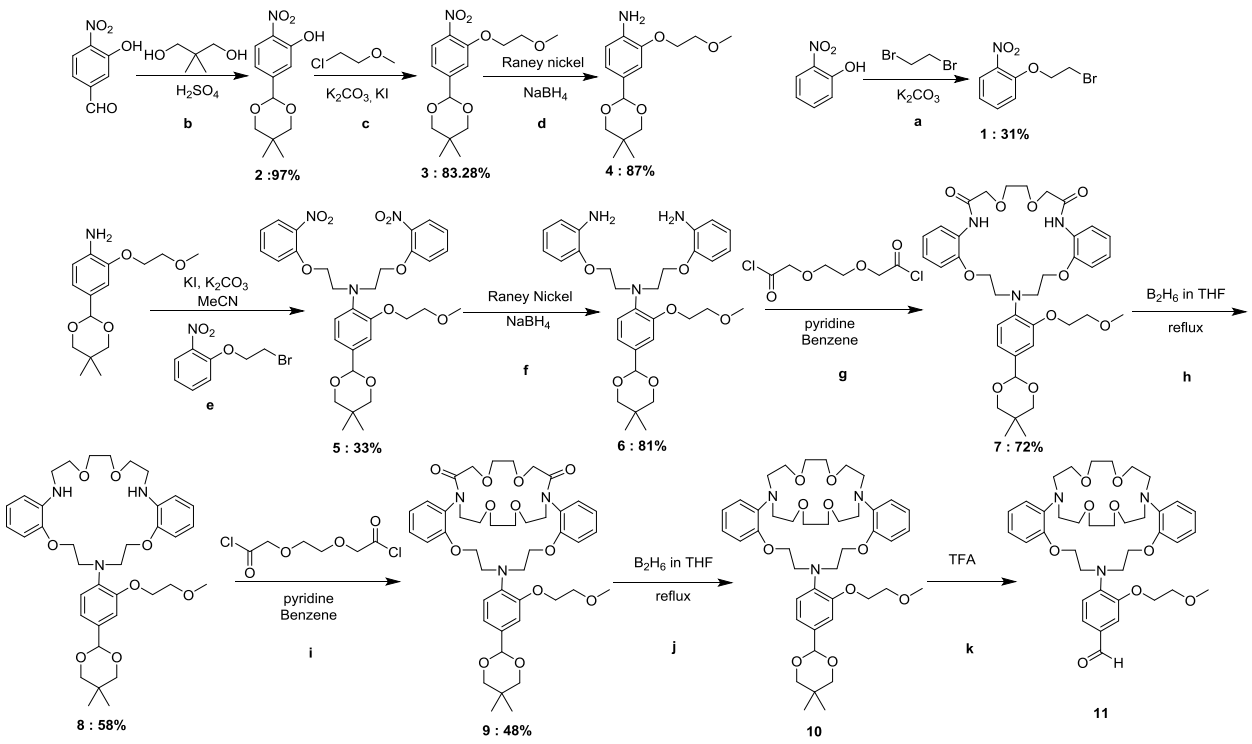

Scheme 2. A complete route towards the synthesis of the aldehyde-functionalized potassium receptor. **Compound 10** is under further purification and **reaction k** still needs to be performed.

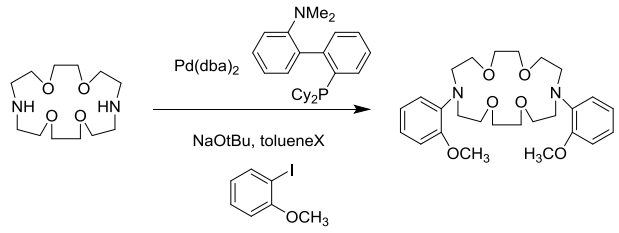

Yield: 23%

Scheme 3. Pd catalyzed *N*-aryl coupling reaction as the first step of the synthesis route from Verkman's group. The best catalyst and ligand with the highest yield are shown

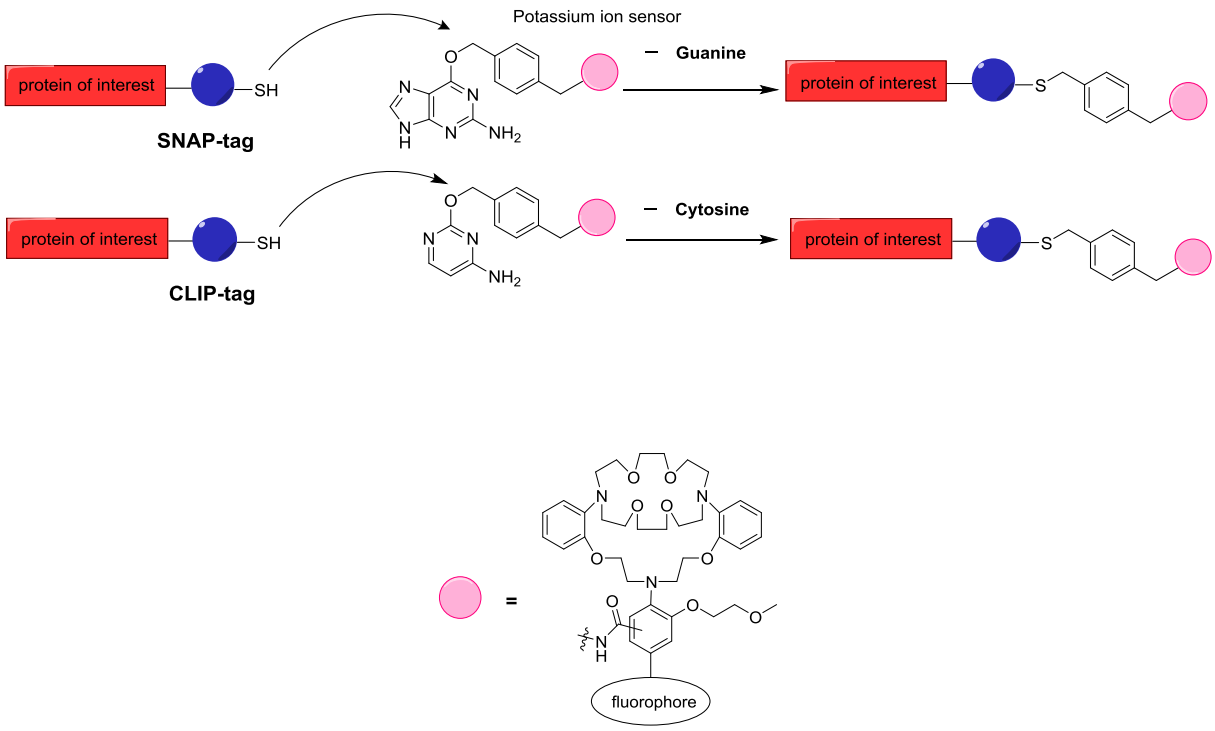

Scheme 4. Schematic for the utilization of SNAP-tag and CLIP-tag based potassium sensors.

Protein of interest is likely to be the cell surface membrane protein. Protein of interest will aid in the targeting of the sensor to the extracellular surface of the cell membrane.

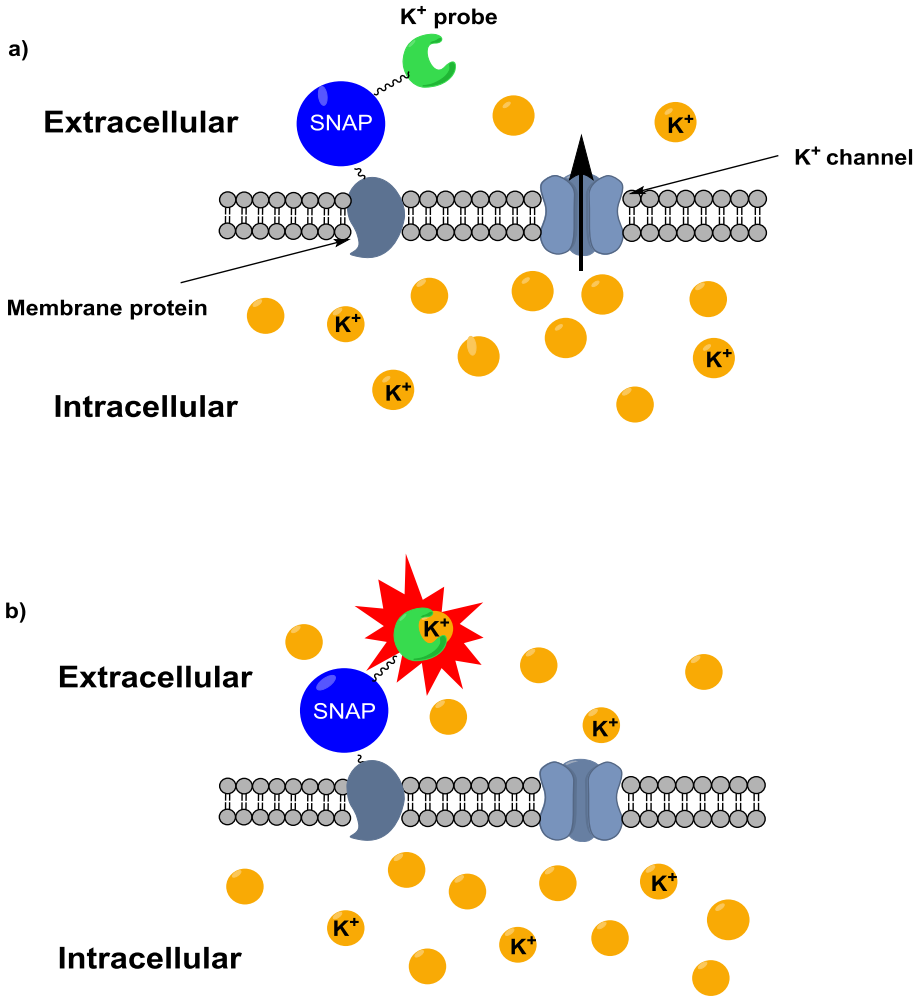

Scheme 5. Mechanism of utilization of SNAP-tag technology for detecting extracellular potassium ions. a) In resting state, the extracellular concentration of potassium is low and the sensor should exhibit low fluorescence. b) After the efflux of potassium ion, the extracellular area close to the cell membrane experiences a raise in potassium level and, at sufficiently high concentrations, potassium is bound by the sensor, thus resulting in the fluorescence.

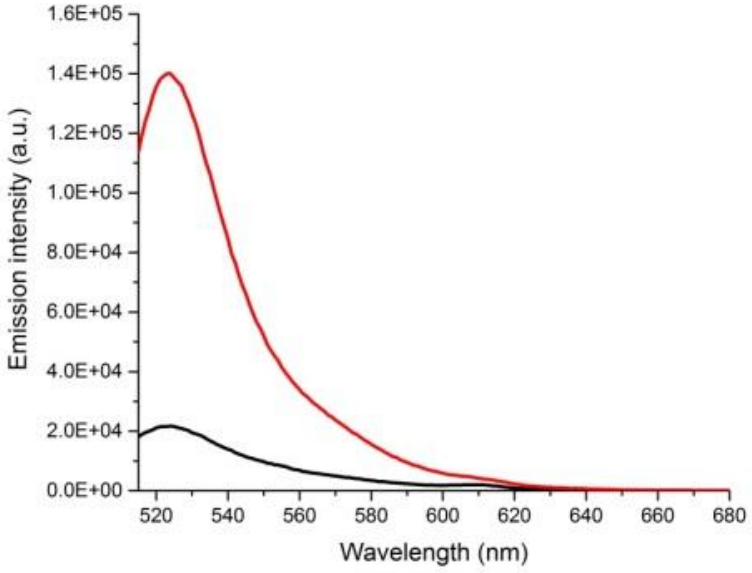

Figure 1.3. Fluorescence intensity of 1 μM TAC-green before (black line) and after (red line) titration of 200 mM K^+. Spectrum were acquired at 37 °C in 50 mM HEPES (pH 7.4) when monitoring intensity on fluorometer, with λ_{ex} = 488 nm, collecting emission between 510 – 680 nm.

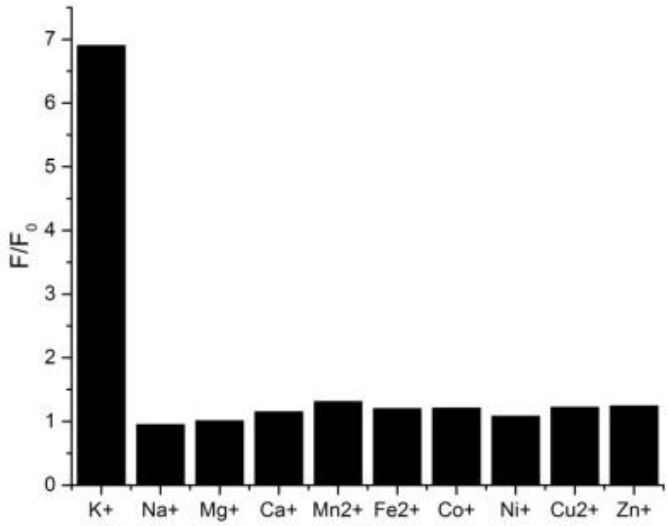

Figure 1.3. Fluorescence response of 1 μM TAC-green to biologically relevant d-block (10 μM) and s-block (1 mM) metals except for Na^+ (150 mM). Spectrum were acquired at 37 °C in 50 mM HEPES (pH 7.4) when monitoring intensity on fluorometer, with λ_{ex} = 488 nm, collecting emission between 510 – 680 nm.

Appendix 2

Development of a platform for imaging synaptic pH in the NIR range using an upconverting nanoparticle conjugated system

Portions of this work were performed in collaboration with the following persons:

Dr. Cheryl Tajon helped synthesize UCNP for this experiment and conducted the conjugation and spectrum analysis (Figure A.2.5)
Dr. Safacan Koleman helped design and synthesized pH sensor (Scheme A.2.1)

A.2.1. Synopsis

Synaptic transmission, which is also known as neurotransmission, is an essential process for neuronal communication in the nervous system1 and it takes place at synapses.[1–6] In a typical chemical synapse, neurotransmission basically involves the release of neurotransmitters from a presynaptic neuron cell (exocytosis), which is followed by binding of these signaling molecules to the specialized receptors on the postsynaptic cell. Synaptic vesicles are at the core of synaptic transmission since they carry neurotransmitters and release them to the synaptic cleft (figure 1). Neurotransmitters are loaded into the synaptic vesicles with the help of vesicular transport proteins. One of the well-known examples is a vacuolar-type H^+- ATPase (V-ATPase). V-ATPase is a proton pump that generates the electrochemical gradient between lumen (interior side) and outside of the vesicles that allows neurotransmitter uptake.[7] Thus, as a result of V-ATPase activity synaptic vesicle's lumen has slightly acidic environment with pH values ranging from 4.5 to 6.0, where pH is accepted to be around 5.0 in general Monitoring synaptic transmission and presynaptic activity are quite important processes since they allow us to understand the signaling pathways, roles of many critical proteins and neurotransmitter trafficking during the neuronal activity which are all directly related with neuronal communication (excitability) and man neurodegenerative diseases. The most straightforward and easy way to visualize neurotransmission is to track synaptic vesicles by pH-sensitive fluorescent probes. As it is mentioned before, due to the V-ATPase activity, pH of the synaptic vesicle is around 5.0 at relax state. Upon exocytosis, since synaptic vesicles are merging with the extracellular medium, pH increases up to 7.4. This pH difference can be used to change the photophysical properties of fluorescent probes (emission turn-on/off).

Initial pH-sensitive probes for neurotransmission visualization involve fluorescent protein based probes. Recently a small pH probe was reported by Nagano group in which the probe is highly emissive at pH 5.0 and almost non-emissive at pH 7.4, thus the emission of their probe is turning-off after exocytosis[8,9]. On the other hand, fluorescent protein based probes are "turn-on" type probes and have their own advantages, however design restrictions, low turn-on ratios and interference with biological compounds are appeared to be some drawbacks and restrict their usage. It is clear that there is still need for neutral pH activatable (turn-on type), photostable and red-emitting small fluorescent probes.[9–11] In the chapter, we described the design and thesis towards a duo-system based sensor of characteristic neutral or slightly basic pH value of secretory vesicles after exocytosis combining bright and red-emitting silicon-substituted xanthone (Si-Xanthone) based small molecular with upconverting nanoparticles (UCNP)

Lanthanide-doped upconverting nanoparticles (UCNPs) absorb multiple NIR photons and emit at higher energies with efficiencies orders of magnitude higher than those of the best 2-photon fluorophores.[12] UCNPs can be imaged in the absence of cellular autofluorescence or measurable photobleaching, even under prolonged single-particle excitation.[13,14] UCNPs make use of energy transfer upconversion between 4^f_N electronic states of neighboring lanthanide ($Ln3^+$) ions, in which sensitizer ions sequentially transfer absorbed energy to luminescent emitter ions, both of which are doped into a low-phonon nanocrystal host matrix. While UCNPs are inherently sensitive to temperature[15,16]and mechanical force,[17] they have little innate chemical sensing ability and require pairing with external probes to act as biosensors. UCNP complexes

with organic fluorophores[18–21]and fluorescent proteins[14,22] have also been reported, but upconverted energy transfer (UET) in these systems is less utilized or optimized.
In this chapter, we report the design and efforts towards making a duo-system NIR pH sensor. UCNP is conjugated with a small-molecule pH sensor. UCNP in the duo-system probe is first excited with NIR laser and convert the energy to visible light emission. Then UET will occur between UCNP and pH sensor, resulting in an emission wavelength around 620 -650 nm. We envision achieving a high signal-to-noise ratio deep tissue NIR imaging using this construct ultimately. It's also worth noted that the structure can be easily modified to response to other bio-analyte as long the excitation of the small molecule probe matches the emission range of UCNP.

A.2.2. Method

A.2.3.1. Synthetic Details

All reactions utilizing air sensitive reagents were performed in flame-dried glasswares under N2 atmosphere. Dry solvents when needed were used after passing over activated molecular sieves. All other reagents were used without any purification. Silica gel P60 (SiliCycle) was used for column chromatography and SiliCycle 60 F253 silica gel plates were used for thin-layer chromatography. 1H NMR, 13C and 31P NMR spectra were collected in CDCl3, CD3OD or (CD3)2SO (Cambrigde Isotope Laboratories, Cambrigde, MA) at 25oC on Bruker AV-300, AVB-400, AVQ- 400 or DRX-500 with operating frequencies of 101 MHz for 13C and 300, 400 or 500 MHz for 1H and 162 MHz for 31P at the College of Chemistry NMR Facility at the University of California, Berkeley. All chemical shifts were reported in parts per million (ppm). Splitting patterns are designated as s (singlet), d (doublet), t (triplet), q (quartet), m (multiplet), dd (doublet of doublets) and br (broad). LC-MS spectral analyses were carried out using a LC-MS (Agilent Technology 6130, Quadrupole (LC/MS).

4,5-Dichloro-3,6-dihydroxy-Si-xanthone :

A solution of 100 mM NaOCl in 0.1 N NaOH aq. (7 mL) was added to a solution of (6) (100 mg, 0.37 mmol) in MeOH (6 mL). The reaction mixture was stirred for 1 h at RT, followed by acidification with 2 N HCl aq. to pH 2.0, and then extracted with EtOAc. Combined organic phases were washed with water and brine, dried over Na2SO4 and solvent was evaporated. Purification by silica gel column chromatography (1:1 / EtOAc: Hexane) gave (14) as a yellow solid (100 mg, 80% yield). 1H NMR (400 MHz, MeOD-d4) δ 8.25 (d, J = 8.8 Hz, 2H), 7.10 (d, J = 8.7 Hz, 2H), 0.78 (s, 6H).

4,5-Dichloro-3,6-diTBDMSO-Si-xanthone:

TBDMSCl (121 mg, 0.80 mmol) was added into a solution of (14) (69 mg, 0.20 mmol) and ImH (55 mg, 0.80 mmol) in DCM (10 mL). Colorless cloudy solution was stirred overnight at RT and then solvent was evaporated and the residue was directly subjected to silica gel column chromatography (1:1 / EtOAc: Hexane) to gave (15) as a white solid (100 mg, 80% yield). 1H NMR (400 MHz, CDCl3) δ 8.36 (d, J = 8.7 Hz, 2H), 7.07 (d, J = 8.7 Hz, 2H), 1.07 (s, 18H), 0.81 (s, 6H), 0.31 (s, 12H).

bis((3-methyloxetan-3-yl)methyl) 4-bromoisophthalate

A mixture of Bromoisophthalic acid (3 g, 12.2 mmol), SOCl2 (3.56 mL, 49.0 mmol) and 1 drop of DMF was stirred at reflux for 18h. After cooling to RT, solvent was removed and the residue was azeotroped twice with toluene. The crude acid chloride was dissolved in 5 mL DCM and added into 3-Methyl-3-oxetanemethanol (4.88 mL, 49.0 mmol) and pyridine (7.92 mL, 98.0 mmol) in 20 mL DCM at 0oC. Ice-bath was removed and reaction mixture was further stirred at RT for 90 min. Solution was diluted with water, extracted with DCM and combined organic phases were washed with satd. NaHCO3 aq. solution and brine. Solvent was evaporated and purification by silica gel column chromatography (1:1 / Hexane: EtOAc) gave (22) as a white solid (3.90 g, 77%). 1H NMR (400 MHz, CDCl3) δ 8.47 (d, J = 2.2 Hz, 1H), 8.02 (dd, J = 8.3, 2.2 Hz, 1H), 7.80 (d, J = 8.4 Hz, 1H), 4.64 (t, J = 5.7 Hz, 4H), 4.52 – 4.40 (m, 8H), 1.46 (s, 3H), 1.44 (s, 3H).

1,1'-(4-bromo-1,3-phenylene)bis(4-methyl-2,6,7-trioxabicyclo[2.2.2]octane:

A solution of (22) (3.75 g, 9.1 mmol) in DCM (35 mL) was cooled to 0oC and BF3.OEt2 (0.64 g, 4.53 mmol) was added to this solution under N2. The reaction was allowed to warm to RT overnight. Et3N (2.5 mL) was added and resulting solution was stirred for 15 min at RT. Solvent was removed and residue was directly purified by silica gel column chromatography (0 to 20% EtOAc in Hexane with continuous addition of 40% DCM) gave (23) as a white solid (1.68 g, 45%). 1H NMR (400 MHz, DMSO-d6) δ 7.81 (d, J = 2.3 Hz, 1H), 7.60 (d, J = 8.3 Hz, 1H), 7.35 (dd, J = 8.3, 2.3 Hz, 1H), 4.01 (s, 6H), 4.00 (s, 6H), 0.84 (s, 3H), 0.83 (s, 3H).

Compound:

(170 mg, 0.39 mmol) was put into a flame-dried 2-necked round bottom flask, which is then filled with N2. 10 mL anhydrous THF was added and the mixture was cooled to -78oC. Then t-BuLi (0.46 mL, 0.78 mmol) was slowly introduced and the solution was stirred for 20 min. (15) (40 mg, 0.077 mmol) in 5 mL anhydrous THF was added to the reaction mixture at -78oC and upon addition reaction was warmed to RT. It was stirred for additional 1 h at RT. 10 mL of 1 M HCl aq. solution was added which yielded purple solution and the mixture was stirred for another 1h. The reaction mixture was poured into 50 mL satd. NaHCO3 aq. solution and extracted with EtOAc. The organic layer was washed with brine, dried over Na2SO4 and solvent was evaporated. Purification by silica gel column chromatography (1:10 MeOH: CH2Cl2) gave (24) as an orange film. (24) was directly dissolved in 6N HCl at stirred overnight at 80oC. The solution was extracted with EtOAc, washed with brine and dried over Na2SO4. Solvent was evaporated and purification by silica gel column chromatography (1:5 / MeOH: DCM) gave (25) (10 mg). 1H NMR (400 MHz, MeODd4) δ 8.48 (s, 1H), 8.20 (dd, J = 8.1, 1.5 Hz, 1H), 7.04 (d, J = 8.0 Hz, 1H), 6.94 – 6.67 (m, 4H), 0.98 (s, 3H), 0.82 (s, 3H).

A.2.3.1. Spectroscopic Materials and Methods

Absorption spectra were acquired using a Varian Cary 50 spectrophotometer and fluorescence spectra were recorded with a Photon Technology International Quanta Master 4 L-format scan spectrofluorometer equipped with a LPS-220B 75W xenon lamp and power supply. In sample

preparation milli-Q water was used and sample solutions were put into 1cm x 1cm quartz cuvettes (Starna).

A.2.3. Reference

(1) Copenhagen, D. R. Synaptic Transmission in the Retina. *Curr. Opin. Neurobiol.* **1991**, *1* (2), 258–262.

(2) Sigal, Y. M.; Speer, C. M.; Babcock, H. P.; Zhuang, X. Mapping Synaptic Input Fields of Neurons with Super-Resolution Imaging. *Cell* **2015**, *163* (2), 493–505.

(3) Abbott, L. F.; Regehr, W. G. Synaptic Computation. *Nature*. 2004, pp 796–803.

(4) Paterson, S. Opioid Receptors. *Asp. synaptic Transm.* **1991**.

(5) Rouach, N.; Koulakoff, A.; Abudara, V.; Willecke, K.; Giaume, C. Hippocampal Synaptic Transmission. *Science* **2008**, *322* (December), 1551–1555.

(6) Kittel, R. J.; Heckmann, M. Synaptic Vesicle Proteins and Active Zone Plasticity. *Front. Synaptic Neurosci.* **2016**, *8* (APR).

(7) Salyer, S. A.; Olberding, J. R.; Distler, A. A.; Lederer, E. D.; Clark, B. J.; Delamere, N. A.; Khundmiri, S. J. Vacuolar ATPase Driven Potassium Transport in Highly Metastatic Breast Cancer Cells. *Biochim. Biophys. Acta - Mol. Basis Dis.* **2013**, *1832* (10), 1734–1743.

(8) Huang, J.; Ying, L.; Yang, X.; Yang, Y.; Quan, K.; Wang, H.; Xie, N.; Ou, M.; Zhou, Q.; Wang, K. Ratiometric Fluorescent Sensing of pH Values in Living Cells by Dual-Fluorophore-Labeled I-Motif Nanoprobes. *Anal. Chem.* **2015**, *87* (17), 8724–8731.

(9) Aigner, D.; Borisov, S. M.; Orriach Fernández, F. J.; Fernández Sánchez, J. F.; Saf, R.; Klimant, I. New Fluorescent pH Sensors Based on Covalently Linkable PET Rhodamines. *Talanta* **2012**, *99*, 194–201.

(10) Zhu, H.; Fan, J.; Xu, Q.; Li, H.; Wang, J.; Gao, P.; Peng, X. Imaging of Lysosomal pH Changes with a Fluorescent Sensor Containing a Novel Lysosome-Locating Group. *Chem. Commun.* **2012**, *48* (96), 11766.

(11) Namkung, W.; Padmawar, P.; Mills, A. D.; Verkman, A. S. Cell-Based Fluorescence Screen for K+ Channels and Transporters Using an Extracellular Triazacryptand-Based K+ Sensor. *J. Am. Chem. Soc.* **2008**, *130* (25), 7794–7795.

(12) Wu, S.; Han, G.; Milliron, D. J.; Aloni, S.; Altoe, V.; Talapin, D. V.; Cohen, B. E.; Schuck, P. J. Non-Blinking and Photostable Upconverted Luminescence from Single Lanthanide-Doped Nanocrystals. *Proc. Natl. Acad. Sci.* **2009**, *106* (27), 10917–10921.

(13) Li, L. Le; Wu, P.; Hwang, K.; Lu, Y. An Exceptionally Simple Strategy for DNA-Functionalized Up-Conversion Nanoparticles as Biocompatible Agents for Nanoassembly,

DNA Delivery, and Imaging. *J. Am. Chem. Soc.* **2013**, *135* (7), 2411–2414.
(14) Shen, J.; Zhao, L.; Han, G. Lanthanide-Doped Upconverting Luminescent Nanoparticle Platforms for Optical Imaging-Guided Drug Delivery and Therapy. *Adv. Drug Deliv. Rev.* **2013**, *65* (5), 744–755.
(15) Zhou, J.; Liu, Z.; Li, F. Upconversion Nanophosphors for Small-Animal Imaging. *Chem. Soc. Rev.* **2012**, *41* (3), 1323–1349.
(16) Peng, J.; Xu, W.; Teoh, C. L.; Han, S.; Kim, B.; Samanta, A.; Er, J. C.; Wang, L.; Yuan, L.; Liu, X.; et al. High-Efficiency in Vitro and in Vivo Detection of Zn^{2+} by Dye-Assembled Upconversion Nanoparticles. *J. Am. Chem. Soc.* **2015**, *137* (6), 2336–2342.
(17) Liu, Y.; Chen, M.; Cao, T.; Sun, Y.; Li, C.; Liu, Q.; Yang, T.; Yao, L.; Feng, W.; Li, F. A Cyanine-Modified Nanosystem for *in Vivo* Upconversion Luminescence Bioimaging of Methylmercury. *J. Am. Chem. Soc.* **2013**, *135* (26), 9869–9876.
(18) Liu, Q.; Peng, J.; Sun, L.; Li, F. High-Efficiency Upconversion Luminescent Sensing and Bioimaging of Hg(II) by Chromophoric Ruthenium Complex-Assembled Nanophosphors. *ACS Nano* **2011**, *5* (10), 8040–8048.
(19) Esipova, T. V; Ye, X.; Collins, J. E.; Sakadžić, S.; Mandeville, E. T.; Murray, C. B.; Vinogradov, S. A. Dendritic Upconverting Nanoparticles Enable in Vivo Multiphoton Microscopy with Low-Power Continuous Wave Sources. *Proc. Natl. Acad. Sci. U. S. A.* **2012**, *109* (51), 20826–20831.
(20) Hesse, J.; Klier, D. T.; Sgarzi, M.; Nsubuga, A.; Bauer, C.; Grenzer, J.; Hübner, R.; Wislicenus, M.; Joshi, T.; Kumke, M. U.; et al. Rapid Synthesis of Sub-10 Nm Hexagonal NaYF4-Based Upconverting Nanoparticles Using Therminol® 66. *ChemistryOpen* **2018**, *7* (2), 159–168.
(21) Wu, S.; Han, G.; Milliron, D. J.; Aloni, S.; Altoe, V.; Talapin, D. V; Cohen, B. E.; Schuck, P. J. Non-Blinking and Photostable Upconverted Luminescence from Single Lanthanide-Doped Nanocrystals. *Proc. Natl. Acad. Sci. U. S. A.* **2009**, *106* (27), 10917–10921.
(22) Gargas, D. J.; Chan, E. M.; Ostrowski, A. D.; Aloni, S.; Altoe, M. V. P.; Barnard, E. S.; Sanii, B.; Urban, J. J.; Milliron, D. J.; Cohen, B. E.; et al. Engineering Bright Sub-10-Nm Upconverting Nanocrystals for Single-Molecule Imaging. *Nat. Nanotechnol.* **2014**, *9* (4), 300–305.

Figure and scheme

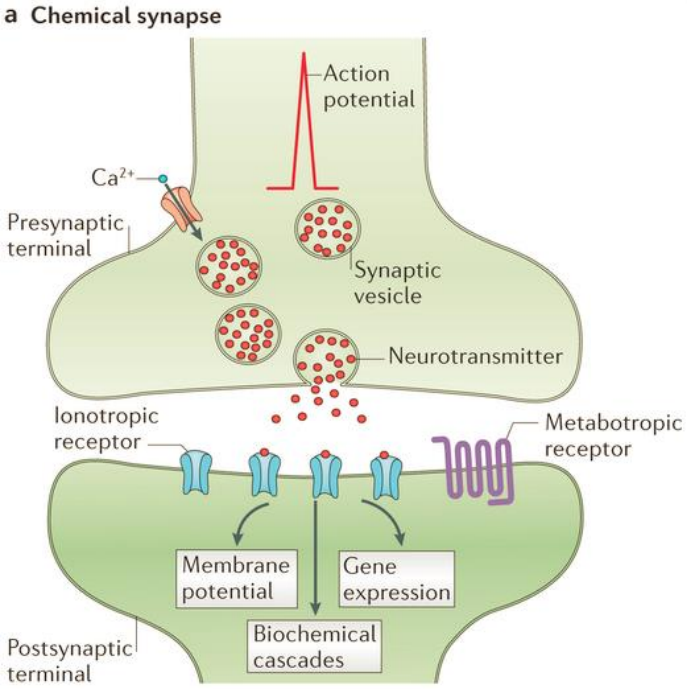

Figure A.2.1. Schematic representation of a typical chemical synapse. Two communicating neuron cells and release of neurotransmitters (exocytosis) from synaptic vesicles and major steps of synaptic transmission.

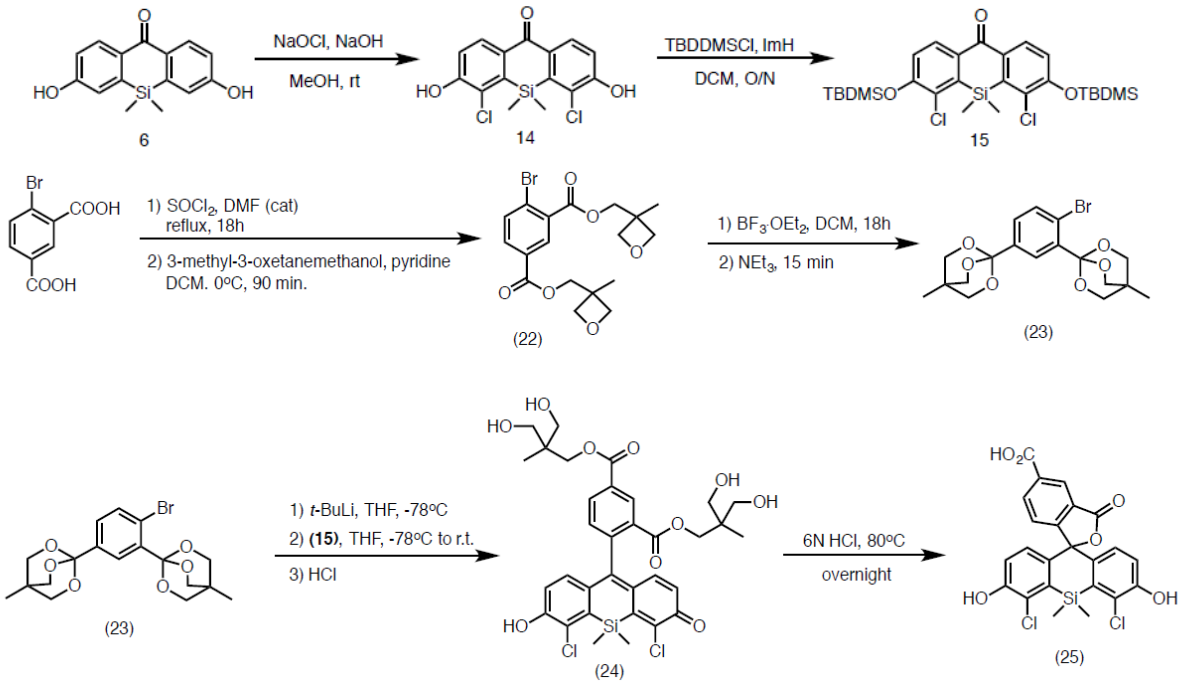

Scheme A.2.2. A briefed route to the synthesis of pH sensor.

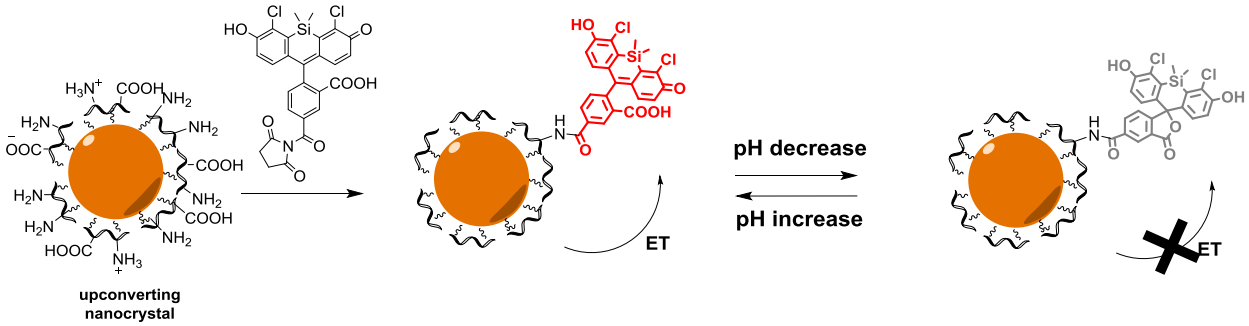

Scheme A.2.3. Proposed mechanism of UCNP-pH sensor conjugate.

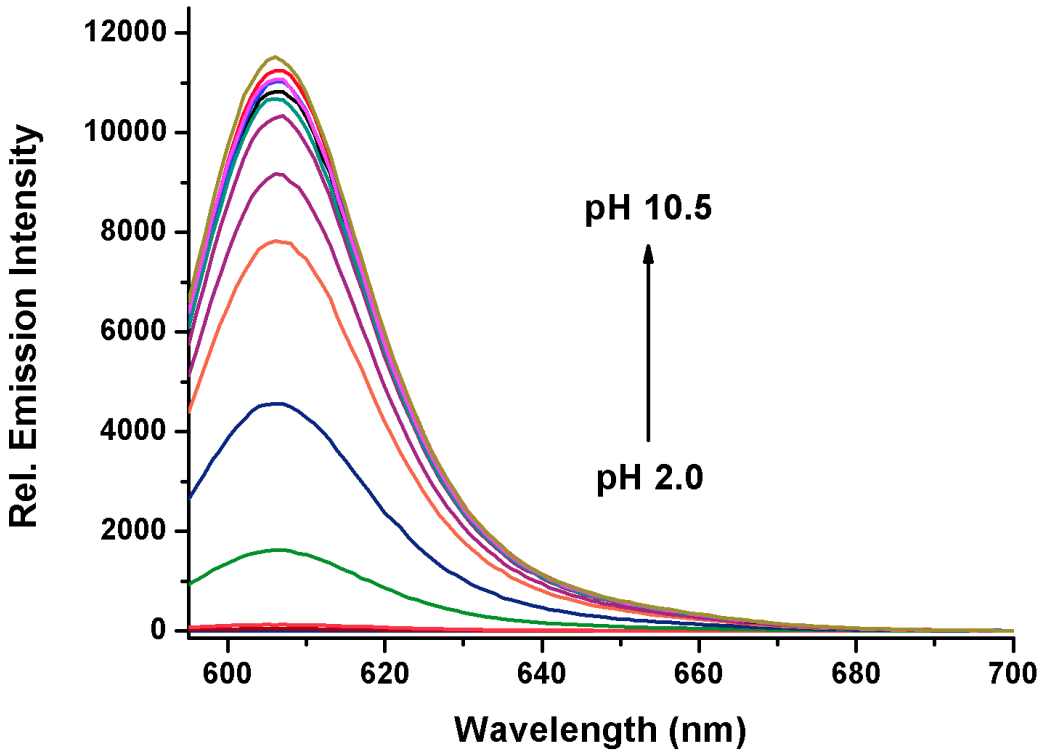

Figure A.2.1. Electronic fluorescence spectra of pH sensor at the following pH values and indicated buffers: 50 mM Glycine (2.0, 2.5, 3.0, 3.5), 50 mM sodium acetate (4.0, 4.5, 5.0, 5.5), 50 mM MES (6.0, 6.4, 6.8), 50 mM HEPES (7.2, 7.4, 7.8, 8.2), 50 mM Tris (8.6, 9.0) and 50 mM glycine (9.5,10.0, 10.5). Probe concentration is 2μM

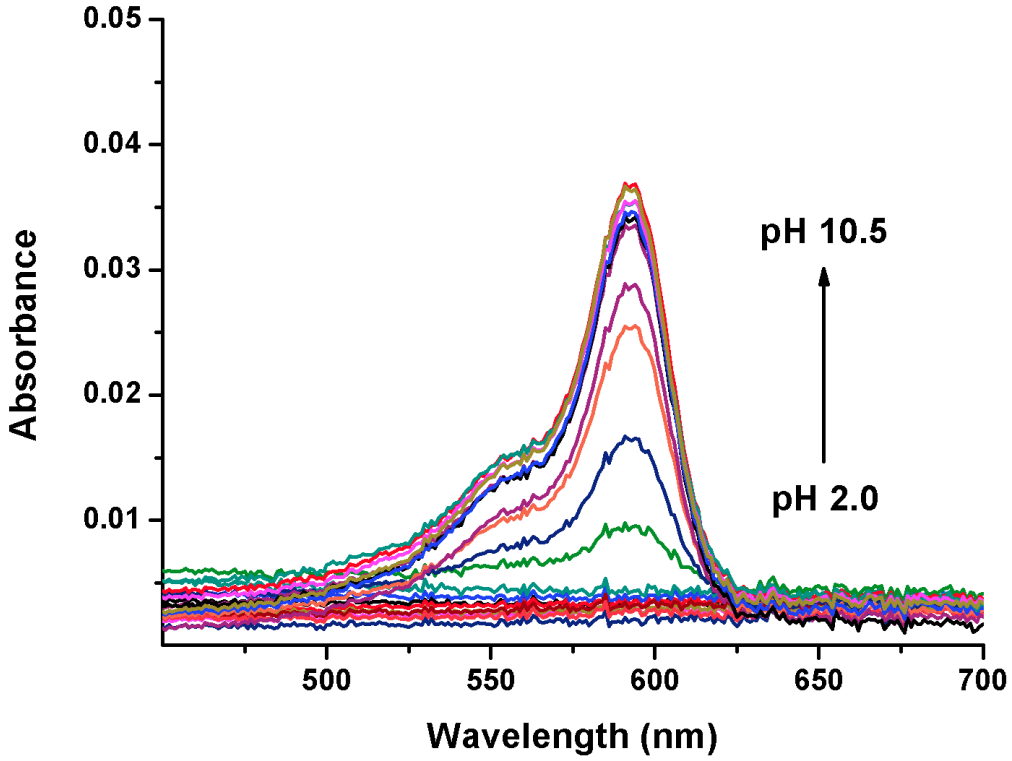

Figure A.2.2. Electronic absorption spectra of pH sensor at the following pH values and indicated buffers: 50 mM Glycine (2.0, 2.5, 3.0, 3.5), 50 mM sodium acetate (4.0, 4.5, 5.0, 5.5), 50 mM MES (6.0, 6.4, 6.8), 50 mM HEPES (7.2, 7.4, 7.8, 8.2), 50 mM Tris (8.6, 9.0) and 50 mM glycine (9.5,10.0, 10.5). Probe concentration is 2μM

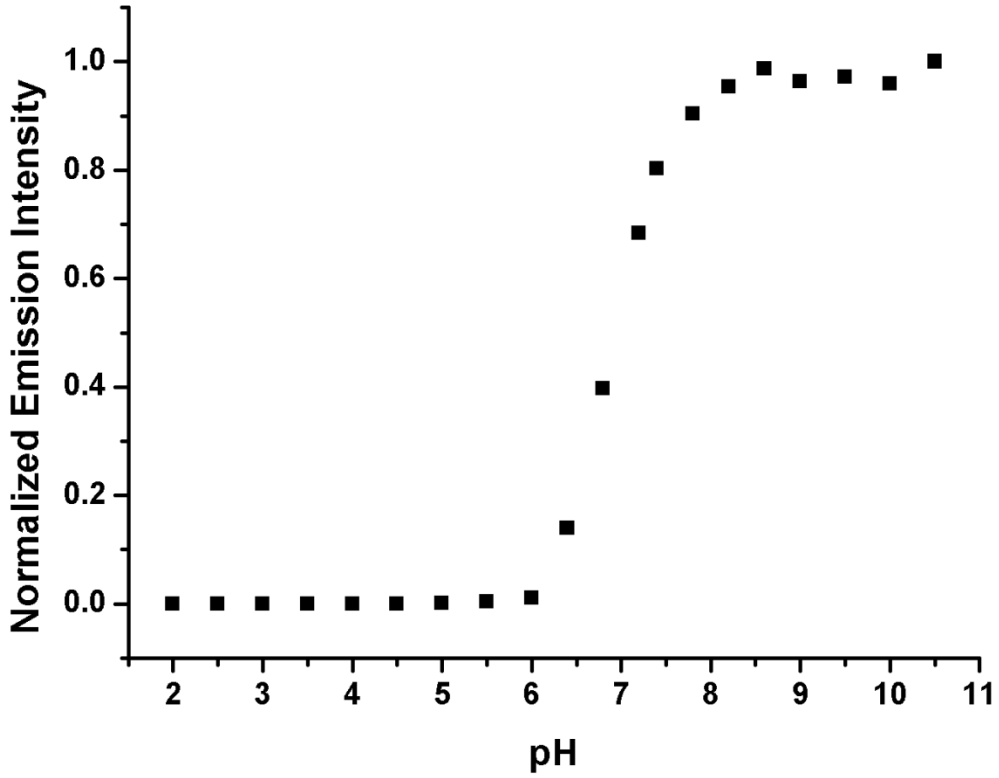

Figure A.2.4. Electronic fluorescence spectra of pH sensor at the following pH values and indicated buffers: 50 mM Glycine (2.0, 2.5, 3.0, 3.5), 50 mM sodium acetate (4.0, 4.5, 5.0, 5.5), 50 mM MES (6.0, 6.4, 6.8), 50 mM HEPES (7.2, 7.4, 7.8, 8.2), 50 mM Tris (8.6, 9.0) and 50 mM glycine (9.5,10.0, 10.5). Probe concentration is 2μM.

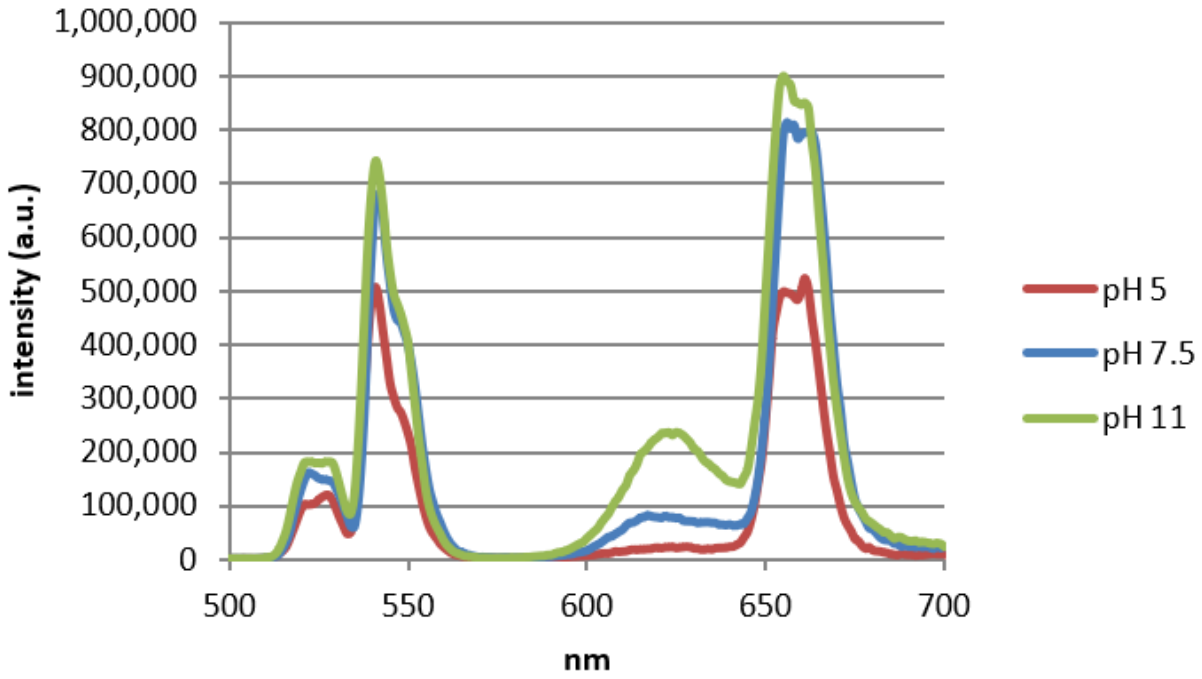

Figure A.2.5. Upconverted emission spectra of covalent core/shell UCNP-fluorophore conjugates bearing ca. 105 pH sensors/UCNP as a function of pH at low 980-nm excitation power density (100 W/cm_2).